Electrostatic Modification of Phospholipid and Lipopolysaccharide Membranes

by

Zheng Ma

A thesis
presented to the University of Waterloo
in fulfillment of the
thesis requirement for the degree of
Master of Science
in
Physics

Waterloo, Ontario, Canada, 2012

I hereby declare that I am the sole author of this thesis. This is a true copy of the thesis, including any required final revisions, as accepted by my examiners.

I understand that my thesis may be made electronically available to the public.

Abstract

Biological membranes are quasi two-dimensional self-assembled structure, primarily serving as a barrier to the leakage of cell's contents. The main constituents of biological membrane are various amphiphilic lipids that form bilayers in an aqueous environment. These lipids carry acidic and/or basic functional groups that ionize in water, giving some of them a net electrical charge. Such a lipid molecule, when integrated into the membrane, experiences electrostatic forces from all other charged objects around it, including ions, surrounding lipids, and other molecules such as cationic peptides. The electrostatic interaction can profoundly influence the membrane, to which many phenomena with physiological significance as well as biophysical interest can be ascribed.

In this thesis, we concentrate on investigating the electrostatic properties of lipid membranes. First, we study how the electrostatic interaction affects their preferred structure. To this end, we adopt a coarse-grain model that preserves the dominant characteristics of the lipids, in which the electrostatic interaction is treated within the "renormalized" Debye-Hückel theory. In particular, we calculate the spontaneous curvature of a phospholipid monolayer, along with other associated quantities. Our results suggest that such divalent ions as Mg^{2+} can stabilize H_{II} phases of lipids (inverted hexagonal phases), which would otherwise form lamellar phases.

Second,we investigate the competitive binding of ions and cationic peptides onto a monolayer of lipopolysaccharide (LPS) molecules, a class of highly charged bio-molecules found in the outer leaflet of the outer membranes of gram-negative (G-) bacteria. Cationic anti-microbial peptides (AMPs) can selectively kill bacteria, and it is suggested that they destabilize the LPS layer, easing their permeation across it, a process of great physiological and clinical interest. To this end, we model the LPS layer as a collection of charged "binding sites", based on which we study the binding of cations (monovalent and divalent) and cationic peptides onto the layer. Our calculations suggest that the peptides can compete with divalent ions on the binding to the layer. It has been empirically known that since the stability of an LPS layer relies greatly on the bridging of divalent ions, the substitution of these ions by the peptides significantly compromises its stability. Our results offer a quantitative basis for this observation, thus providing a possible mechanism of an important step in the action of AMPs against G- bacteria.

Acknowledgements

As the writing of this thesis draws to an end, so is my years as a master graduate student. I want to take this opportunity to express my gratitude to all those who have helped me during this time period.

First and foremost, I want to thank my supervisor, Dr. Bae-Yeun Ha, to whom I owe more gratitude and apologies than anyone else. I still remember the day when I started my academic life in Canada as a naïve, headstrong child, knowing little about the life and responsibility as a graduate student. Dr. Ha took me as his graduate student, as his apprentice, taught me, trained me, showed me what real scientific research is about, and helped me realize what I'm capable of, more important for me at the stage, what I'm actually incapable of. He motivated me to ask myself the question, over and over again: "If this is what the life as a physicist really is like, would you still choose to be one?" Through this, I obtained the potential to be a real physicist, instead of an amateur merely fancied by the superficial magnificence and elegance of physics. He transformed me from an undergraduate student to a true graduate student. During the first two years in Canada, I failed Dr. Ha more times than I can possibly remember. However, he waited, with extraordinary patience, for me to present the correct calculation results, for me to finish the projects, for me to discover myself. He, above and beyond his duty as a supervisor, tolerated all my frustration, dismay, and pause in order for me to be productive during my course of research, silently waiting for me to recover. Each time I get into trouble due to my ignorance and immaturity, he's always willing to give a helping hand. I've always been planning my future career to be a faculty member in a university, and he set a wonderful example for this career, in researching, in teaching, and in being the mentor of graduate students.

I also appreciate the help from other professors in GWPI. Dr. Jeff Z. Y. Chen enlightened me on computational physics during my visit to Hongkong University of Science and Technology, and helped to bring me to Waterloo. Dr. Russell Thompson and Dr. Hartwig Peemoeller, members of my committee, proposed thoughtful questions and constructive guidance in and out of the committee meetings. Dr. Robert Wickham, Dr. John Dutcher and Dr. Leonid S. Brown provided courses that are helpful to my work. Dr. Gary Slater from University of Ottawa met me during the writing of this thesis, and inspired me with his enthusiastic introduction to his work. I also want to thank Dr. Honghao Zhang from Sun Yat-sen University, supervisor of my bachelor degree thesis, whose training as well as passion to science has helped me through the post-graduate years.

I also want to thank the peers around me. Dr. Sattar Taheri-Araghi, before obtaining his PhD degree from our research group in 2010, shared his knowledge, experience and

wisdom with me, helped me familiarize the field of study and get used to the academic life in Canada. He is an excellent graduate student, an exemplar for the students in and out of our group, a benchmark for the performance of all of us. Azadeh Bagheri, who joined our group in 2010, has been working closely with me. We collaborated. We shared what we knew and what we discovered. We supported, encouraged and motivated each other. She added a pinch of femininity to our group, and made the working experience more joyful. I also want to thank other graduate students working on soft matter theory, including Yeongyoon Kim, Kier von Konigslow, Sergey Mkrtchyan, Ying Jiang, Wuyang Zhang and Zijian Long. They all contributed to my graduate study.

I want to show my gratitude to those I love and those who love me. My parents helped develop my life-long habit of reading since I started elementary school. They encouraged me to teach myself of chemistry and physics, buying books for me, when I was 9 years old. One thing I'll never forget is one afternoon in 1996 when I sat on my father's lap and listened to him explaining the chemical composition of table salt. Each of those "Na^+" "Cl^-" "monovalent salt" that appears throughout this thesis traces back to that afternoon. They supported my devotion of physics at the age of 18, and have supported me through every not-so-easy moment during these seven years. Not only are they always ready to support me emotionally, but they're also ready to help me out financially. Most importantly, they instructed me, and set an example for me, on how to be an honest, diligent, responsible person, ready to face all the challenges in life. During these years I study abroad, they've been with the inconvenience of my not being around without complaint. I wish I could treasure every of their remaining days and repay a humble portion of what they've done for me. My current girlfriend, Wen "Lepus" Guan, helped reestablish my confidence, motivation and love of life during these months, encouraged me to fight for our future. During the writing of this thesis, she suffered through, with unparalleled tolerance, the excruciating agony brought about by the lasting, high wavenumber random fluctuation in my temper, and encouraged me to finish this thesis in a timely manner. I also want to thank my ex-fiancee, Chenchen Zhou, who went through those days when I started my life in Canada, bringing me joy and support during our years together.

Finally, I'd love to thank my young friends. Physicists, including Junjie Rao from Sun Yat-sen University, Wei Guo from Zhejiang University, Lichen Liang from University of Victoria, Xuefei Yan from Duke University, Danbo "D-boy" Zhang from Renmin University of China, and Zhuli He from Chinese University of Hongkong, plus one biologist: Yu Gao from Chinese Academy of Science, are some of the most brilliant youngsters I've ever seen. Discussions with them on science and other issues have been fruitful as well as joyful.

This is dedicated to my beloved Lepus and my parents

whose constant support of my cause and concern of my welfare

have allowed me to accomplish everything presented in this thesis

Table of Contents

List of Figures

Chapter 1

Introduction

1.1 Motivation: Electrostatic Force in Molecular Biological Physics

Biological physics, an interdisciplinary science that connects the core of the two largest categories of science—physical science and life science, has been studied for decades and is attracting ever-growing interest. Of all the branches of biological physics, molecular biological physics is most "physical," because it inherited the reductionism of physics, studying life by studying its smallest functional components: biomolecules, nucleic acids, proteins, lipids, polysaccharides, etc. Molecular biological physicists believe that the function of biomolecules is determined by, hence can be explained by, their structure. They attempt to unveil how "the most elaborate machine in the universe" works by establishing such a "structure-function relationship".

Biomolecules such as DNA and protein are macromolecules made up with numerous smaller components. Their size leads to flexibility, allowing components far apart along the molecule to get near and interact with each other. Therefore, the structures they form are not only determined by their chemical structures, but also by the intermolecular force among the components and between the molecule and the environment. Furthermore, smaller biomolecules such as phospholipids self-assemble into structures, which is governed by the intermolecular forces. Therefore, the interactions within biomolecules, among biomolecules and between biomolecules and its surrounding play a central role in molecular biological physics. Besides covalent bond, which is studied in biochemistry instead, the interactions most frequently encountered in molecular biological physics are:

- van der Waals interaction
- electrostatic interaction
- hydrophobic interaction
- H (hydrogen)-bond

Needless to say, entropy is an equally important driving force. Indeed, most of the phenomena studied in molecular biological physics are the results of balances between energy and entropy.

In this thesis, we will focus on one type of interaction among these: electrostatic interaction; and focus on one type of biomolecule: lipids, including phospholipids found in all cellular lives and lipopolysaccharide found almost exclusively in Gram-negative bacteria. We will study: how this type of interaction will contribute to the property of this family of biomolecules.

1.2 Biology: Membrane, Bacteria and AMP

1.2.1 Lipid bilayer as bio-membrane

A biological membrane is a crucial component of many cellular and subcellular processes. Its primary function is compartmentalizing. For example, the plasma membrane distinguishes between the interior and exterior of a cell. It also serves as a substrate for proteins to embed on. For example, ATP Synthase in the mitochondrion and ribosomes on rough endoplasmic reticulum are both embedded on the biological membrane of respective organelles. Therefore, the study of biological membranes becomes an essential step toward understanding many biological processes.

The primary constituents of biological membranes are various lipids, especially phospholipids, not to mention membrane proteins. Over one half of the mass of cell membranes is contributed by lipids. A typical phospholipid molecule (see Fig. 1.1) is an ester of glycerol. Of the 3 carbon atoms of glycerol, two of them are connected with hydrocarbon chains, each of which usually contains 10 to 20 carbon atoms. The third is connected to a phosphate group. The phosphate group usually connects to a small molecule (such as Choline). The hydrocarbon chains are hydrophobic, i.e., they avoids water, while the phosphate group ionizes in water and thus becomes hydrophilic, i.e., it tends to be in contact with water. In most cases, the small molecule attached to the phosphate group

also ionize in water and become hydrophilic. Hence, the phospholipid is an amphiphilic molecule, made up of a hydrophilic "headgroup" and two hydrophobic "tails." When these molecules are present in water at a sufficiently high concentration, they'll self-assemble into a bilayer (see Fig. 1.2), in which tails face inward, avoiding water, while heads face outward, in contact with water. Some other possible constituents of biological membranes, such as lipopolysaccharide (LPS) that would play a central role in the later part of this thesis, may look quite different from typical phospholipids, but they're still amphiphilic, with hydrocarbon chains and phosphate groups.

Electrostatic property of phospholipids

The phosphate group is acidic, deprotonates in water and becomes anionic (carries a negative charge). The pK_a value of the phosphate group is fairly small, so it's safe to say that all phosphate groups immersed in water will dissociate. However, the rest of the lipid head may also carry groups that ionize in water. As a result, a phospholipids may either be zwitterionic (carries both positive and negative charges and neutral overall) or anionic. For example, in Fig. 1.1, phosphatidylcholine (PC) and phosphatidylethanolamine (PE) are zwitterionic while phosphatidylserine (PS) is anionic.

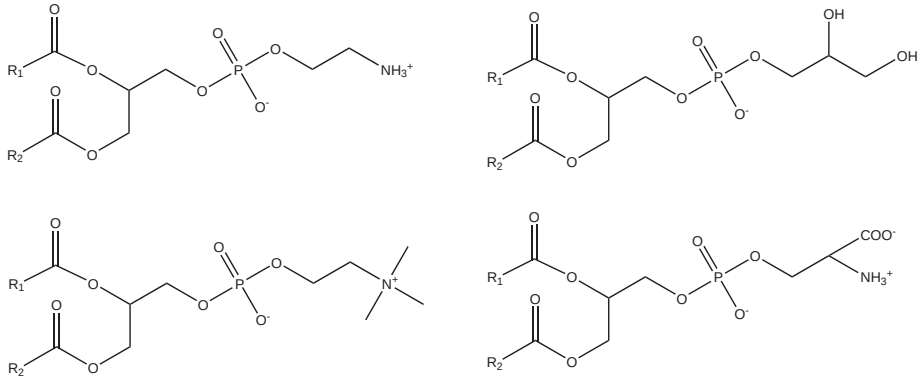

Figure 1.1: Typical phospholipid: PC (Phosphatidylcholine), PG (phosphatidylglycerol), PE (Phosphatidylethanolamine) and PS (Phosphatidylserine)

1.2.2 Bacteria

Bacteria is one of the three domains of cellular life forms along with archaea and eucaryotes [1] [2]. They are prokaryotic (without a cell nucleus) microorganisms (typically $\sim \mu m$

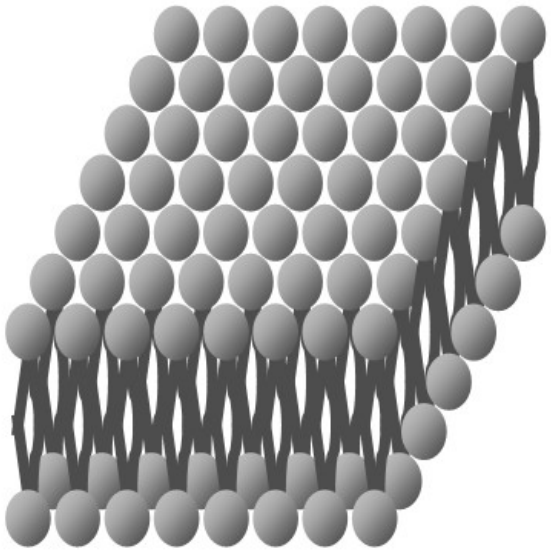

Figure 1.2: A lipid bilayer formed from self-assembly, where the hydrocarbon tails are shielded from the surrounding water molecules.

in dimension) that mostly assume shapes such as spheres (*cocci*), rods (*bacilli*) or spiral (*spirilla* and *spirochetes*). Some bacteria are our allies, while some are our nemesis. Love them or hate them, embrace them or fear them, one fact we have to live with is that we can't avoid them. In fact, human flora, the bacteria that live in peace on the surface of our body, contains ten times as many cells as all the cells of our body [3]. Therefore, bacteria have been studied by the human race for centuries, and will continue to be studied for the centuries to come.

Bacteriology is so tremendous a field that any attempt of comprehensive discussion would take a dozen pages. Therefore, we focus on the aspects that are relevant to our study: their membranes and the electrostatic properties of these membranes.

The lipid composition of several typical bacteria can be found in Ref. [4]. As can be seen, eukaryotic cell membranes are almost electrically neutral looking from outside, while the outer leaflet of bacterial cell membranes carries a large fraction of charged lipids, as detailed in the next section.

For eukaryote cells, one lipid bilayer is all that separates the inside of the cell from the outside. For bacteria, however, there is a cell wall lying outside the plasma membrane. The basic structures and compositions of the cell walls fall into two types, which put all the bacteria into two categories: Gram positive (G+) and Gram-negative (G-). The most

fundamental difference between the two categories lies in their cell walls. As can be seen in Fig. 1.3, the cell wall of G+ bacteria largely consists of peptidoglycan, a copolymer between amino acids and monosaccharides, which accounts for about 90% of the dry weight of Gram positive bacteria. For G- bacteria, there is another lipid bilayer lying outside the plasmic, or "inner", membrane, referred to as the "outer membrane". There is a small amount of peptidoglycan (∼10% of the dry weight of the cell) lying between the two membranes (periplasmic space). While the inner leaflet (lipid monolayer) of the outer membranes consist of ordinary phospholipid, the outer leaflet that faces the environment contains a special type of lipid called lipopolysaccharide(LPS). It's been found that all of the lipid content of this leaflet is LPS [5].

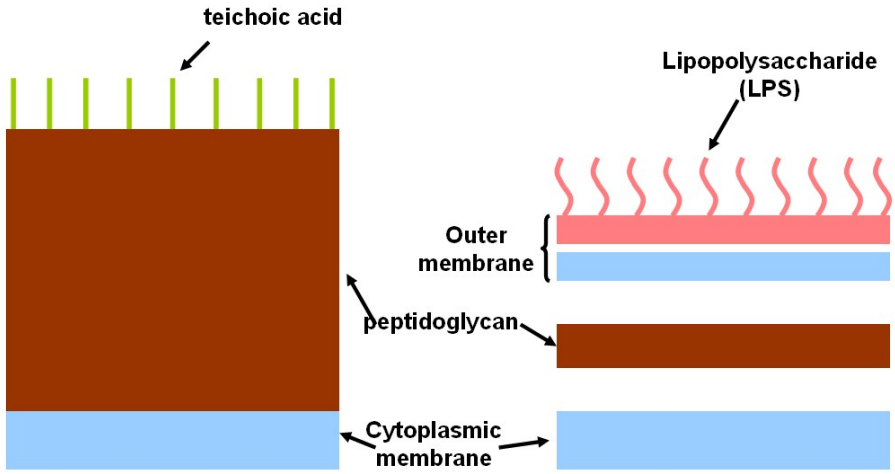

Figure 1.3: The cell wall of Gram positive and Gram negative bacteria (the general layout is inspired by Ref. [6]). If the former has a thick layer of peptidoglycan, the latter has two membranes.

1.2.3 Anti-microbial peptides

A great variety of multicellular, eukaryote organisms are known to be able to produce short (∼ 20 amino acids) peptide molecules as part of their self-defense mechanism, which can selectively destroy foreign prokaryote microbes while posing little or no threat to its own cells. Many of such molecules, known as antimicrobial peptides (AMP), are promising antimicrobial agents that could be used in the treatment of bacterial infection in human. The greatest superiority of AMP over conventional antibiotics is their general mechanism of action: their selective bacterial membrane perturbation. As a result, they will not

easily induce bacterial resistance and show a broad spectrum of activity against pathogenic bacteria [7, 8]. Therefore, various types of AMP or modified AMP are of therapeutic value [8]

After more than two decades of worldwide research, many AMPs have been isolated and sequenced; their structures have been determined and their mechanisms of action have been clarified. It has long been experimentally confirmed that the mechanism of most AMPs does *not* involve interaction with proteins [9] [10]. Typical AMP molecules, such as magainin II [11] [12] [13], are amphiphilic; the polar region is overall cationic (basic) due to the presence of Lys and Arg residues [7]. A fundamental difference between the outer membrane of prokaryotic and eukaryotic cells is that the former contains more anionic lipid while the latter only contains a little that mostly resides on its inner leaflet. This makes AMP molecules much easier to bind on the bacteria cells. This explains their selectivity [8] [14] [15]. Upon binding, AMP molecules may undergo a conformational change, from the unstructured form in the bulk to a specific structure that the polar residues are arranged at one side of the molecule while the non-polar ones on the other, typically including α-helical, β-sheet, loop or extended [16]. Thus it can fit into the amphiphilic lipid bilayer and bind to it. When the density of AMP molecules aggregating on the membrane reaches a certain level, they form toroidal or barrel-stave pores [17] on the outer membrane, compromising its integrity, thus leading to bacterial killing. They can also diffuse across the outer membrane to aim at intracellular targets [8]. The simple picture above, known as Shai-Matsuzaki-Huang (SMH) model [7] [12] [18], forms the basis for theoretical research of the recent years.

However, there is a cell wall lying outside each bacterium, which the AMPs have to cope with before it has the chance to interact with the (inner) membrane. Will the cell wall hinder the electrostatic binding of AMPs onto the inner membrane? The cell walls of both G+ and G- bacteria happen to be negatively charged. The outer surface of the peptidoglycan wall of G+ bacteria contains teichoic acids. As an acid, it becomes anionic after deprotonation. As for G- bacteria, LPS is more highly charged than phospholipid. Hence, electrostatic binding, and consequential permeation, of the cell wall are expected to occur. In this thesis, however, we'll focus only on G- bacteria and their LPS leaflets.

1.2.4 Lipopolysaccharide

Considering the role of LPS in this thesis, it's beneficial to take a closer look at this family of molecules. LPS is a class of large bio-molecules. An LPS molecule consists of 3 parts [19]: lipid A, core oligosaccharide and O-antigen. Lipid A usually consists of a phosphorylated glucosamine disaccharide with multiple (usually 6) hydrocarbon chains attached. The

hydrocarbon chains form the hydrophobic part that is responsible for the integrity of the outer membrane. Core oligosaccharide is connected to one of the glucosamine monomers on lipid A and consists of a variety of sugars, among which are heptose (Hep) and 3-deoxy-D-mannooctulosonic Acid (KDO). O-antigen is a linear glycan polymer (polysaccharide). Fig. 1.4 is a schematic illustration of the structure. When LPS is released from the outer membrane in the hunan body, strong pathophysiological effects such as sepsis, septic shock, and multiorgan failure can be induced. Therefore, LPS are also known as endotoxins.

The major function of LPS is a permeation barrier. An LPS leaflet far more effectively prevents the diffusion of most small molecules than a phospholipid leaflet. If the outer membrane is patched with phospholipid, lipophilic substance can penetrate much faster [5] [20] [21].

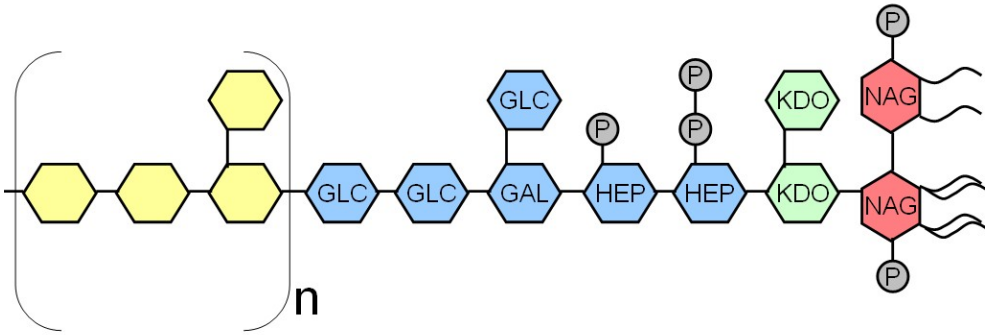

Figure 1.4: Schematic drawling of the structure of LPS (inspired by drawings of similar molecules in Ref. [19] and Ref. [22]). Each consists of three parts: lipid A, core oligosaccharide, and O-antigen

The structure and phase behavior of LPS layer as in G- bacteria has been studied experimentally, mainly by neutron diffraction [24]. Both experiments (on Lipid A from E. coli) and simulations (by energy minimization) indicates that the 6 hydrocarbon chains are located in the nodes of a hexagonal lattice [25]. More details regarding the biochemical and biophysical property of LPS can be found in the following excellent review articles: Refs. [26], [27] and [28].

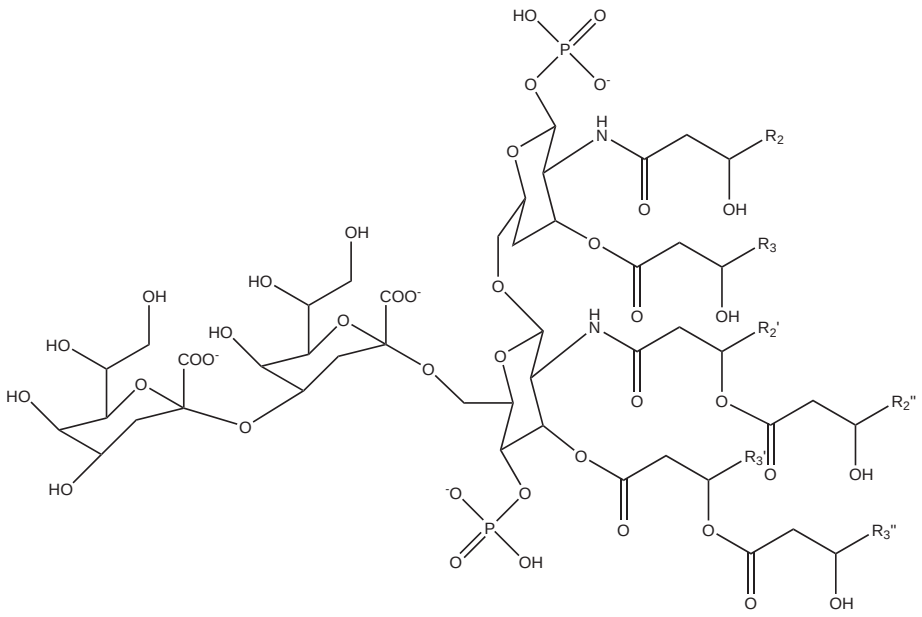

Figure 1.5: Chemical structure of Lipid A (inspired by a similar drawing in Ref. [23]). Note that each has a few negative charges.

1.3 Physics: Self-assembly and Strong Electrolyte

1.3.1 Self-assembly and packing shapes[1]

The formation of a lipid bilayer in aqueous solution is one example of self-assembly, i.e., molecules ("monomers") spontaneously organize themselves into certain structures to minimize the total free energy. Many amphiphilic molecules exhibit such ability in water because assembling helps to keep their hydrophobic parts "dry". Obviously, restricting molecules in an aggregation instead of in the aqueous solution ("bulk") limits its freedom, and has an entropic penalty, but this can be compensated by the benefit in energy. As more molecules aggregates, it eventually comes to a point when the benefit for a molecule to enter aggregation exactly negates the penalty, and the system equilibrates. Hence, it's all about minimizing the free energy by moving particles around, or equivalently, balancing chemical potentials. This is also the main theme in numerous soft matter and biophysics problems.

One of the most fundamental questions we usually ask is: "How does the concentration

[1]This part is largely based on Israelachvili's book [29], but I've also learned a lot from Nelson's book [30].

of monomers determine the concentration of aggregates of various sizes?" This interesting question has been discussed in [29] and [30] in detail. However, this question itself is not the focus of this thesis. Instead, we're going to discuss other aspects:"What are the possible structures amphiphilic molecules can assume?" and "What factors determine the preferred structure the monomers will choose to form?"

Packing Shape

Intuitively speaking, "packing" means stacking many units tightly in the same alignment. For example, grasping a lot of cones in the hand (by the tip) is an example of packing, while lipids aggregate into bilayer is another. Obviously, the shape of the object formed by packing is determined by the shape of each unit that participates in packing (or "packing shape"). A bunch of cones grasped by the tip look like part of a sphere, while a lipid bilayer can form because many lipids found in biological system have cylindrical "shape" (This "shape" may not be identical to what it "appears". It's rather determined by the intermolecular interactions between lipids). If the lipid packing shape deviates much from cylinder, the preferred structure is no longer a bilayer. Furthermore, if the lipid packing shape is somehow changed, the lipid aggregate can adopt a new structure. Hence, the structural preference and phase behavior of a lipid aggregate is largely determined by the packing shapes of its constituting lipids [31]. Typical structures and the corresponding packing shapes are in Fig. 1.6

For typical lipids present in biological system, such as those in Fig. 1.1, conic packing shape is quite unlikely. Their packing shape is usually cylindrical or inverted truncated cone, i.e., they form a bilayer or an inverted hexagonal structure.

However, in a realistic biological membrane, there are almost always more than one type of lipid present. In this case, the overall structure of the membrane will depend on the property of each lipid species and the composition of the entire membrane. Of course, the lipids that prefer structures other than a bilayer will not be in relaxed state, and they'll produce mechanical tension, tending to destabilize the membrane. It's long been experimentally confirmed that PC, a lipid with cylindrical packing shape, stabilizes the bilayer structure, while cholesterol, a lipid with a fairly extreme inverted cone shape, destabilizes it [32]. The membrane may not be a homogeneous mixture of lipids, and demixing is quite common. Lipids of the same species form a domain to lower local energy at the price of entropy. For example, it's been observed that cholesterol accumulates in high curvature region [33].

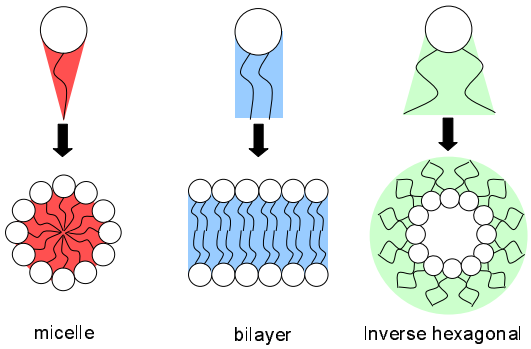

Figure 1.6: Structures and Packing Shapes of lipid aggregates. If double-tailed lipids prefer to form a bilayer, single-tailed ones tend to form micelles. Under the right conditions, inverted hexagonal (H_{II}) structure can form.

Influence by Electrostatic Effect

The structural preferences of lipids can be modulated by a wide variety of physiologically relevant factors such as hydrocarbon unsaturation, temperature, headgroup size, etc, to name a few [34]. Besides these, since the charges of anionic lipids are located at their headgroups, the electrostatic forces among the polar heads of these lipids can change their packing shape. Actually, when physiological functionality calls for changes in the packing shapes of lipids, electrostatics is a most frequently employed means, for at least two reasons:

1. Electrostatic interaction is controlled by tunnable parameters. In later chapters, I'll shown that the electrostatic free energy of a lipid aggregation depends on the fraction of anionic lipids, and the concentration of ions in the surrounding aqueous solution. The former can be changed by changing the pH value so that some lipids don't ionize. Furthermore, even a tiny amount of multivalent cations can drastically alter the electrostatic force (typically leads to an attracting one) between lipids by bridging between them (see Fig. 1.7) [35] [36]. All of these "environmental" parameters are relatively easy to adjust.

2. Other factors that determine the packing shape are harder to change. These usually

involves the inherent properties of lipids, such as chemical structure, and cannot be freely adjusted.

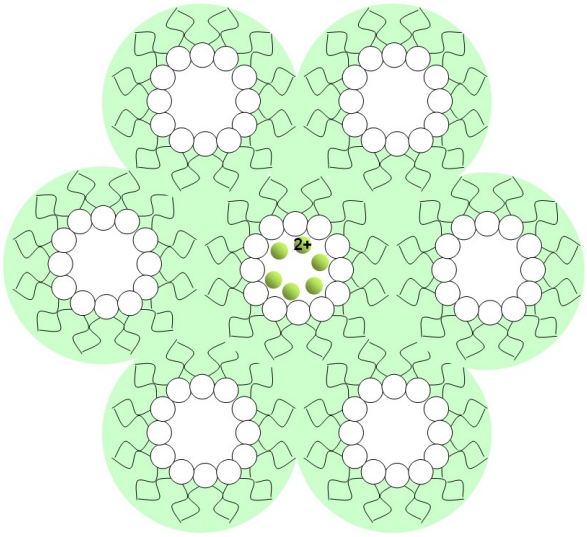

Figure 1.7: Inverse Hexagonal (H_{II}) Structure Induced by Divalent Ion (inspired by a similar drawing in Ref. [36]). The presence of divalent cations can stabilize H_{II} phases of lipids, which would otherwise form lamellar phases.

It has long been found that electrostatic interaction significantly affects the structure and phase behavior of lipid aggregations. By late 1960s, it had been observed that:

1. Bilayers composed of phosphatidylserine (PS) are unstable under conditions of asymmetric distribution of Ca^{2+} or H^{+} [37].

2. Electrostatic interaction affects ordered-fluid phase transition, divalent ions induce a fluid to ordered phase transition while monovalent cations make the membrane more fluid-like [38].

3. For PS, the melting temperature increases by more than 50 K when 1 mM of Ca^{2+} is added to bridge the negative charges [39].

4. PA (phosphatidic acid) forms a bilayer in neutral to basic pH, but forms H2 structure in acidic environment or when Calcium salt is added. CL (cardiolipin) also goes from bilayer to H2 when Ca salt is added [34].

Significance in Physiology

Although it's been known for decades that phospholipids can form non-bilayer structures, people tend to underestimate the significance of lipid polymorphism in a biological context until late 1970s [40]. A realistic biological membrane is usually made up of multiple types of lipids, and well over a hundred different molecular species of lipids have been found in the erythrocyte membrane. The best way to explain such diversity is: they have a wide range of polymorphic behavior which is called for by cellular lives [34]. The major species, such as PC, have roughly cylindrical packing shape, so that a membrane mainly consisting of them stays in a bilayer structure. However, the preferred structure of some lipids is not a bilayer, and integrating them into a bilayer will produce a *packing stress*. An appreciable proportion (30% or more) of membrane lipids either adopt non-bilayer structure in isolation or induce such structure in mixed lipid systems[34]. Such stress can influence the functioning of membrane-embedded protein. There are numerous examples for this. To name a few:

1. Cell fusion and fission. These phenomena are crucial to all the cellular lives. It's difficult to rationalize these events if the structure of cell membranes is inviolate. In other words, at some point in these events, part of the lipids must depart from bilayer structure [40]. It's long been found that Calcium ions, which strongly interact with anionic lipids, play a vital role in these events (see Ref. [39] and references therein).

2. Interaction of proteins and peptides with membranes. On one hand, proteins and peptides have their impact on the structure of the membrane they come into touch. For example, inclusion of protein into a membrane induces deformation [41], and peptides (such as AMPs) are also observed to modulate membrane curvature [42] [43]. For example, "mechano-sensitive channels" can be opened or closed by changing the packing stress of the membrane around it, and it's been experimentally found that some of them can be controlled by multivalent ions [44]. The insulin receptor, a transmembrane protein, is also modulated by the polymorphic property of the membrane [45]. The effect of AMPs is also influenced by the tension and stability of the membrane [46].

3. Drug delivery. In clinical science and pharmacy, people want to deliver drugs to specific sites where they're supposed to exert their effect, such as a cancerous tissue, to maximize the therapeutic effect while minimizing side effects. One strategy is to enclose the drug into liposomes, vesicles made of lipid bilayer. Some of the lipids in the liposome are anionic/cationic. In normal tissue where the pH of body fluid is neutral to slightly basic, the electrostatic force won't compromise the stability of

the liposomes. Once the liposome reaches a cancerous tissue, where the body fluid is more acidic, the ionization of these lipids will change, and the resulting change in electrostatic forces will destabilize the liposome, helping release the drug within. This has been discussed in several literatures [47] [48].

1.3.2 Poisson-Boltzmann and beyond

A major challenge in the study of electrostatic interactions in biological systems, such as bio-membranes, is that they're usually immersed in a body fluid, which is water (aqueous phase) that contains a variety of ions, mostly monovalent (such as proton, Na^+, K^+, OH^-, Cl^-) or divalent (such as Mg^{2+} and Ca^{2+}). For a bio-membrane, the charged lipids can move in 2D, while the ions in the body fluid around it can move in 3D. Hence, we're looking at an electrostatic problem that involves mobile charges. Naturally, the charges will distribute themselves in such a way to minimize the free energy. How will this affect the effective force law between the charged lipids?

In an introductory-level electromagnetic course, systems with mobile charges are also encountered, such as the outer surface of a conductor. However, such systems implicitly adopts the "zero temperature" approximation, so the charge distribution is just about minimizing the electrostatic energy of the system. If we apply this to our "membrane + body fluid" system, the (negatively) charged lipids will form a regular, hexagonal distribution to keep a distance from each other, the cations such as Na^+ will collapse onto the membrane, while anions get as far away from the membrane as possible. However, in biological system where the temperature is typically ≈ 300K, this approximation might be invalid. To check this, we define the *Bjerrum length*, l_b as below:

$$\frac{e^2}{\varepsilon l_b} = k_B T \tag{1.1}$$

$$l_b = \frac{e^2}{\varepsilon k_B T} \tag{1.2}$$

That is, when two elementary charges in a medium of dielectric constant ε are separated by l_b, the electrostatic energy between them will be the thermal energy $k_B T$. The Bjerrum length in water ($\varepsilon_w = 80$) at $T = 300K$ is roughly 7Å, which is of the same order of magnitude as the distance between charges in such systems. Besides, charged lipids and ions usually carries a few elementary charges. Hence, in our system, the thermal energy is comparable to the typical electrostatic energy.

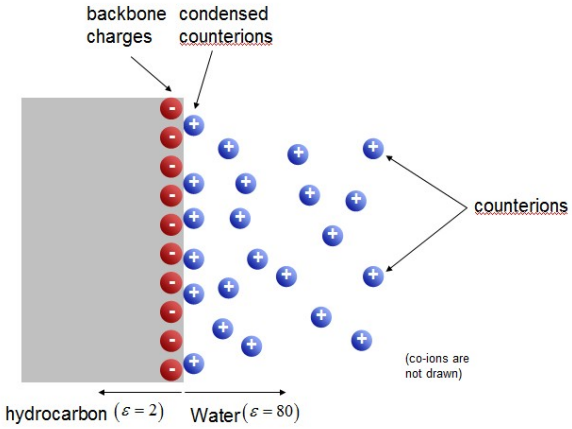

Figure 1.8: Electrostatic Interaction in Electrolyte Solution

Therefore, equilibrium in such system must reflect the balance between minimization of energy and maximization of entropy. While the former pulls the cations towards the membrane surface and push the anions away, the latter prefers the ions to be homogeneously distributed. Hence, we expect the cations to be closer, but not to "collapse," to the membrane. The natural question is then how to quantitatively describe its equilibrium state, namely, the spatial distribution of charges and electrical potential?

Derivation of Poisson-Boltzmann equation[2]

We attempt to find a differential equation for the equilibrium distribution of ions in a medium, typically water (the lipid charges will enter as boundary condition). For simplicity, we assume there are only two types of ions present, a cation and an anion with valence z_+ and z_- respectively. Hence, we seek to determine the following three interrelated quantities simultaneously: the electric potential $\psi(\vec{r})$ as well as the distributions of cations $n^+(\vec{r})$ and of anions $n^-(\vec{r})$. We set infinitely faraway to have $\psi = 0$, where $n^+ = n_0^+$ and $n^- = n_0^-$.

At least, we know the following statements are self-evident:

1. Coulomb's Law always holds, i.e., the electrical potential can be described by *Poisson* equation:

[2]This section is largely written by myself based on what I've learned and figured out myself, instead of copying from any of the literatures. Hence it's not easy to put a citation for each part. This is loosely based on [49], but I've also learned from Ref. [29], [50], [51], [52], [53], and many other sources.

$$\nabla^2\psi\left(\vec{r}\right) = -\frac{4\pi}{\varepsilon_w}\rho\left(\vec{r}\right) = \frac{4\pi}{\varepsilon_w}\left(z_- n^-\left(\vec{r}\right) + z_+ n^+\left(\vec{r}\right)\right) \tag{1.3}$$

2. The ions will obey the *Boltzmann* distribution, i.e., its probability of having a higher electrostatic energy is exponentially lower:

$$n^-\left(\vec{r}\right) = n_0^- \cdot \exp\left(-ez_+\psi\left(\vec{r}\right)/k_BT\right) \tag{1.4}$$
$$n^+\left(\vec{r}\right) = n_0^+ \cdot \exp\left(-ez_+\psi\left(\vec{r}\right)/k_BT\right) \tag{1.5}$$

Combining these two facts, we arrive at a single equation of ψ:

$$\nabla^2\psi\left(\vec{r}\right) = -\frac{4\pi}{\varepsilon_w}\left[z_- n_0^- \cdot \exp\left(-ez_+\psi\left(\vec{r}\right)/k_BT\right) + n_0^- \cdot \exp\left(-ez_+\psi\left(\vec{r}\right)/k_BT\right)\right] \tag{1.6}$$

Naturally, it's referred to as *Poisson-Boltzmann (PB) equation*. It is a second-order, inhomogeneous, non-linear partial differential equation, which is generally hard to solve analytically. Poisson-Boltzmann equation is often applied to two distinct cases with and without added (1:1) electrolyte (e.g. NaCl). A very good discussion on the first case can be found in Ref. [49]. I'll focus on the second case.

PB equation for electrolyte solution and Debye-Hückel equation

Under physiological conditions, the aqueous phase in contact with the membrane always contains some ions. In the simplest case, it contains a 1-1 electrolyte only such as NaCl at a concentration of n_0, so it contains an equal amount of Na^+ and Cl^-. To further simplify the problem, we assume the aqueous is sufficiently large and acts like a reservoir of Na^+ and Cl^-, so $n_0^{\mathrm{Na}} = n_0^{\mathrm{Cl}} = n_0$. Also the concentration of counterions released from the membrane is negligible comparing to n_0, so we can assume there are only Na^+ and Cl^- present in the aqueous phase. In this case, we usually call the ions with the opposite charge with respect to the charged surface (e.g. Na^+) "counterions," while the other ion as "co-ions". Now, Eq. 1.6 becomes:

$$\nabla^2\psi\left(\vec{r}\right) = \frac{8\pi e n_0}{\varepsilon_w}\sinh\left(\frac{e\psi\left(\vec{r}\right)}{k_BT}\right) \tag{1.7}$$

These salt ions will shield surface charges and as a result, ψ decays faster in the presence of added salt ions.

Now we define a quantity κ as below:

$$\kappa^2 = \frac{8\pi e^2 n_0}{\varepsilon_w k_B T} \tag{1.8}$$

With the dimensionless reduced potential $\Psi = \frac{e\psi}{k_B T}$, Eq. 1.7 becomes:

$$\nabla^2 \Psi(\vec{r}) = \kappa^2 \sinh(\Psi(\vec{r})) \tag{1.9}$$

Dimension analysis shows that κ has the dimension of inverse length, so κ^{-1} is called *Debye length*. This length is inversely proportional to n_0, which means a more dilute salt solution has a larger Debye length.

An empirical formula for its calculation is, for aqueous solution at $T = 300K$,

$$\kappa^{-1} = \frac{3.081}{\sqrt{n_0}} \tag{1.10}$$

where κ^{-1} and n_0 are in the unit of Å and mol/L, respectively. In a physiological environment where a typical $n_0 = 100\, mM$, Debye length is roughly 10 Å.

When several types of salts dissolve in water, Eq. 1.9 still holds, with the Debye length defined as:

$$\kappa^2 = \frac{8\pi e^2 \frac{1}{2} \sum_{j=1}^{N} n_{j0} Z_j^2}{\varepsilon_w k_B T} \tag{1.11}$$

where n_{j0} is the concentration of the jth species of charged particle (cations and anions are counted as different species) and Z_j is the valence of the jth species of charged particle. For example, for the typical case considered throughout this thesis: a solution of a 1-1 salt at the concentration of n_1 and a 2-1 salt (such as $MgCl_2$) at the concentration of n_2, the Debye length would be: $\kappa^{-1} = \frac{3.081}{\sqrt{n_1 + 3n_2}}$.

Eq. 1.9 is still non-linear and extremely hard to solve analytically even for simple geometries (e.g. cylindrical and spherical surface). As we can see, when Ψ is small, $\sinh \Psi \approx \Psi$. Hence Eq. 1.9 can be approximated as:

$$\nabla^2 \Psi(\vec{r}) = \kappa^2 \Psi(\vec{r}) \tag{1.12}$$

Eq. 1.12 is called linearized Poisson-Boltzmann equation or *Debye-Hückel equation*. In Appendix A, we present the solutions of Eq. 1.9 and Eq. 1.12 in various cases.

Beyond Poisson-Boltzmann theory: fluctuation and correlation

Despite the complexity of and difficulty in solving the Poisson-Boltzmann equation, it has limitations, since it is based on a mean-field picture. That is, the actual charge distributions are replaced by their thermal averages and stay at such averages over time. Therefore, it fails to capture any charge-charge correlation, which can be important in some cases, especially in the presence of multivalent counterions.

Fig. 1.9 is to illustrate how a mean-field theory can break down. In this figure, some positive and negative point charges, carrying equal but opposite charges, are discretely organized on a square lattice (the left panel); there will be the same numbers of positive and negative charges if the lattice is infinitely large. That is, the average charge density on the lattice plane is zero. A mean-field approximation is equivalent to replacing a (local) charge distribution by the (local) average charge, which is zero in the case shown in Fig. 1.9. However, if we pick one charge and sum up the Coulomb force exerted by all other charges, we'd see it's not zero, but some value that is the same for each charge (positive or negative)[3]. Therefore, the electrostatic interaction energy of the plane is none-zero, and mean-field theory gives a qualitatively wrong prediction.

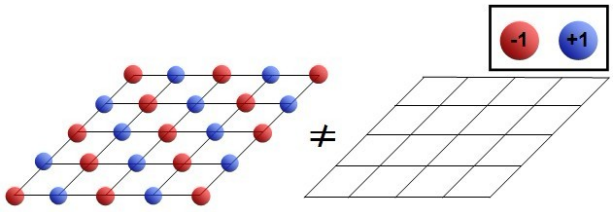

$$\bar{\sigma} = 0, E_{mean-field} = 0$$

$$E_{site} = \frac{l_b}{a}\left(-4 + \frac{4}{\sqrt{2}} - \frac{8}{\sqrt{5}} + \frac{4}{2} + \frac{4}{\sqrt{2}} + \cdots\right)$$

Figure 1.9: Illustration of the limitation of a mean-field approach. On the left, charge discreteness and charge non-uniformity are well preserved. All this feature will be lost if the charges are smeared out, as in a mean-field approach (left panel).

Note that the overall neutral lattice on the left has lower energy. If we don't restrict the charges on the lattice sites, but allow them to move freely, positive and negative charges will immediately start to pair with each other, and the surface will becomes more electrically neutral locally than indicated in the left panel. However, any physical system

[3]This configuration plays an important role later in this thesis, and the calculation is detailed in Appendix. D

doesn't always stay in the lowest free energy state, and fluctuations occur. Even if we do not restrict the charges on the lattice, and the surface is *on average* neutral at every point, some charges may still fluctuate away from the thermodynamically most favorable position. Local non-zero charge densities rise and fall, making the energy of the surface, averaged over time, non-zero. For instance, Casimir effect, in which the fluctuation of a vacuum (production and annihilation of virtual photon pairs) leads to a non-zero force between metal plates. In electrostatic systems, dipoles can be "produced" (ionized) and "annihilated" (neutralize) in a conceptually similar way.

Just like in Casimir effect, charge fluctuation and correlation usually create attractive forces. Intuitively speaking, by varying charge distributions while keeping the average charge density constant, we're making some regions more "positive" and some other regions more "negative." This induces attractive forces. This also explains why multivalent ions in soft condensed matter systems, such as those we studied in this thesis, often lead to attractive forces. A divalent cation, for example, is different from two monovalent ones in that the two electrical charges in the former always stick together, or, less "smeared out". If we neutralize the former with two monovalent anions, these anions will also tend to be spatially closer. A mean-field theory such as Poisson-Boltzmann theory cannot account for such subtleties, and these effects can only be appreciated by accounting for the electrostatic correlation between the charges.

Much effort has been put into quantitatively studying the effects of charge correlations and fluctuations on charged objects immersed in an electrolyte solution, most of which are based on a continuum model, such as the attraction between parallel membranes [54] [55].

In parallel with such an effort to account for charge correlations and fluctuations, an attempt to go beyond Poisson-Boltzmann equation has been made. For example, Borukhov [56] [57] introduced the finite size of ions into the classical Poisson-Boltzmann equation. However, since these are not used in our work, we're not going further on these topics.

1.4 Overview of the Thesis

Following the general background in chapter 1, we first present two similar but closely-related problems and our strategies for solving them in chapter 2 and 3; from these studies, we draw several conclusions, which are relevant in a variety of contexts: nano-biotechnologies and the microbe-killing activity of antimicrobial peptides. We conclude this thesis with some possible directions to work in.

In chapter 2, we attempt to establish a model to study the structural preference of a mixed anionic and zwitterionic phospholipid system. We will adopt from earlier works a molecular model of phospholipids that accounts for the non-electrostatic intermolecular interactions between them. Then, we'll consider a mixed lipid monolayer that can be bent into cylindrical shape, write down the free energy (including non-electrostatic and electrostatic parts) as a function of its geometrical parameters. By minimizing the free energy, we can determine the preferred geometry of the monolayer, which reflects the average packing shapes of the lipids in the monolayer, and thus the structure they tend to form and be stable in. To account for electrostatic interaction more accurately, we adopted the viewpoint of "counterion condensation" and utilized renormalized Debye-Hückel (DH) approach. We then account for fluctuations and charge correlations in the condensed layer, especially when multivalent ions are present.

In chapter 3, we study the action of cationic peptides against an LPS leaflet. We establish a model, in which the charges of LPS are distributed onto a square lattice; ions and peptides are allowed to be bound onto them. Based on the model, we study the binding behavior of the ions and peptides. Our approach is distinct from molecular dynamics [22] [58] and Monte-Carlo [59] simulations, which have been used to tackle similar problems. It allows us to calculate readily various physical quantities such as the (excess) lateral pressure contributed by electrostatic interactions and its impact on the leaflet.

Chapter 2

Effects of Electrostatics on Lipid Membranes

2.1 Introduction

As discussed in the last chapter, electrostatic interactions can effectively modulate the packing property of lipids and thus eventually their phase behavior, important aspects of lipid aggregation. It is thus of great interest to study electrostatic modification of lipids: their packing shape and the structures they form.

Over the last few decades, there has been much effort to unravel the intriguing role of electrostatics in reshaping lipid membranes. For instance, in late 1980s to early 1990s, Winterhalter et al. [60] [61] calculated a a number of membrane parameters such as the bending rigidity and spontaneous curvature of a membrane carrying charge lipids using the Debye-Hückel equation. Later, Chou et al. [62] tackled a similar problem by solving the full Poisson-Boltzmann equation without suppressing dielectric discontinuities. Thus their results are numerically more accurate. However, both Debye-Hückel and Poisson-Boltzmann approaches rely on on mean-field approximation and have limitations. They cannot correctly capture the effect of multivalent ions. Furthermore, in these past studies, a membrane is viewed as a continuous, homogeneous "slab". Thus some molecular details of individual lipids are left out. More recently, Ha [63] [64] studied the effect of multivalent ions on lipid bilayers based on a continuous treatment of charge fluctuation and correlation, Li and Ha [65] attempted to determine c_0 by relating it to Δa_0, lipid headgroup-area changes induced by electrostatic interactions. Lau and Pincus [66] studied the unusual (non-analytical) softening of a membrane at low salt limit due to charge fluctuations, effects

of which diverge logarithmically with membrane dimensions. Finally, Taheri-Araghi and Ha [67] developed an accurate approach by combining a molecular model of individual lipids and the Poisson-Boltzmann equation. However, this method is numerically involved.

Here we aim at developing a more analytically tractable approach to lipid membranes that captures important lipid and charge properties of the membrane as discussed in the work by Taheri-Araghi and Ha [67].

2.2 Theoretical Methods

2.2.1 Deformation of lipid bilayers and monolayers

Helfrich free energy

A homogeneous, relaxed membrane (bilayer or monolayer) adopts certain geometry, characterized by two parameters: area A_0 (optimized area) and curvature c_0 (spontaneous curvature) that are constants throughout the membrane. "Deformation" is defined as deviation from *this* relaxed state. We can expand the free energy *per unit area*, $F(A, c)$ as a power series to the leading terms. For a cylindrically bent bilayer or monolayer:

$$F(A,c) = F(A_0,c_0) + \frac{1}{2}\frac{\partial^2 F}{\partial A^2}(A-A_0)^2 + \frac{1}{2}\frac{\partial^2 F}{\partial c^2}(c-c_0)^2 + \frac{\partial^2 F}{\partial A \partial c}(A-A_0)\cdot(c-c_0) \quad (2.1)$$

Define stretching modulus λ, bending modulus k and stretching-bending coupling coefficient χ as below:

$$\lambda = A_0^2 \cdot \frac{\partial^2 F}{\partial A^2}, \quad k = A_0^2 \cdot \frac{\partial^2 F}{\partial c^2}, \quad \chi = A_0 \cdot \frac{\partial^2 F}{\partial A \partial c} \quad (2.2)$$

And rewrite Eq. 2.1 as:

$$F(A,c) = F(A_0,c_0) + \frac{1}{2}\lambda\left(\frac{A}{A_0}-1\right)^2 + \frac{1}{2}k(c-c_0)^2 + \chi\left(\frac{A}{A_0}-1\right)\cdot(c-c_0) \quad (2.3)$$

The sign of curvature c for a bilayer is defined to be the same as its "outer" monolayer. In this chapter, monolayer bending from the polar heads to the hydrocarbon tails i.e. the

hydrophilic side bulges outward leads to positive c, while bending from the tails to the heads leads to negative c [50] [68]. When "outer" can't be unambiguously defined, special convention might be adopted to define the sign of c of a bilayer.

For geometries other than cylinder, such as sphere, we have two curvatures, c_1 and c_2 at each point, measured on two perpendicular directions. The bending free energy will become:

$$\Delta F_{bending} = \frac{1}{2}k(c_1 + c_2 - c_0)^2 + k_G c_1 c_2 \tag{2.4}$$

The product $c_1 c_2$ is called *Gaussian curvature*, and k_G is the corresponding modulus.

This is the so-called *Helfrich free energy* [69]. It's originally adopted to describe lipid bilayers, but the elastic free energy of a lipid monolayer takes the same form. For convenience, we'll use area *per molecule* a and a_0 in the place of A and A_0 in the equations above to study monolayers.

Neutral surface

To discuss parameters such as a, c and corresponding moduli, we have to specify the surface on which are measured, or their values will be ambiguous. For example, if the chosen surface is closer to the bulging side, we'll arrive at a larger a and a smaller c. For convenience, we want to choose such a surface so that $\chi = 0$. This surface is referred to as the *neutral surface*.

On the neutral surface, stretching and bending decouples. If a membrane (or any slab of fine thickness) is bent (without overall stretch in the tangential direction), some surfaces are compressed while some others are stretched. However, there is one particular surface whose area is unaffected, and this is the neutral surface.

For a symmetrical bilayer, neutral surface always coincides with the middle plane. However, for a lipid monolayer that is inhomogeneous and asymmetrical in the transverse direction, the neutral surface must be located by the criterion $\chi = 0$.

Besides the neutral surface, there are other choices. Another popular choice is the "pivoting surface", on which the torque of all kinds of tensions in the membrane balance with each other [70]. However, in most of the scenarios we study in this chapter, the pivoting surface almost coincides with the neutral surface. Yet another choice is the surface on which $k_G = 0$, which might be different from both above [50].

Spontaneous curvature and preferred structure

The spontaneous curvature, c_0, of a lipid bilayer with two chemically symmetrical monolayers is always 0. However, a monolayer, in its relaxed state, is a "close" packing of the constituent lipids. Hence, its geometry, namely c_0, reflects the packing shape of individual lipids.

From the definition of the sign of c for a monolayer introduced in the previous section, it's easy to see that those lipids with large positive c_0 tend to form micelle, those with small positive c_0 tend to form bilayer, while those with negative c_0 tend to form inverse hexagonal structure, as shown in Fig. 1.6. For example, the spontaneous curvature of pure DOPE and DOPS monolayers are $1/c_0 = -3$ nm and $1/c_0 = 14.4$ nm, respectively [71]. More experimental data on c_0 of pure phospholipid monolayers are summarized in Ref. [68].

2.2.2 Model of a lipid molecule

A Molecular-level Model for Elasticity of Lipid Aggregation

There have been many attempts to model the intermolecular interactions between lipids. In some models, the free energy is written in terms of areas measured from various surfaces, while in some other models the free energy takes a harmonic spring form.

May and Ben-Shaul [72] proposed a molecular-level model that falls in the former category to study the elasticity and preferred structure of lipid aggregates. In this model, they assumed a lipid molecule has the geometry in Fig. 2.1, and argued that the *molecular* free energy can be written as $f = f_h + f_i + f_c$ i.e. each term on the right-hand side accounts for a distinct effect.

1. Steric repulsion between lipid headgroups. The corresponding term $f_h = K/a_h$, is inversely proportional to the headgroup area per lipid i.e. it's repulsive.

2. Surface tension on the water-hydrocarbon interface. The corresponding term $f_i = \gamma \cdot a_i$ is proportional to the interfacial area per lipid i.e. it's attractive.

3. Interaction between hydrocarbon tails. The corresponding term $f_c = \tau \cdot b^2$ is proportional to the square of the tail length. The hydrocarbon chains are largely incompressible i.e. it's volume ν is almost constant. As their end-to-end lengths increases, the cross-section of the hydrocarbon region shrinks. Hence, this term is also repulsive in effect.

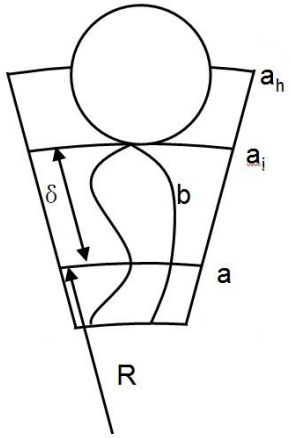

Figure 2.1: Geometry of a lipid molecule (inspired by a similar drawing in Ref. [72]). The area occupied by this lipid a and curvature $c = 1/R$ are measured on a surface at a distance δ from the water-hydrocarbon interface (labeled as a_i in the figure). In practise, this surface is chosen to be the neutral surface by adjusting the value of δ. The meaning of the neutral surface is discussed in section 2.2.1.

Therefore,

$$f = K/a_h + \gamma \cdot a_i + \tau \cdot b^2 \tag{2.5}$$

From the geometry depicted in Fig. 2.1, it can be derived that:

$$a_i = a\,(1 + c\delta) \tag{2.6}$$

$$a_h = a\,[1 + c\,(\delta + l_h)] \tag{2.7}$$

$$b = b_p \left[1 + c\left(\frac{b_p}{2} - \delta\right) + \frac{c^2}{2}\left(b_p^2 - 3b_p\delta + 2\delta^2\right)\right],\ b_p = \frac{\nu}{a} \tag{2.8}$$

in which c is the curvature measured on the surface at a distance δ from the water/hydrocarbon interface. When $c = 0$, each molecule assumes a cylindrical shape. $a_h = a_i = a$, $b = b_p = \nu/a$.

Hence, the molecular free energy is a function of area per lipid on a surface a, curvature measured on the neutral surface c and distance from interface to this surface δ. Determine δ so that this surface coincide the neutral surface, and rewrite f into such form:

$$\frac{f(a,c)}{a_0} = \frac{f(a_0,c_0)}{a_0} + \frac{1}{2}\lambda\left(\frac{a}{a_0}-1\right)^2 + \frac{1}{2}k(c-c_0)^2 \tag{2.9}$$

in which a_0, c_0, λ and k can all be expressed by energetic parameters and geometric parameters, namely: K, γ, τ, δ and l_h.

Choice of parameters

Typical values of these parameters, consistent with experimental measurements [73], are:

1. Interface repulsion $\gamma = 0.12\, k_BT/\text{Å}^2$
2. Repulsion of hydrocarbon tails $\tau = 0.004\, k_BT/\text{Å}^2$
3. Total volume of hydrocarbon tails $\nu_{hc} = 918\ \text{Å}^3$
4. Distance from headgroup repulsion surface to water-hydrocarbon interface $r_h = 1.74$ Å
5. Strength of steric headgroup repulsion $K = 401.38\, k_BT\text{Å}^2$

Similar values are also adopted in Ref. [67] and [72].

2.2.3 Model of electrostatic interaction

Charge renormalization

Although Debye-Hückel equation is a satisfactory approximation to Poisson-Boltzmann equation in many applications, the errors introduced by this approximation become intolerably large for many realistic biophysical problems. The source of such disagreements can be intuitively understood in the following example (inspired by Ref. [52]): since k_BT at $300K$ is just 25 meV, if the surface potential reaches 100 mV, which is not impossible, reduced surface potential becomes $\Psi = 4$, and according to Eq. A.6, the concentration of counterion near the surface, $n(0)$, will be $e^4 \approx 55$ times larger than its concentration faraway from the surface, n_0. For the typical value of $n_0 = 100$ mM, $n(0)$ will be 5.5 molar, greatly exceeding the solubility of table salt in water. In other words, solving Debye-Hückel

equation may yield unreasonably large concentration of counterions. This is expected, because the approximation $\sinh \Psi \approx \Psi$ is no longer a good one for large Ψ. However, as shown by Eq. A.17, Ψ_{PB} behaves similarly to Ψ_{DH} at large z: decaying almost exponentially. Or more precisely, Ψ_{PB} at large distance is very close to a Ψ_{DH} with σ_0 replaced by another surface charge density, σ_{eff}.

An intuitive interpretation of this phenomenon is [1]: there is a layer of counterions trapped or "condensed" in the close vicinity of the charged surface. This layer can be regarded as a 2D charge distribution with a surface charge density σ_1. Observed faraway from the surface, the condensed layer almost overlap with the original charged layer, partially neutralizing it, hence equivalent to a charged surface with an "effective" or "renormalized" charge density, $\sigma_{eff} = \sigma_0 - \sigma_1$. Outside the condensed layer, ψ is small, and the potential is well described by Debye-Hückel equation.

Hence, by considering this phenomenon, known as "counterion condensation", we can make predictions more accurately while still working in the much more analytically tractable Debye-Hückel framework. This is referred to as "renormalized Debye-Hückel approach".

Naturally, we want to start by explicitly relating σ_{eff} to known quantities. To this end, the most straightforward method is to "match" the solution of Poisson-Boltzmann equation to the form of the solution of Debye-Huckel equation (providing an analytical solution is available). For a slab of dielectric constant ε_l immersed in electrolyte solution, in the limit of $\varepsilon_l/\varepsilon_w \kappa d \to 0$, we already have Eq. A.17 and Eq. A.5, which gives [74]:

$$\sigma_{eff} = \frac{\gamma \kappa}{\pi l_b} \tag{2.10}$$

in which γ is defined by Eq. A.15.

Taheri and Ha [75] considered the effect of dielectric discontinuity. In there calculation, $\varepsilon_l/\varepsilon_w \kappa d$ ranges from 0.005 to 0.02, and their result is quite similar to what's given above.

Another perspective: two-state model

Another way of understanding counterion condensation is to introduce the concept of "state": a conterion can either be in the "condensed state" i.e. in the condensed layer, or be in the "bulk state", i.e. in the aqueous bulk outside the condensed layer. When

[1] Assume only 1-1 salt is present in the surrounding solution

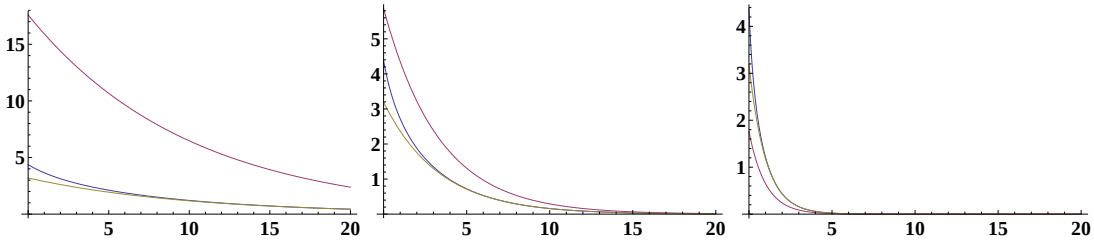

(a) $\kappa = 0.1\,\mathrm{nm}^{-1}$ (b) $\kappa = 0.3\,\mathrm{nm}^{-1}$ (c) $\kappa = 1.0\,\mathrm{nm}^{-1}$

Figure 2.2: Potential predicted by D-H, P-B and renormalized D-H approaches. The *vertical axis* is potential in unit of k_BT/e, the *horizontal axis* is the distance from surface in unit of nm. The purple, blue and yellow curves are potentials predicted by D-H approach, P-B approach and renormalized D-H approach, respectively. $\sigma_0 = 0.2\,\mathrm{nm}^{-2}$, $\varepsilon_l/\varepsilon_w\kappa d \to 0$. Predictions based on renormalized D-H approach is closer to those based on P-B approach at reasonably large distance, especially at low κ.

chemical equilibrium is reached between the two states, the chemical potential of the same type of particles in either state must equate each other [75]:

$$\Delta\mu_i = \mu_i^{bulk} - \mu_i^{cond} = 4\pi Z_i \sigma_{eff} \kappa^{-1} l_B \frac{\varepsilon_l + \varepsilon_w \kappa d}{2\varepsilon_l + \varepsilon_w \kappa d} + \ln\left(\frac{n_i l_c^i}{\sigma_i}\right) = 0 \tag{2.11}$$

in which i labels the types of ions, with valence Z_i respectively.

The only ambiguity here is the thickness of the condensed layer, l_c^i. In Ref. [75], it's given by:

$$l_c \approx \left(\frac{\kappa^{-2}}{\lambda}\right)\left(\frac{4}{\exp(4)}\right) \tag{2.12}$$

so as to correspond with the result from matching method. However, l_c diverges as $\kappa \to 0$, contradicting the concept of "condensation". This is because in the small κ limit, Eq. 1.9 and Eq. 1.12 no longer hold. The counterions released from the ionization that produces surface charges can't be neglected any longer, and the system approaches "no electrolyte added" scenario, where most counterions are in the proximity ($\sim \lambda$, which is but a few Angstroms for reasonable σ_0) of the charged surface.

As can be seen in Fig. 2.3:

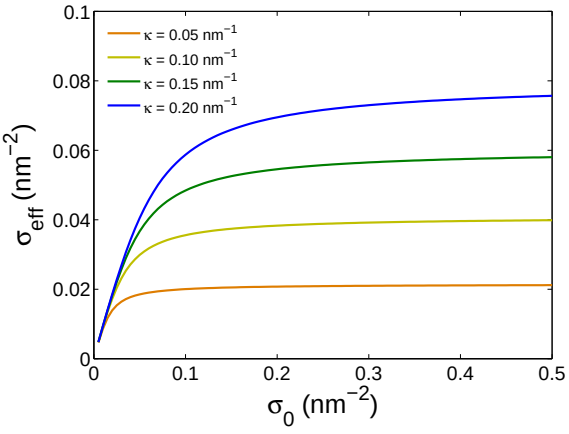

Figure 2.3: Charge renormalization predicted by two-state model. Only 1-1 salt is present in the solution. The four curves, from the lowest one to the highest one, correspond to $\kappa = 0.05\,\mathrm{nm}^{-1}$, $\kappa = 0.1\,\mathrm{nm}^{-1}$, $\kappa = 0.15\,\mathrm{nm}^{-1}$, $\kappa = 0.2\,\mathrm{nm}^{-1}$, respectively.

1. At small σ_0 (criteria: $\lambda \gg 1$), $\sigma_{eff} \approx \sigma_0$. This can be verified by expanding Eq. 2.10 to the leading order for small σ_0. When σ_0 is small, Debye-Huckel approximation work well, and the correction from charge renormalization is minor.

2. At large σ_0 (criteria: $\lambda \ll 1$), $\sigma_{eff} \to \frac{\kappa}{\pi l_b}$. In this region, σ_{eff} is almost independent of σ_0.

These conclusions only apply to the case when there's only 1-1 salt present in the solution. When multivalent ions are involved, all mean-field approaches would give qualitatively inaccurate predictions. Because of the strong charge correlation effect, multivalent ions have a significant privilege in condensing, and can become the dominant constituent of the condensed layer even even when their concentration in the bulk is low. "Charge inversion" in which so much ions (mainly multivalent) condense onto the surface that the sign of σ_{eff} is inverted. See Ref. [74] [75] [76]. Charge inversion has been experimentally observed by electrophoresis [77] and theoretically discussed [78].

In this chapter, we choose Na^+ and Mg^{2+} to be the representative monovalent and divalent cations, respectively. However, all the methodologies discussed here can be applied to other cations of the same valence, such as K^+, Ca^{2+}, or even NH_4^+. In fact, the effects of these ions on lipid aggregates are qualitatively similar to Na^+ and Mg^{2+}, and the quantitative difference can largely be ascribed to the differences in sizes.

2.2.4 Location of the charged surface

In a recent paper, Ref. [67], two assumptions have been made:

- The lipid charges all lies on the water-hydrocarbon interface.
- The electrostatic energy per lipid is given by $\mathcal{F}_{WS} \cdot a_h / A_{WS}$, in which $\mathcal{F}_{WS}/A_{WS}$ is the electrostatic energy per area.

The two assumptions contradicts each other. If the first assumption holds, the area on the interface a_i should be used in the place of a_h in the second assumption. If we want to keep the second assumption, the lipid charges should locate at a distance away from the interface. Either of these adjustments will make the model more self-consistent. Which one is closer to the reality?

In a phospholipid molecule, phosphate group always contributes a negative charge $-e$. Therefore, an anionic lipid has either a zwitterionic headgroup or an electrically neutral headgroup. PG and PS are the examples of the two cases, respectively. For the former case, the lipid charge can be treated as locating on the interface; For the latter case, overall lipid charge can locate in the aqueous phase a few Angstroms away from the interface. The distance may or may not coincide with l_h, and a detailed discussion of its chemical structure is needed.

In our calculation, charges are always assumed to be locating on the interface, and molecular electrostatic energy is the surface electrostatic energy density (similar to $\mathcal{F}_{WS}/A_{WS}$ above) times a_i instead of a_h. When the lipid charges are away from the interface, electrostatic energy can be calculated with formulas in Appendix C providing we know their distance from the interface.

2.2.5 Chemical equilibrium and free energy

Based on two-state model, we can study counterion condensation by determining the density of each species of condensed ions from chemical equilibrium, based on which we can calculate the electrostatic free energy of the system. Other properties can naturally be derived from free energy.

Chemical equilibrium

In the absence of Mg^{2+}, the chemical equilibrium is determined by the equation below:

$$\ln(n_1 v_1) = -\frac{2\mathcal{F}_{mf}(\sigma_0, \sigma_1, \kappa, c)}{(\sigma_0 - \sigma_1)} + \ln\left(\frac{\sigma_1 v_1/l_c}{l_c/v_1 - \sigma_1 v_1/l_c}\right) + \frac{\partial}{\partial\sigma_1}\mathcal{F}_{corr}(\sigma_0, \sigma_1, \kappa) \quad (2.13)$$

in which v_1 is the volume of a Na^+ ion, $\mathcal{F}_{mf}$ is determined from the potential in Eq. A.7, Eq. A.8 and Eq. A.9. $\mathcal{F}_{corr}$ is given by Eq. B.1.

Similarly, in the presence of Mg^{2+}, we have:

$$\begin{aligned}\ln(n_i v_i) &= -\frac{2Z_i\mathcal{F}_{mf}(\sigma_0, \sigma_1, \sigma_2, \kappa, c)}{(\sigma_0 - \sigma_1 - \sigma_2)} + \ln\left(\frac{\sigma_i v_i/l_c}{l_c/v - \sigma_1 v_1/l_c - \sigma_2 v_2/l_c}\right) \\ &\quad + \frac{\partial}{\partial\sigma_i}\mathcal{F}_{corr}(\sigma_0, \sigma_1, \sigma_2, \kappa) \quad (2.14)\end{aligned}$$

in which $i = 1, 2$ stand for Na^+ and Ca^{2+} ions, respectively. v can be chosen as, for example, $max\{v_1, v_2\}$, for the convenience in the calculation of free energy.

With given σ_0 and n_1, n_2, numerically solving these equations would yield σ_1 (as well as σ_2 if Mg^{2+} ions are present).

Free energy

The free energy *per area* for given σ_0, σ_1, σ_2, n_1 and n_2 is:

$$\begin{aligned}F &= F_{mf} + F_{entr} + F_{corr} \quad (2.15)\\ F_{mf} &= \mathcal{F}_{es} \quad (2.16)\\ F_{entr} &= \sigma_1\ln\left(\frac{\sigma_1 v_1}{l_c}\right) + \sigma_2\ln\left(\frac{\sigma_2 v_2}{l_c}\right) + \left(\frac{l_c}{v} - \sigma_1 - \sigma_2\right)\ln\left(1 - \frac{\sigma_1 v_1}{l_c} - \frac{\sigma_2 v_2}{l_c}\right) \\ &\quad -\sigma_1\ln(n_1 v_1) - \sigma_2\ln(n_2 v_2) \quad (2.17)\\ F_{corr} &= \mathcal{F}_{corr} \quad (2.18)\end{aligned}$$

The total free energy *per lipid* is determined by combining the equation above with Eq. 2.5:

$$f = K/a_h + \gamma \cdot a_i + \tau \cdot b^2 + F \cdot a \tag{2.19}$$

in which $a = a_h$ or $a = a_i$, depending on which surface you assume the charges to be locating on.

2.3 Results and Discussion

2.3.1 Counterion condensation

In order to reassuringly adopt the renormalized Debye-Hückel approach in the study of structural preference of phospholipid aggregates, we have to systematically examine counterion condensation (to be specific, density σ_i). At least 4 questions are of our interest:

1. How well does matching method and 2-state model agree with each other over a large range of σ_0 and κ?
2. In 2-state model, how much difference does it make to use a fixed l_c in contrast of a varying one in Eq. 2.12?
3. In the absence of Mg^{2+}, how much difference does charge correlation make? Is the popular viewpoint true that charge correlation is sub-dominant in the absence of multivalent ions?
4. Will the presense of divalent Mg^{2+} result in charge inversion, as we expected?

In the absence of Mg^{2+}

To begin with, we studied the case in which $n_2 = 0$. As can be seen in Fig. 2.4:

1. Matching method and 2-state model agree with each other better at low n_1 (low κ) and low σ_0. However, for the typical range of σ_0 and n_1 in our problem, the agreement is dissatisfactory.
2. As expected, results based on a varying l_c coincide with those based on a fixed l_c when the l_c values determined by Eq. 2.12 coincide with those values we fix at. Otherwise, the difference is fairly large, indicating the choice of l_c has an impact on the prediction we make.

3. Charge correlation lowers the chemical potential of the surface state and enhances condensation, resulting in a lower σ_{eff} value. Furthermore, it *inverts* the way σ_{eff} varies with n_1. As n_1 increases, mean-field calculation predicts less condensed ion and a higher σ_{eff}, but correlation effect would allow more counterions to condense and therefore a lower σ_{eff}.

In the presense of Mg^{2+}

Fig. 2.5 shows that charge inversion can't be predicted in the mean-field limit. In fact, σ_{eff} predicted in this limit doesn't deviate much from the no-Mg^{2+} case. Ions in the condensed layer mainly consist of Na^+, simply because they're of a higher concentration in the bulk. The privilege of multivalent ion in condensing is not at all reflected. Therefore, mean-field approach is not satisfactory in the presence of multivalent ions, and charge correlation must be accounted for.

After accounting for charge correlation, as seen in Fig. 2.6, Mg^{2+} exhibit a significant privilege in condensing, as they constitutes the majority of the condensed layer. Charge inversion is observed for $n_2 \gtrsim 1\,\mathrm{mM}$, consistent with earlier theoretical predictions [75].

2.3.2 Structural preference reflected by geometrical properties

After all these preparations, we're eventually ready to study the structural preference of phospholipid aggregates by constructing a lipid monolayer and calculate its spontaneous curvature c_0. To simplify the problem, we approximate the surface of the monolayer as *uniformly charged*, neglecting the fact that the surface charges are carried by individual, discrete lipids and lipid demixing could occur. We assume that a fraction $\bar{\alpha}$ of the constituent lipids carry $-e$ of charge each, while the rest are electrically neutral. Experimentally, $\bar{\alpha}$ can be controlled through the pH value of the environment. In this section, we compare seven cases:

1. $\bar{\alpha} = 10\%$, 20%, 30% in the absence of Mg^{2+}.
2. $\bar{\alpha} = 10\%$, 20%, 30% in the presense of $5\,\mathrm{mM}$ of Mg^{2+}.
3. $\bar{\alpha} = 0$ i.e. (electrically) neutral.

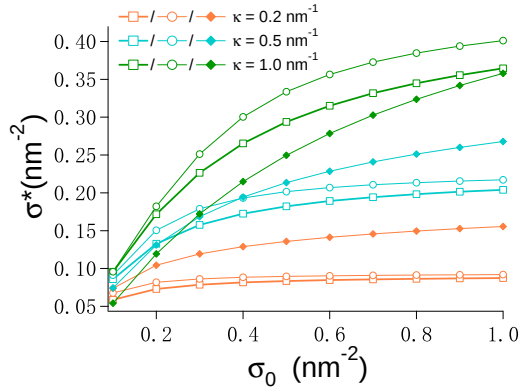

(a) σ_{eff} v.s. σ_0 calculated in the mean-field limit, based on matching method (empty squares) and two-state model that adopts l_c varying as in Eq. 2.12 (solid circles) or fixed at 5 Å (solid diamonds).

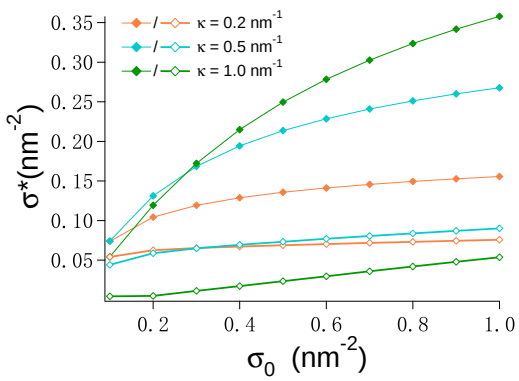

(b) σ_{eff} v.s. σ_0, with (solid diamonds) or without (empty diamonds) accounting for correlation. $l_c = 5$ Å

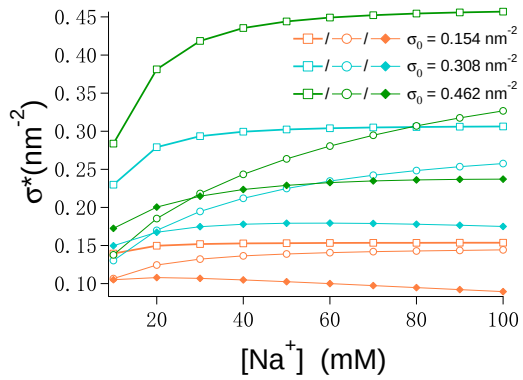

(c) σ_{eff} v.s. n_1 calculated in the mean-field limit, based on matching method (empty squares) and two-state model that adopts l_c varying as in Eq. 2.12 (solid circles) or fixed at 5 Å (solid diamonds).

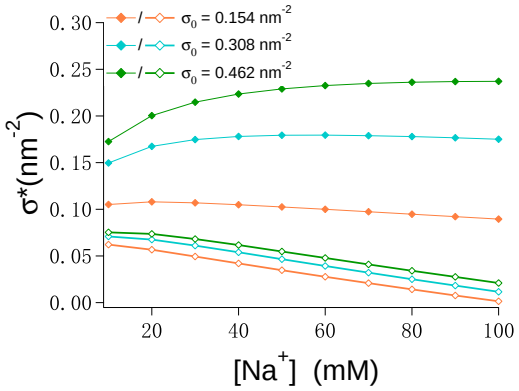

(d) σ_{eff} v.s. n_1, with (solid diamonds) or without (empty diamonds) accounting for correlation. $l_c = 5$ Å

Figure 2.4: Counterion condensation calculated in the absence of Mg^{2+}. Surface charge density is consistent with a typical phospholipid monolayer on which 10 percent of the lipids are anionic. Matching method and 2-state model agree better at low n_1 and low σ_0, the choice of l_c makes an obvious difference in the prediction of σ_{eff}, and charge correlation enhances condensation to yield a lower σ_{eff}.

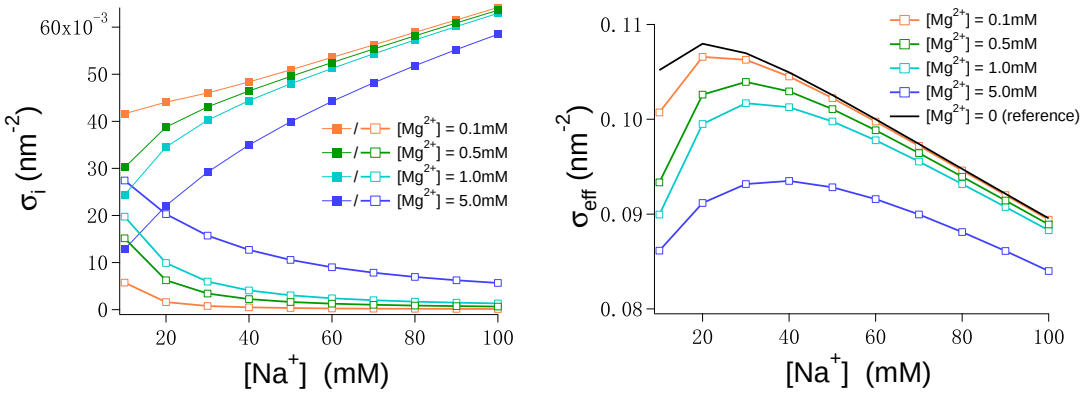

(a) Graph of σ_i (b) Graph of σ_{eff}

Figure 2.5: Density of condensed counterion, σ_1 (filled squares) and σ_2 (empty squares), calculated in the mean-field limit. $\sigma_0 = 0.154\,\mathrm{nm}^{-2}$ corresponding to a typical phospholipid monolayer containing 10 percent of anionic lipids. Mg^{2+} doesn't have a significant advantage in the competition with Na^+, and the latter still dominates in the condensed layer. Charge inversion never occurs.

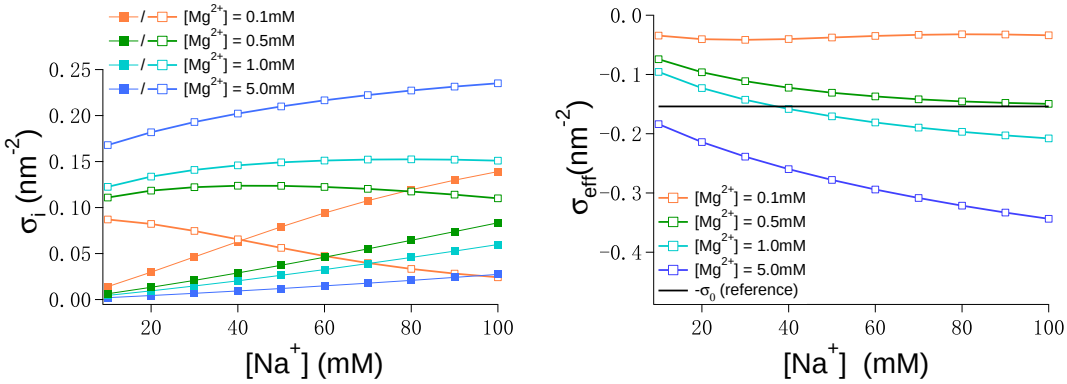

(a) Graph of σ_i (b) Graph of σ_{eff}

Figure 2.6: Density of condensed counterion, σ_1 (filled squares) and σ_2 (empty squares), with charge correlation accounted for. $\sigma_0 = 0.154\,\mathrm{nm}^{-2}$. Now the privilege of Mg^{2+} is exhibited as they start to dominate in the condensed layer, and charge inversion occurs at around $n_2 = 1\,\mathrm{mM}$.

Optimized headgroup area

Optimized headgroup area a_0 reflects the attractive/repulsive nature of the electrostatic force. The results are presented in Fig. 2.7. As can be seen here, in the absence of Mg^{2+}, the electrostatic force results in an outward tension, pushing lipids apart, resulting in a larger a_0. However, Mg^{2+} ions bridge between the anionic lipids, leading to an inward tension that draws lipids closer to each other. The tension becomes stronger when $\bar{\alpha}$ (or equivalently, σ_0) increases, and becomes weaker when n_1 (or equivalently, κ) becomes higher. This is consistent with other literatures, such as Ref. [65] and [67]. Notably, for $\bar{\alpha}$ = 30%, with and without Mg^{2+} respectively, the a_0 results quantitatively coincide fairly well with the results in Ref. [67] achieved by a much more sophisticated, computationally resource-demanding algorithm that is considered to be the most accurate result to date.

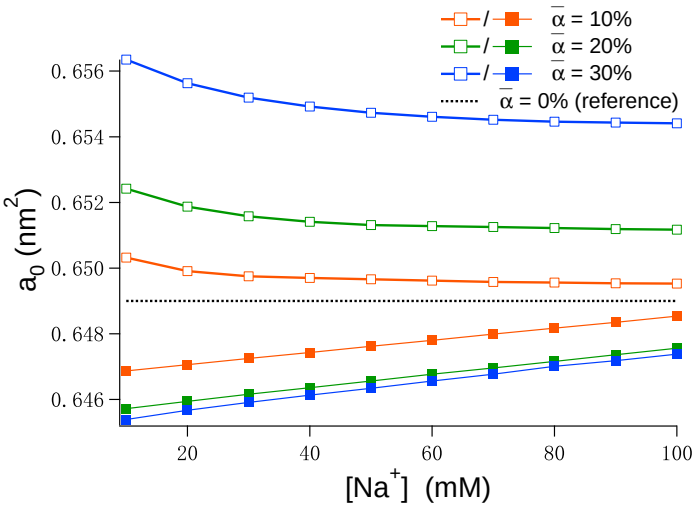

Figure 2.7: Optimized headgroup area per lipid, a_0, in the absence (unfilled squares) or the presense of 5 mM (filled squares) of Mg^{2+}. Without Mg^{2+}, the electrostatic force between the headgroups are repulsive, leading to a larger a_0, while Mg^{2+} allow the electrostatic force to go from repulsive to attractive, leading to a smaller a_0. Higher $\bar{\alpha}$ naturally leads to stronger electrostatic force, and at higher n_1, Debye screening weakens the electrostatic force.

Impact of the location of the neutral surface

Considering the complexity and expected inaccuracy of locating neutral surface, we'd better take a look at how much error in c_0 will result from error in the location of the neutral

surface. In Fig. 2.8, c_0 was calculated by assuming different surfaces to be the neutral surface. Define a parameter $\theta = \delta/b$: $\theta = 0$ means the "free" end of all hydrocarbon tails lies on the surface, while $\theta = 1$ means the surface coincides with the water-hydrocarbon interface. As can be seen, the variation is quite significant when θ varies from 0 to 1.

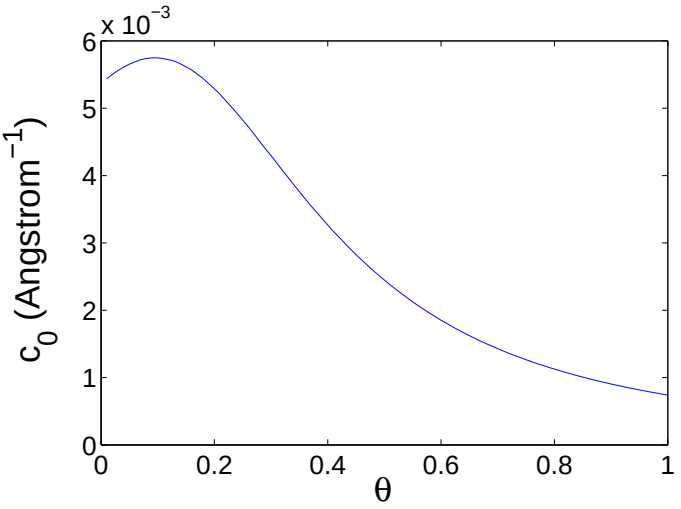

Figure 2.8: Influence of neutral surface location. $\bar{\alpha} = 30\%$, $n_1 = 10\%$, no Mg^{2+} present. Interestingly, the maximum on the curve coincide with the calculated δ value and c_0 value, as in Fig. 2.9 and 2.10.

The neutral surface can be located accurately for an electrically neural monolayer. Hence, the error in locating the neutral surface is dominated by the inclusion of electrostatic force. In Fig. 2.9, we presented the δ values. As can be seen, in the absence of Mg^{2+}, the outward electrostatic tension brings the neutral surface farther away from the water-hydrocarbon interface, because it enhances the K term in Eq. 2.5; while in the presense of Mg^{2+}, the inward electrostatic tension brings the neutral surface closer to the water-hydrocarbon interface. However, such effects are not pronounced, because the vertical axis of Fig. 2.9 only spans 0.1 Å to 0.2 Å, changing θ only by 0.01. Therefore, the accuracy of c_0 calculation won't be compromised even if the error in δ were relatively larger.

Spontaneous curvature

After all these preparations, we're finally ready to calculate c_0, the quantity that reflects the structural preference we've been talking all along. The results are presented in Fig. 2.10.

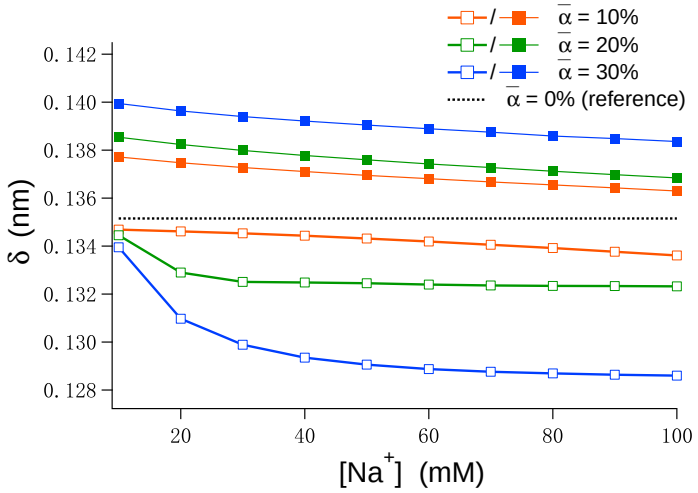

Figure 2.9: Position of neutral surface. Electrostatic force only makes around 1 percent of change in the position of neutral surface. Without Mg^{2+}, the neutral surface shifts away from headgroup, while the presense of Mg^{2+} brings it closer to the headgroup.

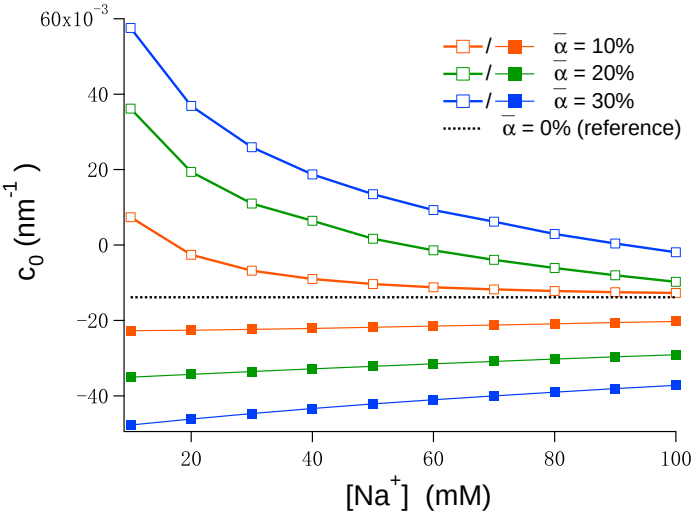

Figure 2.10: Spontaneous curvature, c_0, in the absence (unfilled squares) or the presense of 5 mM (filled squares) of Mg^{2+}. In the absence of Mg^{2+}, the electrostatic force stabilizes the lamellar phase (bilayer structure) by making c_0 slightly positive. The presense of Mg^{2+} leads to a more negative c_0, suggesting that Mg^{2+} can stabilize H_{II} phases of lipids that would otherwise stay in lamellar phase.

As can be seen, for an electrically neutral monolayer, c_0 is slightly negative, suggesting an unstable tendency for a bilayer to transit to inverse-hexagonal structure. In the absence of Mg^{2+}, the electrostatic force invert the sign of c_0, allow the lipid bilayer to stay stable. However, at a relatively high n_2, the c_0 becomes even more negative, and the bilayer is more likely to transit into, and be stable in, inverse-hexagonal structure. These are consistent with the experimental and computational results presented in the references we mentioned at the beginning of this chapter.

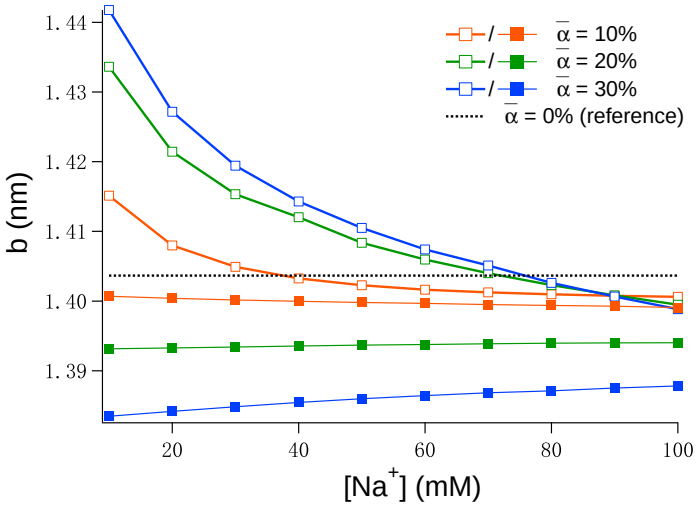

Figure 2.11: Hydrocarbon chain length at relaxed state. The general layout of this graph is slightly different from the graph of a_0 and c_0 in that the two sets of curves (in the absence/presence of Mg^{2+}) doesn't lie on either side of the reference line. This might be due to the accumulated error in the calculation, in which case it's in fact not pronounced.

2.4 Conclusions

Now, we've proven that our model and our algorithm can make predictions on the electrostatic impact of structural preference and phase behavior of phospholipids that are not only qualitatively correct, but quantitatively accurate to some extent (as compared with Ref. [67]). Considering the conciseness and computational efficiency of our model, it's indeed a triumph.

Chapter 3

The Destabilization of LPS Leaflet by Cationic Peptide

3.1 Introduction

As we have learned in section 1.2.2, LPS is the dominant, if not only, lipid constituent of the outer leaflets of the outer membranes of Gram-negative bacteria. LPS is a polyanionic molecule that carries several acidic (phosphate and carboxyl) groups that mainly distribute in the lipid A and oligosaccharide core region. On first glimpse, the highly anionic nature of LPS makes an outer leaflet highly negatively charged, and the strong repulsive electrostatic force between the molecules will render the leaflet unstable. In physiological environment, despite some contribution from the interaction between neighboring O-chains [79], the dominant contributors to the stability of an LPS leaflet are the cations attracted to its vicinity, especially divalent cations (Mg^{2+} and Ca^{2+}): at least half of the negative charges are neutralized by cations [80] that help neutralizing and bridging the LPS charges. It turns the repulsive electrostatic forces between the LPS molecules into effectively attractive ones, greatly enhancing their tendencies to stay together. In fact, LPS molecules strongly prefer to stick together in an LPS-phospholipid mixed monolayer in the presense divalent ions [81].

Similar phenomena in phospholipid membranes have been verified both theoretically [63] [82] and experimentally [39]. For an LPS leaflet, considering its higher surface charge density, such stabilization is expected to be more pronounced. Much experimental works support the significant role of polycationic ions in the stabilization of LPS layer. It was found in 1970s that substituting monovalent ions trapped around an LPS layer with divalent ions has a profound impact on the aggregation state of LPS [83], and aggregates of isolated

LPS in the presence of 10 mM of Mg^{2+} show no thermal melting up to 350 K [84]. More interestingly, when some G- bacteria enter an environment that lacks divalent ions (e.g. phagocytic vacuoles), they will modify their LPS leaflets to avoid destabilization [85]. For example, *P. denitrificans*, when grown in a media in which the concentration of divalent cations is lower than normal, produces more of the zwitterionic ornithine lipids, possibly to substitute for LPS [86].

For many substances, the LPS leaflet is a formidable permeability barrier (see Ref. [28] and references therein), which is why it's evolutionarily chosen to be a first line of defense. However, both controlled experiments and clinical observations confirm that AMPs are fairly effective against G- bacteria such as E. coli (for example, see Ref. [87]). Questions naturally emerge: how do AMPs cope with the LPS leaflet? What allow AMPs to permeate the LPS leaflet with apparent ease? In particular, what role does the electrostatic interaction play in the permeating of the leaflet by AMPs, given that it plays a key role in both the selective binding of AMP onto bacteria and in the stabilization of LPS leaflet?

Interestingly, recent works reveal that AMPs activate the PhoPQ system (and consequently the PmrAB system) in *S. enterica* [88], and directly activate the PmrAB system in *P. aeruginosa* [89]. It's known that PhoPQ system is activated when the bacteria is in low Mg^{2+} environment [90], and some of the genes activated by PmrAB system modify the LPS molecules to reduce the charged groups on them [91]. It indicates that: maybe AMPs can effectively decrease the amount of Mg^{2+} on it, probably by competing with them for the chance of binding, and render it unstable. Similar assumption has also been made in other works [92].

This work aims at proposing an approach to quantitatively investigate the interaction between cationic peptides and the LPS leaflet as found on G- bacteria. To this end, we established a model for the LPS layer, cations (monovalent and divalent), and cationic peptides, formulated the interactions between them, and carried out calculations as below. Firstly, we assumed there are monovalent ions (Na^+), but *no* divalent ions or cationic peptides surrounding the LPS leaflet, to verify the intuition that electrostatic interaction tend to destabilize the leaflet in the absence of divalent ions. Secondly, we add divalent ions into the scenario above, while still keeping peptides out of the picture, to verify the stabilizing effect of the divalent ions. Finally, we allowed both species of ions as well as peptides to be present in the environment, to determine the impact made by the presence of these peptides. Stabilization and destabilization are quantitatively reflected by excessive surface tension $\Delta\Pi$, the part of the surface tension contributed by electrostatic interaction. However, we will only focus on whether AMPs destabilize the leaflet i.e. whether they make the leaflet more vulnerable to permeating. We will not concern about the dynamic process of permeating itself, or what these peptides do after going through the leaflet.

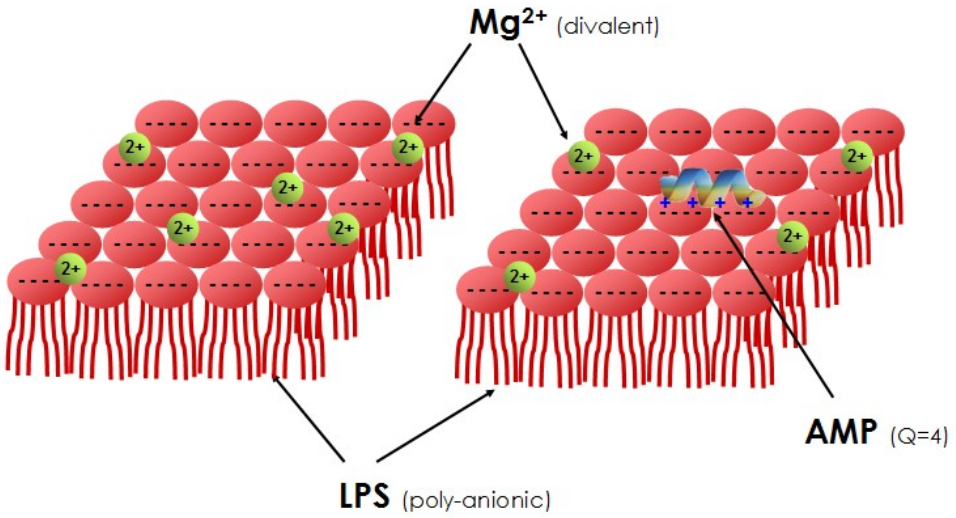

Figure 3.1: Competitive binding between AMP and divalent ions, during which the latter is partially substituted by the former, easing the penetration process

3.2 Theoretical Model: Establishing

LPS is a class of relatively large and complex molecules that arrange themselves on the surface of G- bacteria in a fairly complicated way. Therefore, the first step to tackle the problem, as before, is to establish a model that depicts the system of interest, the LPS leaflet and the charged objects on or around it. The model shall bear sufficiently resemblance to reality yet computationally manageable.

Before thinking of a new model, we should consider the applicability of the model we adopted in the previous chapter in the current problem. That model accounts for the molecular properties of phospholipids, while treating the electrostatic effects in a continuous, largely smeared-out, mean-field manner that focuses more on the influence of geometry (curvature). It is because in physiological reality, only 10% to 30% of a charged leaflet in a plasma membrane consist of anionic lipids, and we assumed that lipid demixing is minimal, that these anionic lipids are homogeneously distributed on the monolayer on average without organizing into any particular structure. Besides, the moderate backbone charge density makes renormalized Debye-Hückel approach suitable. However, almost 100% of the lipids on the outer leaflet of outer membrane is LPS that is more densely charged than phospholipids. Besides, experiments show that LPS molecules on the leaflet tend to have well defined formation [25] [93]. Furthermore, the scenario we study here is "binding".

Beside being restricted in the transverse [1] direction, as in simple "counterion condensation", a "bound" ion also have less freedom in the lateral direction. To be more specific, it can only stay in the vicinity of a set of discrete "binding sites", coinciding with the acidic functional groups in our problem.

Therefore, we found it necessary to establish a new model. According to the discussion above, we have already determined a number of features expected in this model.

1. It has to account for charge discreteness. In other words, we'd like to depict each charged object as an individual entity, with its own charge of an integer number of e's, maybe even with their own size and geometry, instead of working in continuous limit as before.

2. The arrangement of the binding sites shall reflect the organized nature of the LPS leaflet.

3. It has to put an emphasize on "binding". The concept of "binding" bears some resemblance with "condensing" as discussed in the previous chapter, but the latter is merely a means of compensating the error of Debye-Hückel equation, as in the naive renormalized Debye-Hückel approach, they're indeed playing a leading role in our calculation, whose pairwise interaction with other charges, especially the binding site, should be accounted for as accurately as possible. We define "binding" as *arriving at and staying in the vicinity of a binding site due to Coulomb attraction*. To be specific, two ions are considered as "bound" as long as the Coulomb interaction energy between them exceeds k_BT.

The model we eventually arrived at is detailed below. This model is inspired by a number of previous works, especially Ref. [94] and [95]. We will start by explaining a few aspects, among others, of the model in detail, followed by a summarized description of the model to make it easier for the readers to follow.

Note: in the calculation we performed based on this model, we used Na^+ and Mg^{2+} as representative monovalent and divalent ions, respectively, as we did in the last chapter. However, we will mostly use "monovalent ions" and "divalent ions" in this section instead of mentioning specific types of ions, because in principle, the model applies to all types of ions of these valences.

[1] See Fig. 3.7 for the concept of transverse.

3.2.1 Binding sites on a square lattice?

It's reasonable to argue that each acidic functional group (phosphate and carboxyl) acts as a binding site that carries one elementary charge. For the sake of computational convenience, the best approximation is to assume that each site occupies a node on a *square* lattice. However, before doing that, we have to confirm that this arrangement bears sufficient resemblance with a biochemical realistic LPS leaflet to avoid qualitatively absurd result.

As can be seen in Fig. 3.2a, the four charges of an LPS Re molecule can be approximately arranged onto an isosceles right triangle. Fig. 3.2b shows that a square lattice can be covered only by these triangles. Hence, it's indeed plausible to argue that: the charged groups on an LPS leaflet, acting as electrostatic binding sites [2], roughly forms a square lattice.

However, it's by far not the only way to approximate the spatial positions of these charged groups, and, unfortunately, not even the most accurate one. A more accurate approximation, referred to as "minimum model", was used in Ref. [59] and references therein. However, we will stick to the square lattice, since it's not too faraway from reality, yet much simpler to work with.

3.2.2 Binding sites on the interface?

When the amphiphilic LPS molecules self-assemble into a monolayer in water, there is clearly an interface between the hydrophilic headgroups and the hydrophobic hydrocarbon tails, much like the case of phospholipids. Do the charged groups locate at the interface? If not exactly, is it safe to approximate their location as such?

More sophisticated models, such as the "minimum model" [59], depict all the charged groups slightly above the interface. However, for the convenience of mathematical treatment, we assume that all the charged groups locate at the interface. In more sophisticated future works, we'd love to model the charges to be out of the interface. Some mathematical preparation has already been accomplished (See Appendix C).

[2]The term "backbone charge", as used in the previous chapter, may also be applied occasionally to refer to these charged groups, putting an emphasize on their electrostatic properties

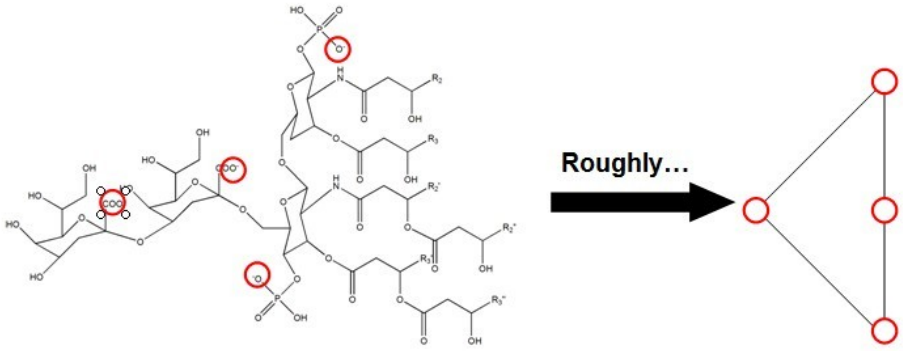

(a) Abstracting the relative locations of the charged groups. The left half is inspired by Ref. [23].

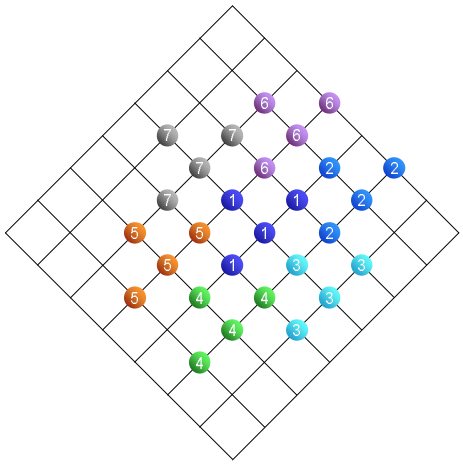

(b) Arranging the charges on a square lattice

Figure 3.2: Aligning the charges of LPS Re on a square lattice. We abstract the positions of the four charged groups in the lipid A of one LPS molecule along an isosceles right triangle as depicted in (a), and tile them onto a square lattice as depicted in (b).

3.2.3 "All anions are created equal"?

In our model, "binding" is purely electrostatic. The only relevant properties in the binding of two objects are their respective charges an sizes [3]. In this sense, an anion in the bulk (e.g. Cl^-) carries the same charge, $-e$, as a binding site on the LPS leaflet. We naturally ask: if a binding site has a considerable probability to bind to a cation, shouldn't an anion in the bulk have a same, at least comparable, probability to bind to a same cation and form a pair? Aren't all monovalent anions created equal when it comes to Coulomb force? From our common sense, if we solve some table salt in a glass of water, there would be hardly any NaCl molecule in it i.e. little pairing/binding. Does that mean the chance for a binding site to be bound by monovalent ions shall be comparably small? It's reasonable to make the hypothesis that the anions in the bulk and the binding sites on the leaflet are somehow different. In that case, once we manage to make them as symmetrical as possible, will the binding probability be comparable? We have to verify this to ensure the self-consistency of our model.

Ion pairing in the bulk

Firstly, we have to admit: the chance for pairs such as Na^+Cl^- to form is, tiny as it should be, non-zero. To quantitatively determine this chance, the most natural approach is to use the concept of association constant:

$$K_b = \frac{[AB]}{[A]\,[B]} \tag{3.1}$$

in which $[A]$ and $[B]$ are the concentration of the two species of particles the solute dissociates into (e.g. Na^+ and Cl^-), while $[AB]$ is the concentration of pair (e.g. Na^+Cl^-). When the binding can be solely ascribed to Coulomb force, this constant is calculated as [96] [97] [98]:

$$K_b = 4\pi \int_d^{|Z_i Z_-| l_b/2} dr r^2 \exp\left(|Z_i Z_-|\, l_b/r\right) \tag{3.2}$$

in which Z_i and Z_- are the valence of the ith type of the cation and the anion, respectively. d is the *minimal* distance between the two charges. The physical meaning of Eq. 3.2 is: two charges of opposite signs are regarded as "bound" if the Coulomb energy between

[3] In the following discussion, we implicitly assume that the binding sites on the LPS leaflet has the same size as the anions in the bulk

them exceeds thermal energy k_BT. To this end, a bound cation shall be in a spherical shell centered at the anion with radius between d and $Z_iZ\_l_b/2$, see Fig. 3.3.

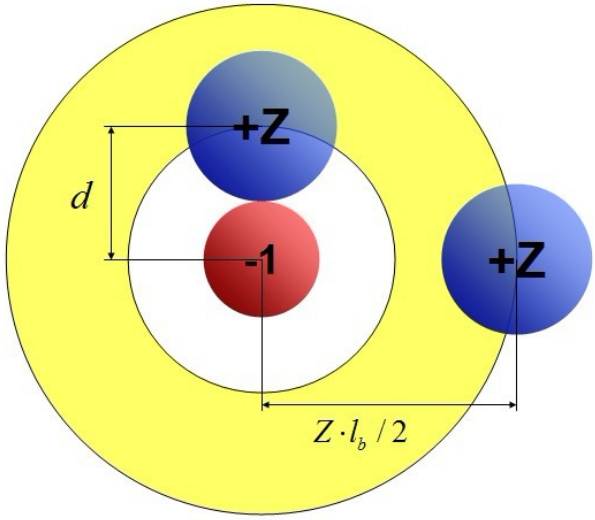

Figure 3.3: Physical meaning of Eq. 3.2. The yellow part is a cross section of the spherical shell the cation can explore. We integrated over the yellow region in Eq. 3.2.

Eq. 3.2 can be transformed into [98]:

$$K_b = 4\pi(Z_iZ\_l_b)^3 \int_2^{Z_iZ\_l_b/d} dz \cdot z^{-4}e^z \tag{3.3}$$

Notice that K_b is *not* a dimensionless constant. The integral is dimensionless, while l_b has the dimension of length. Therefore, K_b has the dimension of volume. However, this is not surprising, because all the concentrations in Eq. 3.1 has the dimension of inverse volume. If the concentrations are in the unit of particle per nm^3, the unit of K_b will be nm^3. However, it is the logarithm of K_b that will enter the chemical potential, and we prefer to avoid taking the logarithm of a quantity that is not dimensionless.

Take the logarithm of both sides of Eq. 3.1:

$$\ln([A]) + \ln([B]) = \ln([AB]) - \ln K_b \tag{3.4}$$

Add $2\ln\nu$ on both sides, in which ν is the common volume of these particles *providing that A, B and AB all have exactly the same volume*, we have:

$$\ln\left([A]\,\nu\right)+\ln\left([B]\,\nu\right)=\ln\left([AB]\,\nu\right)-\ln\left(K_b/\nu\right) \tag{3.5}$$

In Eq. 3.5, everything we take logarithm of is dimensionless, and the first 3 logarithms in the equation are nothing but the ideal gas chemical potential (in unit of k_BT) of the respective particle species, and $\ln\left(K_b/\nu\right)$ is the energy benefit for binding reflected in chemical potential. Of course, the "same volume" assumption is a crude one, but the resulting error is expected to be small. Therefore, terms of the form $\ln\left(K_b/\nu\right)$ will enter our chemical potential to account for binding.

To account for binding in the bulk, we assume that only the "free" cations not associated with anions can contribute to the cation concentration in the bulk. Therefore, we numerically solve Eq. 3.1, namely:

$$\left(n_i-n_i*\right)/\left(n_i*\right)^2=K_{bi}, i=1,2 \tag{3.6}$$

in which n_i is the total concentration of the i$^{\text{th}}$ type of cation in the bulk, while n_i* is the corresponding "effective" concentration after taking the paired ones out of the picture. There are more subtleties when divalent cations are included, because they can bind to either one or two anions. Entities such as $MgCl^-$ cannot be simply ignored, as they should be treated as monovalent cations. However, n_2 is almost always far smaller than n_1 in our calculation, and it's safe to assume that (n_2-n_2*) is far smaller than n_1*. This assumption can be discarded in future works to improve the calculation in the high n_2 limit.

To calculate the chemical potentials of the cations in the bulk, μ_{1b} and μ_{2b}, we should use the corresponding effective concentrations in the place of the original ones. Since the effective concentration is always smaller, the chemical potentials are lowered as a result of pairing in the bulk.

For the bound cations, the same approach can be employed. Similar to the last term in Eq. 3.5, we have:

$$\Delta E_i^{binding}=-\ln\left(K_{Ii}/\nu_i\right) \tag{3.7}$$

However, K_I in Eq. 3.7 doesn't equal to the K_b in Eq. 3.2, because a bound cation cannot diffuse into the other side of the interface. Furthermore, the dielectric discontinuity at the interface affects the strength of electrostatic interaction. Without dielectric discontinuity, we have [98]:

$$K_I=\frac{1}{2}K_b \tag{3.8}$$

Make them equal, and see!

If cations can bind to either the anions in the bulk or the sites on the surface, what leads to the drastically different (as we expect) binding probabilities? There are at least 3 obvious factors contributing to it.

1. Dielectric discontinuity at the surface enhances the Coulomb force to be almost twice as strong.
2. Cations cannot explore the hydrocarbon region, leading to Eq. 3.8.
3. Cations experience forces from neighboring binding sites, accounted for by the mean-field term and the lateral correlation term.

Therefore, if we eliminate these differences respectively, namely: set $d = 0$, set K_I and K_b equal to each other [4] and set the distance between nearest neighbor sites a to be so large that they're effectively uncoupled. Calculation based on these parameters Fig. 3.4.

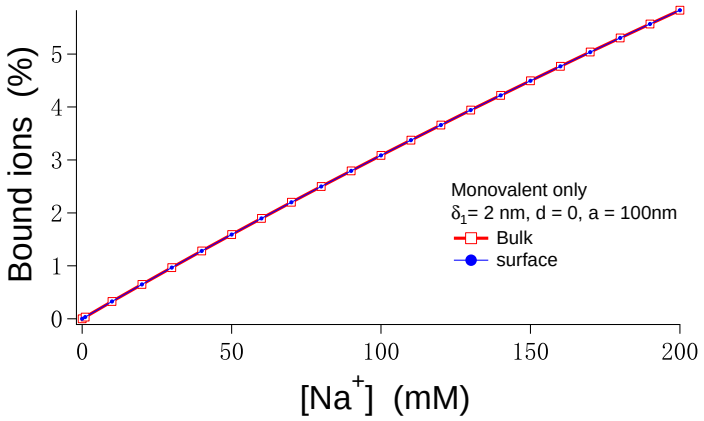

Figure 3.4: Binding probability in the bulk and on the surface. Dielectric discontinuity has been eliminated, and the sites are sufficiently sparse. The very nice coincidence between the two curves suggests that we didn't introduce any artificial discrimination between binding sites on the surface and anions in the bulk.

As can be seen in Fig. 3.4, the binding probability in the bulk and on the surface match each other very nicely. The negative charges on the surface and in the bulk are indeed

[4] Physically, it naturally occurs when $d = 0$. However, this change have be manually made in the computer code we used.

treated equally (providing they has the same size), and we can be reassured that such inconsistency has been excluded in our model.

Interaction ions

The unpaired ions interact with each other through long-range (even after screening) Coulomb force, leading to another term in the chemical potential.

We know from elementary physical chemistry (see, e.g. the one by E. A. Moelwyn-Hughes [99] and the one by T. Engel and P. Reid [100], also see Ref. [97]) that: for a very dilute ($< 1\,\mathrm{mM}$) electrolyte solution, this term in chemical potential follows Debye-Hückel limiting law:

$$\Delta\mu_i/k_BT = -\frac{1}{2}Z_i l_b \kappa \tag{3.9}$$

For higher concentration, the finite size effect is no longer negligible, and a better approximation is:

$$\Delta\mu_i/k_BT = -\frac{1}{2}Z_i l_b \kappa \cdot \frac{1}{1+\kappa\delta_i} \tag{3.10}$$

There are some other empirical equations, such as Davies equation, but they're empirical and phenomenological, so we prefer not to use them.

Finally, concentrations are usually given in molar, but in our calculation, the most convenient and consistent unit is particle per nanometer cubed. So we have to do the conversion: $1 molar = 0.602\,\mathrm{nm}^{-3}$.

3.2.4 Summary of the model

1. There is an infinite plate of finite thickness d, made of a material with dielectric constant ε_l, immersed in an aqueous electrolyte solution.

2. On one of the interfaces (referred to as "the surface" in the following context) between the plate and the aqueous solution, there is a 2D square lattice, with lattice constant a. On each lattice site there is an electric charge (negative by default), which is fixed there and doesn't have any freedom to move. All these charges make up *the backbone charges*. Obviously, the surface charge density for these charges is $\sigma_0 = 1/a^2$.

3. The electrolyte solution contains a 1-1 salt (e.g. NaCl) of concentration n_1 and a 2-1 salt ($MgCl_2$) of concentration n_2 [5], and cationic peptides, each carries Qe of positive charge, of concentration n_p. For simplicity, the two salts share the same type of anion (Cl^- in the example above). The cations serve as "counterions" in the system. In principle, backbone charges should release their own counterions to ensure electrical neutrality, but this is neglected in our calculation.

4. In this solution (referred to as "bulk" in the following context, also referred to as "aqueous phase" in other literatures), cations can pair with and bind to anions i.e. being in each other's vicinity, moving around as one entity, due to Coulomb attraction. To be specific, two ions of opposite charges are considered as "bound" as long as the Coulomb interaction energy between them exceeds k_BT. The bound cations are in chemical equilibrium with the "free" ones.

5. The cations and peptides can also bind to the backbone charges. However, since the other side of the surface cannot be accessed by the ions, and there is a dielectric discontinuity across the surface, the energy gained through binding with backbone charge can be quite different from that with anions in the bulk. Besides, we emphasize that each backbone charge can bind to at most one cation, either monovalent or divalent, or one of the Q charges on a peptide. (In the following context, we don't distinguish "bind to a site" and "bind to a backbone charge (on this site)".)

6. Water is abstracted as a continuous, homogeneous background characterized by its dielectric constant $\varepsilon_w = 80$. Beyond this, water results in a hydration shell around all the ions, increasing their effective radii.

7. When a cation bind to a negative charge (binding site or anion in the bulk), the smallest possible distance between their centers is denoted as δ_1 for monovalent cation or δ_2 for divalent cation, which is roughly the sum of the radii of the charges. Obviously, we can have different δ_i's for binding in the bulk and on the surface, because a backbone charge (for phospholipid and LPS, O^-) may have quite different size from an anion in the bulk (typically Cl^-). In a more primitive model, we can make the approximation that δ_i is the only possible distance between the bound ion pairs. However, in a more sophisticated model, the distance is allowed to vary between δ_i and $Z_i/2 \cdot l_b$, with l_b being the Bjerrum length. We also assume that $\delta_i < Z_i/2 \cdot l_b$, because otherwise no binding as defined above would occur. In my work, the latter model is adopted for the ions, and the former model is adopted for peptides, because ions are smaller and more mobile while peptides are more bulky and more inflexible.

[5] In principle, the model can be generalized to 3-1 salts e.g. $GdCl_3$, but the lateral correlation may have to be calculated in a drastically different way

8. When the discreteness and the finiteness of size of the ions have to be taken into account, the ions are depicted as spheres with their respective radii. The interaction between "free "ions in the bulk is calculated based on Debye-Hückel limiting law, which implicitly assumes the ionic charges are distributed on the surface of the spheres. However, when ion pairing and binding is discussed, we assume the electrical charge is concentrating at the center of the sphere. The apparent contradiction in these assumptions is expected to produce negligible error (because the "free" ion in the bulk are much farther apart).

9. In the system we study (LPS leaflet), the distances between bound ions are far smaller than the lattice constant: $\delta_i < Z_i/2 \cdot l_b \ll a$. Therefore, a lattice site on which the backbone charge is bound by a monovalent/divalent ion, as seen from other lattice sites, is electrically neutral/carrying $+e$ charge. In other words, we neglect the dipole moment of "backbone charge + bound ion". Furthermore, we assume that a is comparable to the Debye length κ corresponding to the electrolyte solution.

Therefore, the general scenario is as depicted in Fig. 3.5.

3.3 Theoretical Model: Mathematical Formulation

In principle, since all the charges are discrete and their position can be determined (in classical limit), a summation of the Coulomb energy of all the charge pairs shall yield the total electrostatic energy of the system. Since that's obviously unrealistic, we have to make simplifying approximations and adopt tricks to ease the pain.

Consider a square lattice of lattice constant a that contains N_0 lattice sites. Originally, each lattice site carries one $-e$ charge. Then, as depicted in Fig. 3.5 (except that we don't want peptides to be involved for now), there are N_1 monovalent ions and $\frac{1}{2}N_0 + N_2$ divalent ions bound onto the lattice. Notice here that $-\frac{1}{2}N_0 \leq N_2 \leq \frac{1}{2}N_0$. When $N_2 < 0$, it simply means that less than half of the lattice sites are bound with divalent ions. Now, there are N_1 sites that are electrically neutral, $\frac{1}{2}N_0 + N_2$ sites carrying $+e$ charge each, and $\frac{1}{2}N_0 - N_1 - N_2$ sites carrying $-e$ charge each. These sites are arranged on the square lattice in a certain configuration.

In principle, it's always possible to decompose such a configuration into the superposition of two parts according to the scheme depicted in Fig. 3.6. In the first part (mid-left in the figure), $+e$ and $-e$ charges are respectively carried by N sites, and the remaining $N_0 - 2N$ sites are neutral. Here, $N = min\{\frac{1}{2}N_0 + N_2, \frac{1}{2}N_0 - N_2\} = \frac{1}{2}(N_0 - 2|N_2|)$.

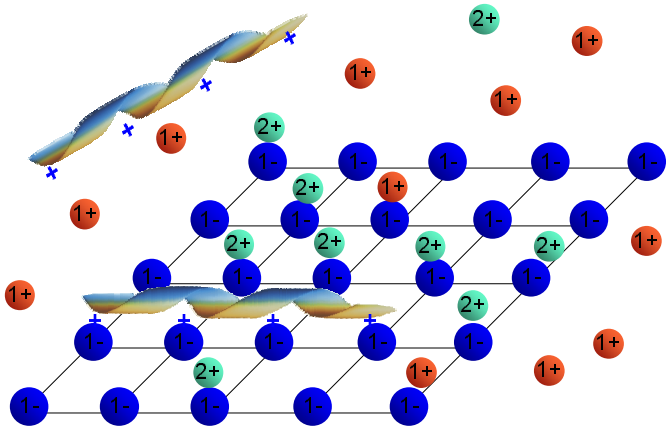

Figure 3.5: Schematic drawing of the binding scenario. Each lattice site carries $-e$ of negative charge (red sphere), and monovalent/divalent ions (blue/green spheres) in the bulk can be attracted to the vicinity of lattice sites and be "bound". Peptides (blue-and-yellow helices) in the bulk can also bind to the surface, occupying a number of lattice sites equal to its charge Q.

Therefore, the average surface charge density of this part is always zero. In the second part (mid-right in the figure), $+e$ ions (if $N_2 > 0$) or $-e$ ions (if $N_2 < 0$) are positioned at corresponding lattice sites, so that the superposition of these two parts leads to the original configuration. Of course, there are more than one way to decompose a particular configuration, but it doesn't hinder us from carrying out the treatment below.

For the first part, we make the lattice more *sparse* while keeping its total area constant, so the number of lattice sites changes from N_0 to $2N$. The new lattice constant is $a/\sqrt{1-2\left|N_2/N_0\right|}$. Then, we rearrange the $2N$ charges on it into an alternative configuration (bottom-left in the figure). This is referred to as the *"initial state"*. For the second part, we simply smear it out into a uniformly charged surface. The surface charge density is $\left(N_1+2N_2\right)/a^2$.

Therefore, if we pick out one bound cation to study, all the other charges in the system fits in the following categories.

1. Free ions in the bulk (mean-field screening);
2. The backbone charge to which it is bound (transverse correlation);
3. All the other charges in the initial state (lateral correlation);
4. Excessive cations or anions (mean-field term arising from non-zero σ).

Hence, the Coulomb force on this cation is the sum of the forces exerted by all these charges, and its Coulomb energy (or the electrostatic part of its chemical potential) is the sum of the Coulomb energy contributed by each of these categories.

A few simplest cases are analyzed below to help the readers see how to work with the model. To simplify our discussion, we assume that both sides of the lattice are aqueous phase, so as to remove the complexity due to the dielectric discontinuity. Peptides are not involved at this stage.

3.3.1 Example calculations

$N_1 = N_2 = 0$

In this case, the surface is electrically neutral, and is in an "initial state" already. Only the first 3 out of the 4 categories listed above need to be accounted for (since there's no excessive charge).

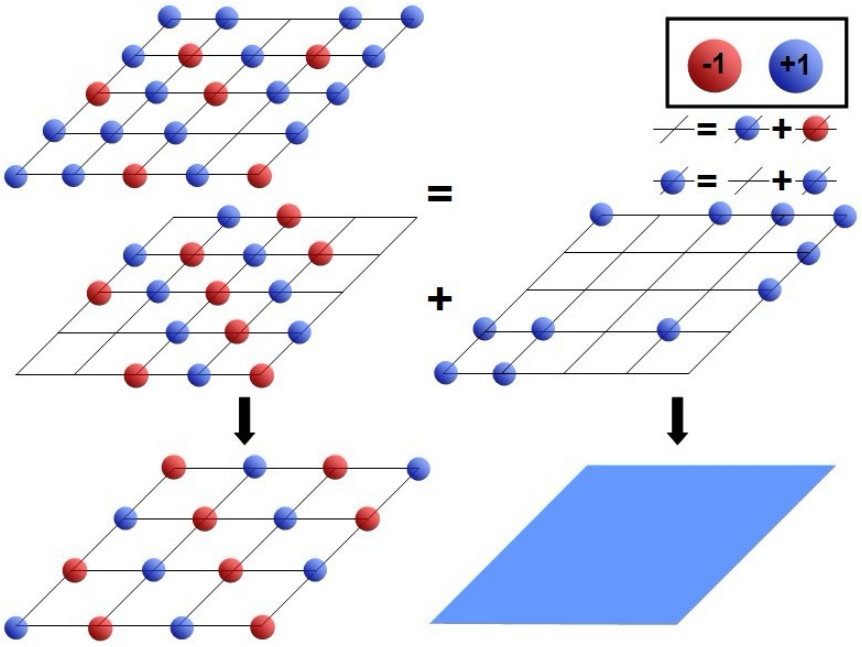

(a) positive overall σ_0

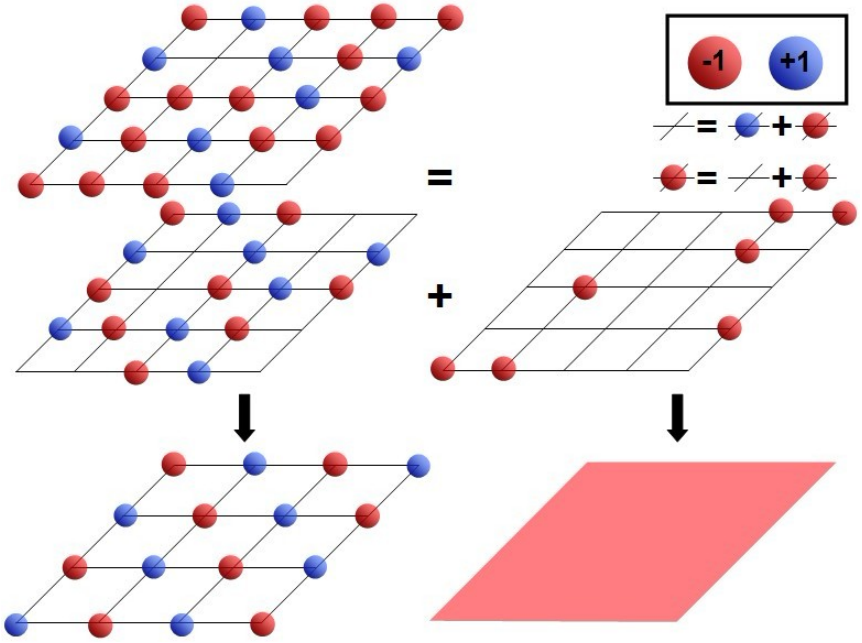

(b) negative overall σ_0

Figure 3.6: Each configuration of bound charges can be approximated by the superposition of two parts: a lattice on which positive and negative charges are alternatively arranged, and a uniformly charged surface.

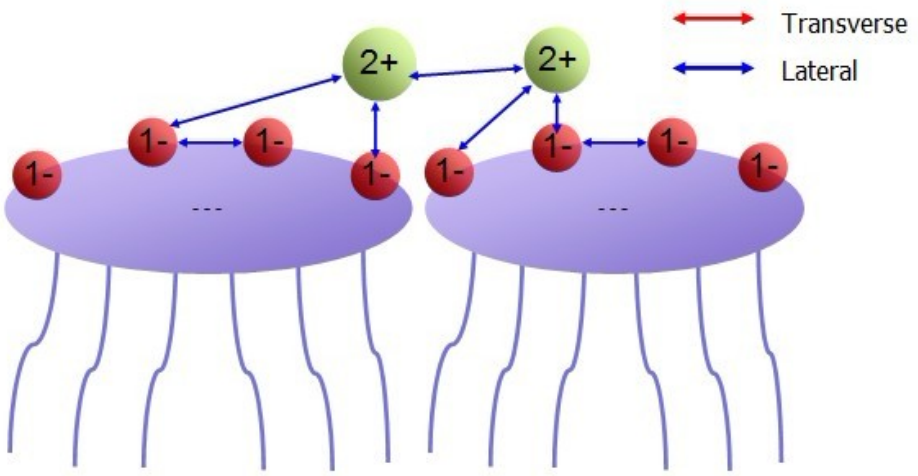

Figure 3.7: Lateral v.s. Transverse correlation

We denote the pairing energy between a backbone charge and a divalent ion as E_2, whose exact value is not of our concern for now. As to the lateral interaction energy in the initial state, we can take advantage of the regularity: for any site ($+e$ or $-e$), the nearest neighbors carry opposite charges, and the second nearest neighbors carry same charges, and so on. So, we can write it down as:

$$E_{site} = k_B T \cdot l_b \cdot \Sigma\left(a_i\right) \tag{3.11}$$

in which Σ is the electrostatic energy of one site in an initial state of lattice constant a_i due to its interaction with all other charges in the initial state. Its value is calculated by a summation explained in detail in Appendix D.

Hence, the total electrostatic energy of this system with N_0 lattice sites, among which $\frac{1}{2} \cdot N_0$ are bound with divalent ions, is:

$$E_{init} = \frac{1}{2} \cdot N_0 \cdot E_2 + N_0 \cdot k_B T \cdot l_b \cdot \Sigma\left(a\right) \tag{3.12}$$

1 excessive cation

In this case, since there is no "other" excessive cation, we still consider only the first 3 out of the 4 categories. We'll calculate the change of energy ΔE as compared to the

$N_1 = N_2 = 0$ case. Besides, considering $N_0 \gg 1$, the lattice constant of the initial state is almost a.

We denote the pairing energy as E_i, $i = 1, 2$ is the valence. Note that $E_2 = 2E_1$ may not hold. The contribution from other sites can be figured out as below. If the excessive cation is monovalent, it effectively neutralize the lattice site. The lateral correlation energy for this site will drop from $k_BT \cdot l_b \cdot \Sigma$ to 0, changing by $-k_BT \cdot l_b \cdot \Sigma$. If this cation is divalent, it effectively inverse the sign of the charge on this site, and the lateral interaction energy will also change sign, going from $k_BT \cdot l_b \cdot \Sigma$ to $-k_BT \cdot l_b \cdot \Sigma$, changing by $-2k_BT \cdot l_b \cdot \Sigma$. Hence, we can easily write the change in energy (comparing to E_{init})as:

$$\Delta E_{i,+1} = E_i - Z_i \cdot k_BT \cdot l_b \cdot \Sigma\,(a) \tag{3.13}$$

in which $i = 1, 2$ denotes for the valence of the cation.

2 excessive divalent cations

To keep our discuss concise, we assume both cations are divalent, but it's really trivial to generalize the idea to 2, or n, arbitrary cations. As above, the lattice constant of the initial state is approximated to be a.

All 4 categories of charges are present in this case. However, for the effects due to the first 3 categories, there isn't any difference i.e. we can treat the two excessive cations as independent. Beyond that, we'll have to deal with the 4th category i.e. adding the interaction between excessive cations. Because the respective positions of the two cations can basically be anywhere, the simplest treatment will be the mean-field picture i.e. to study one of the cations, smear out the other cation, so the interaction energy will have the Debye-Huckel form: $k_BT \cdot \pi l_b \kappa^{-1} \cdot \sigma^2$. Still, there is one restriction. Only one cation can bind to any one of the lattice sites, so the other cation cannot be simply smeared out over the entire surface, but the entire surface *subtracting* a certain region around the cation of interest (see Fig. 3.8), leading to a correction term $-E_{hole}$. When N_0 is very large, smearing over a area of $N_0 \cdot a^2$ or over $(N_0 - 1) \cdot a^2$ will have almost no difference, and the restriction above can be enforced by subtracting a term E_{hole}. The calculation of E_{hole} is detailed in Appendix E.

Hence, the change in energy is:

$$\Delta E_{2,+2} = 2E_2 - 2Z_2 \cdot k_BT \cdot l_b \cdot \Sigma\,(a) + k_BT \cdot \pi l_b \kappa^{-1} \cdot \left(\frac{1}{N_0 \cdot a^2}\right)^2 - E_{\text{hole}} \tag{3.14}$$

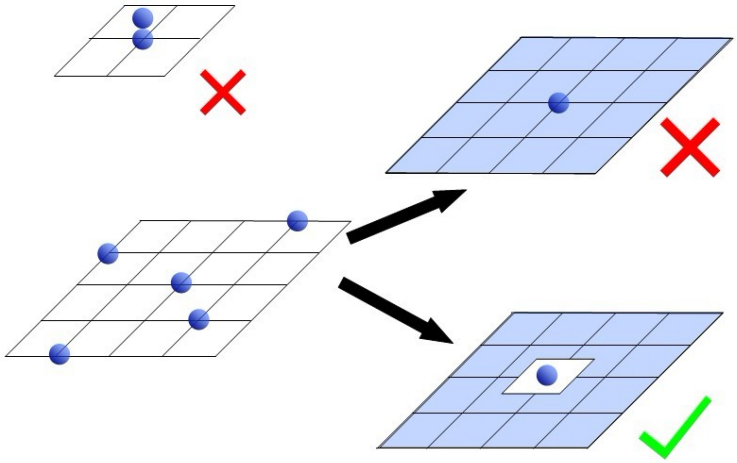

Figure 3.8: Since one lattice site can only be associated with one charged object at any given time, we have to take this into account in the calculation of mean-field effects.

$N_2 = -N_0/2$

This case, equivalence to the absence of divalent cations, is of great interest, because similar calculation can be found in earlier works [95]. As $N_2 \to -N_0/2$, $a_i = a/\sqrt{1 - 2\,|N_2/N_0|} \to \infty$. As the lattice becomes infinitely sparse, we expect $\Sigma \to 0$. Therefore, the change in energy is:

$$\Delta E_{N_2 \to -N_0/2} = -N_0/2 \cdot E_2 + k_B T \cdot \pi l_b \kappa^{-1} \cdot \left(\frac{N_1}{N_0 \cdot a^2} \right)^2 - E_{hole} \tag{3.15}$$

Notice that this is different from the energy for the same scenario in Ref. [95] by a constant only. That is, in the monovalent-only limit, our model naturally degenerate into the model in earlier works.

3.3.2 Chemical equilibrium and free energy

Now, we are ready to write down the chemical potentials and free energy in our model explicitly. In the following context, subscripts $i = 1, 2$ denote quantities associated with monovalent and divalent ions, respectively. $Z_1 = 1$ and $Z_2 = 2$ are their valences.

Chemical equilibrium

The chemical potentials of particles in the bulk are:

$$\mu_i^b(n_i) = 0.6022 n_1 \cdot \frac{4}{3}\pi r_i^3 - \frac{Z_i^2}{2} l_b \frac{\kappa}{(1+\kappa\delta_1)} \tag{3.16}$$

$$\mu_p^b(n_p) = 0.6022 n_2 \cdot \frac{4}{3}\pi v_p \tag{3.17}$$

in which $0.6022\,\mathrm{nm}^{-3} \cdot L/\mathrm{mol}$ is the conversion factor mentioned earlier. r_i is the radii of monovalent and divalent ions in the bulk, respectively. Finally, v_p is the volume of a peptide molecule.

The chemical potentials of particles binding to the surface are:

$$\mu_i^s(N_1, N_2, N_p) = \Delta(\kappa) l_b \cdot \left[- Z_i \Sigma \left(\frac{a}{1 - 2\left|N_2/N_0\right|} \right) + \frac{N_1 + 2N_2 + QN_p}{a^2} \times \left(2\pi Z_i \kappa^{-1} - \mathcal{M}_1(\kappa, a) \right) \right] - \ln(K_{I,i}) + \ln \frac{N_i'}{0.5N_0 - N_1 - N_2 - QN_p} \tag{3.18}$$

$$\mu_p^s(N_1, N_2, N_p) = \Delta(\kappa) l_b \cdot \left[- Q \Sigma \left(\frac{a}{1 - 2\left|N_2/N_0\right|} \right) + \frac{N_1 + 2N_2 + QN_p}{N_0 a^2} \times \left(2\pi Q \kappa^{-1} - \mathcal{M}_p(\kappa, a) \right) \right] + \Delta(\kappa) l_b \frac{Q}{\delta_p} - \frac{N_p \cdot (N_0 - QN_p)^{Q-1}}{(N_0 - QN_p - N_1 - N_2)^Q} \tag{3.19}$$

in which we've defined dielectric discontinuity constant $\Delta = \frac{2(\eta+\kappa d)}{2\eta+\kappa d}$, $\eta = \varepsilon_l/\varepsilon_w$. The meaning of Σ is the same as the examples above and is calculated in Appendix D. $\mathcal{M}_1$ and $\mathcal{M}_p$ are correction integrals as depicted in Fig. 3.8 and detailed in Appendix E.

By solving the equation system below:

$$\begin{cases} \mu_1^b = \mu_1^s \\ \mu_2^b = \mu_2^s \\ \mu_p^b = \mu_p^s \end{cases} \tag{3.20}$$

We can obtain a set of $\{N_1, N_2, N_p\}$. However, in real calculation, it's more convenient to choose $\{N_1/N_0, N_2/N_0, N_p/N_0\}$ as the outputs.

If $n_p = 0$, we set $N_p \equiv 0$ in Eq. 3.18, and solve the first two equations in Eqs. 3.20. If $n_2 = n_p = 0$, we further set $N_p \equiv 0, N_2 \equiv -0.5$ in Eq. 3.18, and solve the first equation in Eqs. 3.20.

Free energy

The complete form of the free energy is:

$$
\begin{aligned}
F &= F_{es} + F_{ent} + F_{corr} && (3.21)\\
F_{es} &= \Delta \cdot \pi l_b \kappa^{-1} \frac{(N_1 + 2N_2 + QN_p)^2}{N_0^2 \cdot a^4} && (3.22)\\
F_{ent} \cdot N_0 a^2 &= N_1 \ln N_1 + (N_2 + 0.5)\ln(N_2 + 0.5) + N_p \ln N_p \\
&\quad + (0.5 - N_1 - N_2 - QN_p)\ln(0.5 - N_1 - N_2 - QN_p) \\
&\quad \frac{1-Q}{Q}(1 - QN_p)\ln(1 - QN_p) \\
&\quad -N_1 \cdot \mu_1^b - N_2 \cdot \mu_2^b - N_p \cdot \mu_p^b && (3.23)\\
F_{corr}/(\Delta l_b) &= \frac{\mathcal{M}_1}{2} \cdot \frac{(N_1 + 2N_2)^2}{N_0^2 \cdot a^4} - N_p(N_0 - 0.5N_p)\mathcal{M}_p - Q(N_1 + N_2 + 0.5N_0)\mathcal{M}_1 \\
&\quad -\frac{(N_0 - N_1 - 2N_2 - QN_p)}{N_0 \cdot a^2} \cdot \Sigma\left(\frac{a}{1 - 2|N_2/N_0|}\right) \\
&\quad -[N_1 \cdot \ln(K_{I1}/\nu_1) + N_2 \cdot \ln(K_{I2}/\nu_2)]/\left(N_0 \cdot a^2\right) && (3.24)
\end{aligned}
$$

3.3.3 Choosing parameters

In this model, the parameters yet to be accurately determined are: the smallest distance for transverse correlation δ_i and δ_p, the charge Q and the volume v_p of the peptide. These parameters are taken as: $\delta_1 = 3$ Å, $\delta_2 = 2.5$ Å, $Q = 4$, $v_p = 2.5\,\mathrm{nm}^3$.

3.4 Results and Discussion

3.4.1 Ion binding

Monovalent ion only

The simplest case that our model can study is when $n_2 = 0$ and $n_p = 0$ i.e. there are only monovalent ions in the solution. Calculations based on this scenario serve as a step stone towards more sophisticated ones. Since this scenario has been extensively studied in previous works, checking whether our work is consistent with others' would help us to determine the viability of our model.

Firstly, we attempted to verify the statement of Pincus et al. that ion binding is an extra effect due to charge discretization [94]. We set out verifying that: when backbone charges are smeared out, discrete, pairwise ion binding shall disappear, and mean-field effect shall dominate, and the amount of bound ions shall asymptotically approach counterion condensation in continuous limit. We smear out the backbone charges by introducing a parameter called "partition", allowing me to modify the lattice as in Fig. 3.9.

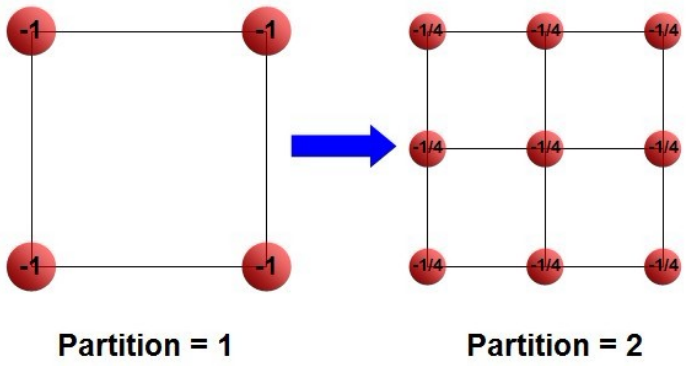

Figure 3.9: Smearing out the backbone charges to verify the consistency with results in continuous limit.

Note that "partition" need not to be an integer. We calculated with different partitions, and make the plots in Fig. 3.10.

As evident in these plots, when the partition is large i.e. the charges are better smeared out, σ_{eff} approaches the one predicted in continuous limit fairly quickly.

Furthermore, enlarging δ_1 has similar effect. See Fig. 3.10d. However, enlarging δ_1 too much won't lead to a better match, because when $E_{\text{binding}} < l_b M_1$, σ_{eff} would become significantly larger than that in continuous limit.

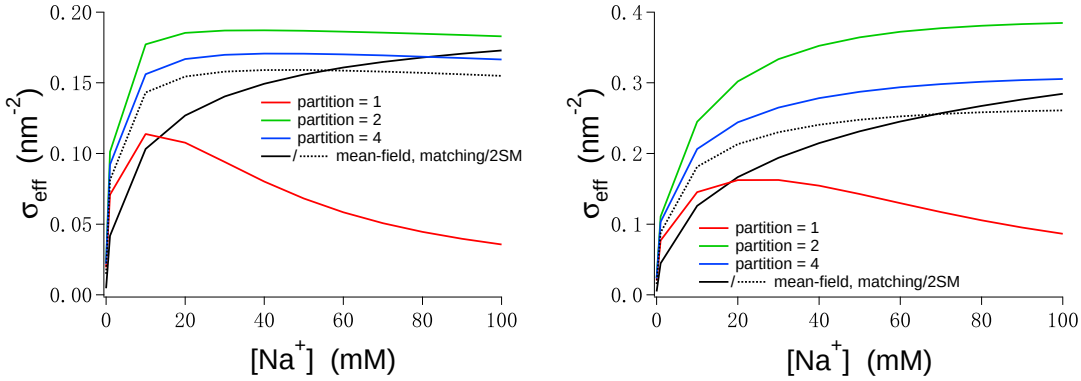

(a) $a = 2.24\,\mathrm{nm}$, $\sigma_0 = 0.20\,\mathrm{nm}^{-2}$

(b) $a = 1.49\,\mathrm{nm}$, $\sigma_0 = 0.45\,\mathrm{nm}^{-2}$

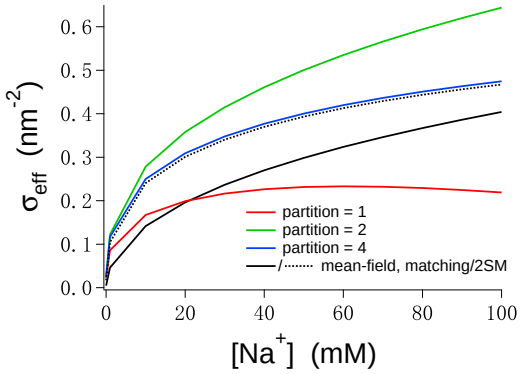

(c) $a = 0.80\,\mathrm{nm}$, $\sigma_0 = 1.56\,\mathrm{nm}^{-2}$

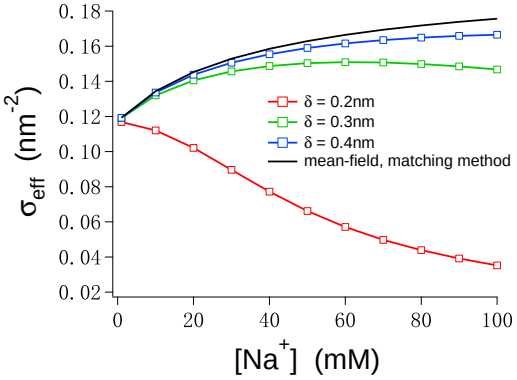

(d) $a = 2.24\,\mathrm{nm}$, $\sigma_0 = 0.20\,\mathrm{nm}^{-2}$

Figure 3.10: Binding in the absence of divalent ions, compared to counterion condensation in continuous limit calculated from 2-state model. In (a), (b) and (c), the backbone charges are gradually smeared out by increasing the "partition" number, and in (d), δ is gradually increased. In either case, the results based on our discrete model approach those calculated in the continuous limit, demonstrating the consistency.

Divalent ions added

In the case of $n_2 \neq 0$, $n_p = 0$, we chose 3 typical values of n_2 and calculated $\sigma_1/\sigma_0 = N_1/N_0$, $\sigma_2/\sigma_0 = N_2/N_0 + 0.5$ and $-\sigma_{eff}/\sigma_0 = N_1 + 2 \cdot N_2$. Results for $n_2 = 0$ are also presented for comparison. The results are shown in Fig. 3.11.

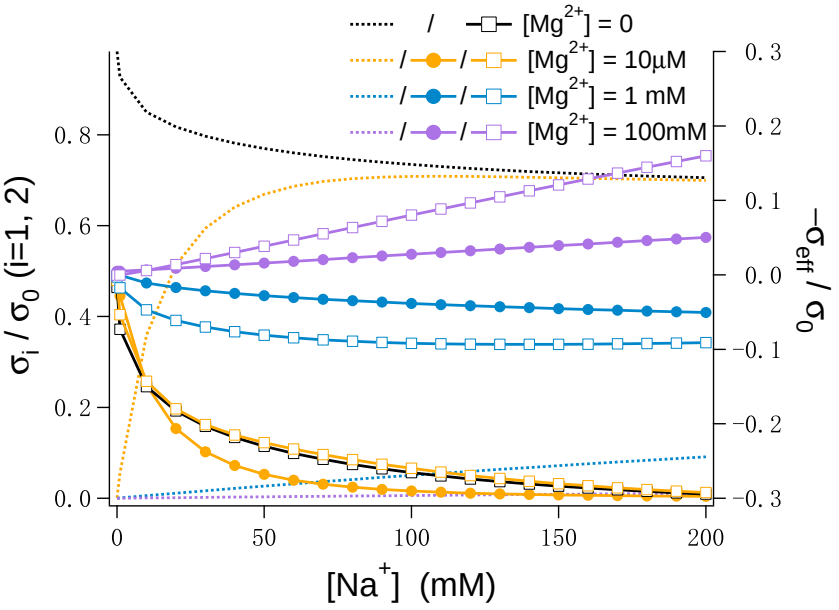

Figure 3.11: Surface charge density in the absence of peptides. At small n_2, σ_2 approaches 0 and ion binding approaches the $n_2 = 0$ limit. As n_2 increases, so is σ_2, but overcharging is not pronounced, consistent with experimental works e.g. Ref. [80].

Our results reveals that:

1. When $n_2 = 10\mu M \ll n_1$, σ_2 asymptotically approaches 0, and σ_1 approaches the value in the monovalent-only case. Since the monovalent-only case is calculated based on models in earlier works, it confirms that our results are consistent with those works in the limit of $n_2 \to 0$. Interestingly, the value of σ_{eff} for $n_2 = 10\mu M$ and $n_2 = 0$ coincide very well in a very wide range of n_1 values, indicating that ion binding in low n_2 limit is dominated by mean-field effect.

2. σ_2 increases as n_2 increases, eventually resulting in overcharging. However, there were no overcharging when $n_2 = 1$ mM, and even for 100 mM of Mg^{2+}, which is a very high concentration even in lab experiments, the overcharging is still merely

10% - 20%. However, previous experimental works indicates that overcharging does not occur (surface potential is still negative) even when $n_2 = 10$ mM [80], which is qualitatively consistent with our calculation.

Excessive lateral pressure

Firstly, we calculated the lateral pressure $\Delta\Pi$ as a function of n_1 for the same set of n_2 values above, and present the results in Fig. 3.12.

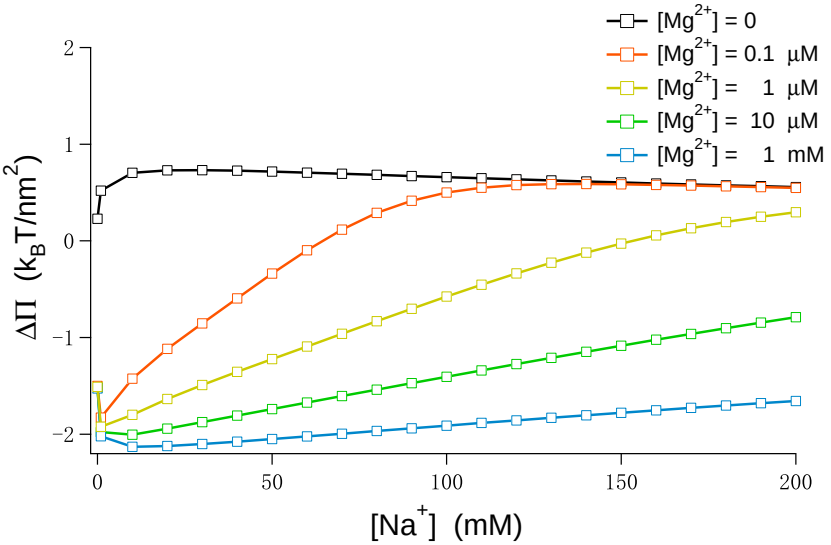

Figure 3.12: Excessive lateral pressure $\Delta\Pi$ in the absence of peptides. Without divalent ions, $\Delta\Pi$ is always larger than 0 (outward), and it stays so when $n_1 \gg n_2 \approx 0$. At higher n_2, $\Delta\Pi$ becomes negative (inward), indicating that the divalent ions are stabilizing the LPS leaflet.

It can be seen that:

1. In the absence of divalent ions, $\Delta\Pi$ is always positive (outward), indicating the LPS leaflet is highly unstable without the bridging effect of divalent ions.
2. In low n_2 limit, $\Delta\Pi$ asymptotically approaches the monovalent-only case at larger n_1, which is a natural result of the ion-binding behavior discussed earlier.
3. A relatively low concentration of divalent ions would lead to a negative $\Delta\Pi$, indicating how effective divalent ions can stabilize the LPS leaflet.

4. As n_2 goes higher, the stabilization does not get significantly better. The decrease in $\Delta\Pi$ is roughly the same when n_2 change from 1 μM to 10 μM (10^1 fold) and from 10 μM to 100 mM (10^4 fold).

5. The absolute value of $\Delta\Pi$ generally decreases as n_1 increases because of the screening.

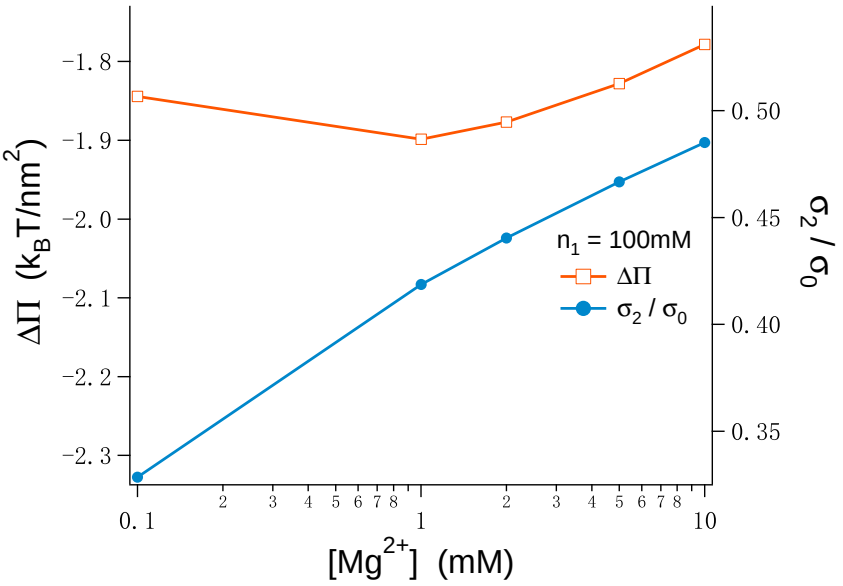

Figure 3.13: $\Delta\Pi$ varies with n_2. A minimum at $n_2 \approx 1$ mM can be seen.

3.4.2 Competitive binding

Now we move on to the central subject of our study: when $n_2 \neq 0$ and $n_p \neq 0$, does our model predict competitive binding? Fig. 3.14 gives a confirmative answer. Note that its vertical axis is chosen to be "Portion of occupied sites" which is σ_2 for divalent ions and $Q \cdot \sigma_p$ for peptides, instead of using σ_p itself [6]. It clearly shows that, for all the chosen values of n_2, as n_p goes up, more and more divalent ions leave the LPS leaflet as peptides moves in. At high Mg^{2+} concentration of $n_2 = 100$ mM, peptide can hardly bind to the surface, which is consistent with the result in Ref. [92]. At lower Mg^{2+} concentration, however, peptide can easily bind to the surface, and occupy 5% to 30% of the binding sites in physiological conditions (see Fig. 3.16).

[6] Although there's not much difference in a logarithm graph, we do it for the sake of consistency with other figures

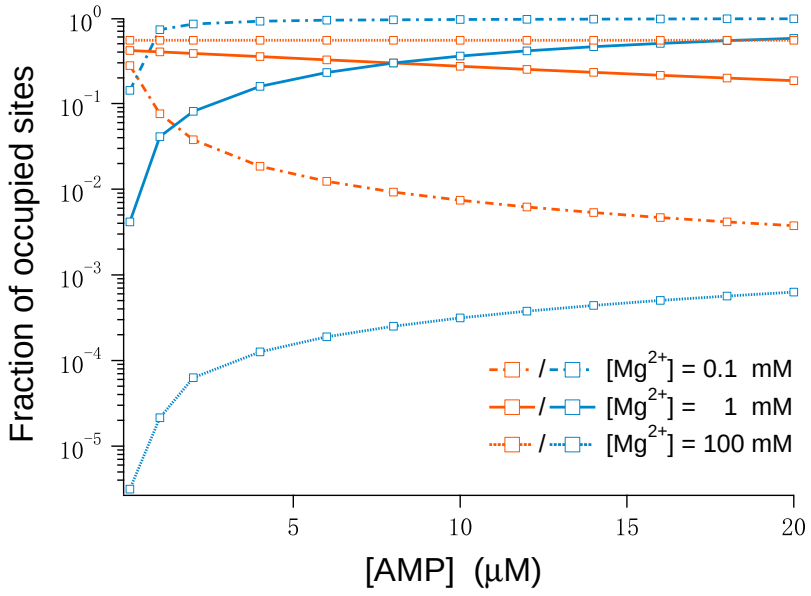

Figure 3.14: Competitive binding between peptides (blue) and divalent ions (orange). As n_p increases, more and more bound divalent ions leave the surface, being replaced by the peptides. A higher n_2 value can hinder, but not eliminate, such replacement.

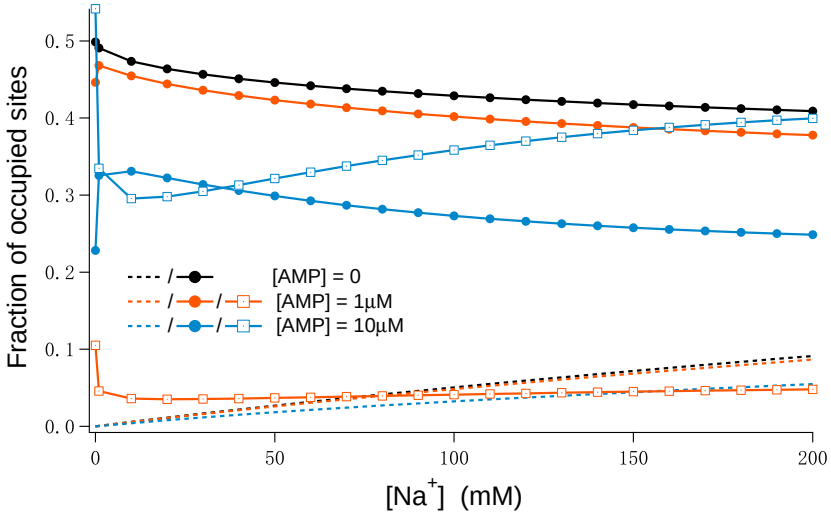

Figure 3.15: Concentration of Na^+ (dashed lines), Mg^{2+} (solid circles) and peptide (empty squares) showing competitive binding. A higher n_1 gives the peptides some edge in the competition, but generally the effect is not pronounced.

3.4.3 Excessive lateral pressure

Competitive binding has been hypnotized, even reported to have been observed, in other works like Ref. [92] and [95], and is not too much of a big news for us. What we'd like to see is how the binding of peptides affects the excessive lateral pressure $\Delta\Pi$ that reflexes the stability. As we can see in Fig. 3.16, at relatively low concentration of Mg^{2+} ($n_2 < 1\,\mathrm{mM}$), the excessive lateral pressure becomes strongly outward even with moderate n_p, indicating that the LPS leaflet becomes highly unstable, easier to permeate and rupture, in the presense of peptides. It evidently shows that *cationic peptides, via competitively bind onto the LPS layer, can destabilize it by making its constituent molecules tend to break away from each other instead of sticking together.* However, at higher n_2, the divalent ions inhibit the peptides from binding, and the lateral pressure remains negative and largely unchanged as n_p increases, consistent with the results in experimental works (e.g. Ref. [92]).

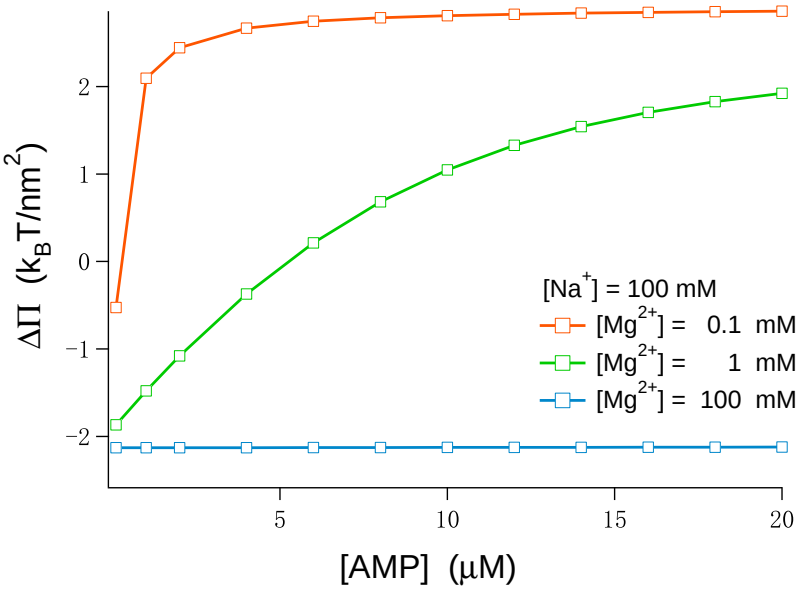

Figure 3.16: Change in excessive lateral pressure due to the binding of peptides. At lower n_2, a little peptides in the bulk can convert the excessive lateral pressure from inward to outward, destabilizing it. At higher n_2, the LPS leaflet is more resistant to such destabilization.

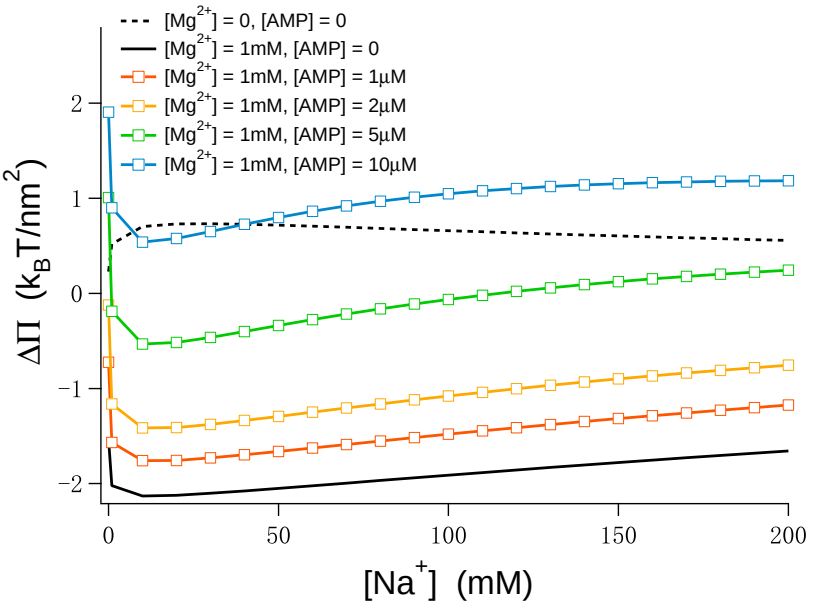

Figure 3.17: Excessive lateral pressure in the presence of peptides. The destabilizing effect of the peptides is shown to be quite strong, and $\Delta\Pi$ can even be more positive than the monovalent-only case.

3.4.4 Stabilization effect of divalent ions

"Competition" is a two-way concept. On one hand, the presence of peptides forces divalent ions to leave the LPS leaflet, making it more unstable; on the other hand, the presence of divalent ions prevent too much peptide from binding, protecting the LPS layer and contributing to the inhibition of AMPs. We'd love to explicitly see how increasing the concentration of divalent ions would allow the LPS leaflet to be more resistent to the attack of AMPs. The results are presented in Fig. 3.18.

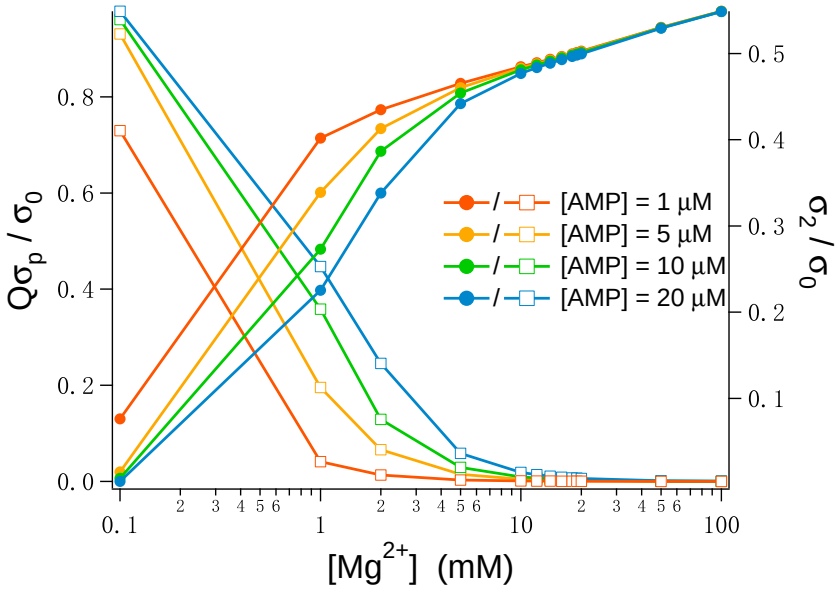

Figure 3.18: Competitive binding between peptide (empty squares) and divalent ions (filled circles) as n_2 increases. It presents what's already evident in Fig. 3.16 and Fig. 3.17 from another perspective. At higher n_2, peptide binding is not pronounced even at fairly high n_p, indicating the protection, or "immunity", against AMPs brought about by divalent ions.

3.4.5 Effect of Q

The last subject we're interested in is: how the value of peptide charge Q affects its effectiveness in terms of increasing $\Delta\Pi$. As shown in Fig. 3.19, for $n_2 = 1\,\text{mM}$, which is typical in physiological environment e.g. blood, $Q \leq 3$ is hardly effective. This explains why the Q value of most AMPs is 4 to 6.

Some may find that Fig. 3.19 indicates "the larger Q is, the better", which is contradictory to some other works, such as Ref. [15] and [101], that indicates an optimized peptide charge of $Q = 4$, above which the effectiveness of AMPs (against phospholipid membrane) will go down. Part of the reason is that in those works, the area occupied by each peptide on the membrane is considered as roughly fixed, while in our work, the number of binding sites occupied by a peptide is assumed to be always equals to Q.

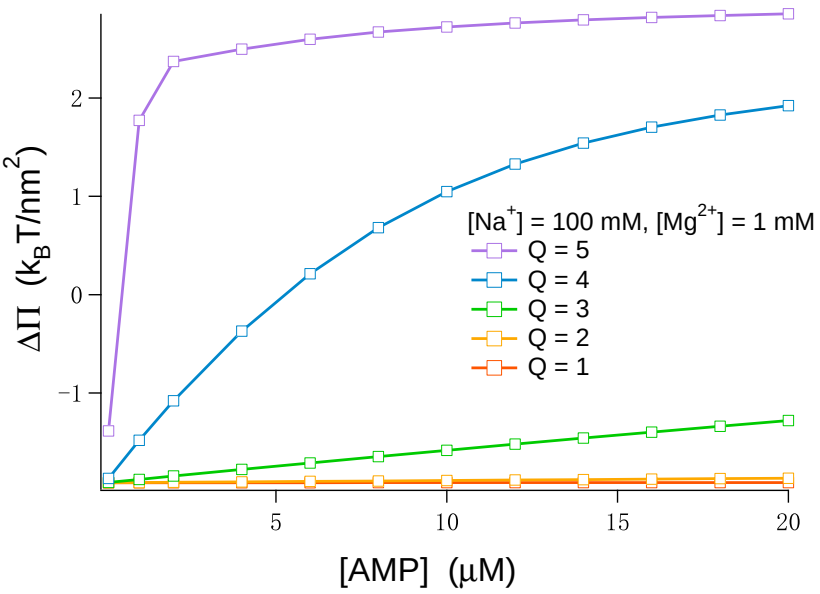

Figure 3.19: Impact on lateral pressure for peptides with various charges. For $n_2 = 1\,\mathrm{mM}$, typical in physiological environment, $Q \leq 3$ is hardly effective. This explain the typical charges carried by AMPs is from 4 to 6.

3.5 Conclusions

In this work, we've established a coarse-grain model of the interaction between ions, cationic peptides and a LPS leaflet, based on which we predicted competitive binding between divalent ions and peptides, and the resulting change in lateral pressure that leads to the destabilization of the leaflet. Our result is, at least qualitatively, consistent with the experimental works by others.

Chapter 4

Conclusions and Prospect of Future Works

So far, we have presented the details of the research we've been doing. It's time to give a more conclusive summarize of our work and, more importantly, discuss what can be done in the future based on these works.

4.1 What Has Been Done

In this thesis, we have tackled two problems: electrostatic influence on structural preference of lipid aggregation, and the stability of LPS as affected by ions and cationic peptides. Though we have, to some extent, solved these two problems and yielded some results, it may not be our greatest triumph. What is more significant than solving two particular problems is our contribution to a set of theoretical formulations and computational techniques, a system of methodology, that can be applied to solve countless problems that shares some features with those we've studied here.

By putting the two problems together and examine them, we can see the features they share:

1. The system consist of two parts. The first part is an aggregation of amphiphilic molecules in water, at least some of these molecules carries net charges, forming a two-dimensional charged surface. The second part is the aqueous environment around

it, containing charged objects i.e. ions from dissolved salts and possibly charged biomolecules (for convenience, we refer to them collectively as "ions" in the following context). The property of the system depends heavily on electrostatic interaction.

2. Most of the ions stays in the aqueous environment, effectively screens the Coulomb force between surface charges.

3. Some of the ions condense to the vicinity of the charged surface, altering the effective surface charge density.

4. The surface charges along with condensed ions form a 2D interacting gas/liquid/crystal, in which correlation and fluctuation plays a crucial role in its property, and hence the property of the entire system.

5. The hydrophobic part of the aggregation has quite different dielectric constant against water, which affects the strength of electrostatic force.

Therefore, to summarize the works in this thesis with only one sentence, we've been studying "the electrostatic force in two-dimensional systems self-assembled from amphiphilic molecules in water". There are countless implements of such systems in cellular life-forms, and countless questions can be raised regarding the physical properties of these systems. Surely, not all of these properties can be ascribed to electrostatic interaction, but as we've mentioned earlier, electrostatic interaction is more flexible, more "tunable", than other interactions commonly involved in biological physics like van der Waals force and hydrophobic force. It's expected that electrostatic interaction will play a central role in many biological and physiological phenomena. Therefore, though we've only studied two particular problems out of a large family of problems, the methodology we developed in the process would contribute to the solving of them all. The methodology can be summarized as below:

1. Find a proper way to depict the charged surface.

2. Consider each species of ions in the aqueous environment as being in one of the two states: either "in the bulk" or "condensed near the surface", and assume the two species to be in chemical equilibrium.

3. For each species of ions, analytically express the chemical potential for the two states. The chemical potential for the condensed ions should be a function of the density of them on the surface.

4. Equating the chemical potential of the two state for each species, and we arrive at a system of equations. Numerically solve the system to determine the density of each species on the surface.

5. Calculate the free energy, which is a function of the surface ion densities just solved for and ion concentration in the aqueous environment.

6. Calculate quantities by numerically taking derivatives of the free energy.

How good is this method comparing to other methods? A completely analytical approach is less fruitful, because the analytical solution of P-B equation, or even D-H equation, is extremely involving, even impossible, in the presence of complex geometries and dielectric discontinuity, say nothing of charge fluctuation. Numerically solving P-B equation, as in Ref. [15] and [67], would yield more accurate result than our approach, but it'll consumes much more computational resources. On the other hand, "hard-core" numerical methods, especially Monte-Carlo and molecular dynamic simulations, are brute-force ways to address these problems, and usually yield satisfactory result. Besides, the simulations are done in finite systems, and the results suffers significantly from finite-size effect. To avoid the problem, besides choosing appropriate boundary conditions, the system should be made larger, which would greatly increase the computational cost of these simulations. Furthermore, in previous works that address similar problems as we've addressed in the thesis, such as Ref. [59] and Ref. [67], the confidence in computational power leads to complication of the model, preserving many details of the corresponding realistic systems, leading to a blur of the physical picture. Our method keeps a balance between two pairs of conflicting expectations: firstly, the semi-analytical calculation analytically modeled each of the contributing effects, and numerically avoided involving algebraic and analytical solving of equations; secondly, our modeling accounted for the most dominant factors, producing reasonably good results while avoid over-complicating the picture.

Despite the general idea in the ways we tackle these two problems respectively is similar, we do introduced some variation. In the first problem, we modeled the charged property of the (mixed) phospholipid monolayer in a continuous manner, treating both the backbone charges and the condensed ion layer as continuous, and mathematically accounted for the fluctuation/correlation effects with continuous functions. It's because typical phospholipid aggregation at physiological temperature is in a more "fluid-like" phase. On the other hand, we considered the individual lipid molecules as discrete objects, and treated electrostatic force as an addition to the 3 types of intermolecular forces. It's because those 3 types of forces, despite much less "tunable", determines the elastic property of the monolayer more dominantly. In the second problem, we modeled the charged property of the LPS

leaflet with a lattice, and utilized the concept of "binding" in the treatment of electrostatic effects, because the structure of an LPS leaflet at physiological temperature is much more organized. On the other hand, we didn't consider other biophysical properties of LPS molecules or other intermolecular forces between them, because the elastic property of the leaflet is less of our concern (stabilizing/destabilizing is merely reflected in $\Delta\Pi$). Therefore, the problems we chose to attack are actually rather representative.

4.2 What To Do

In scientific research, having an idea doesn't necessarily means having the resource to actually carry it out. By the end of my life as a master graduate student, there are ideas in my mind that are yet to be executed, there are questions I'm curious at that are yet to be answered. Therefore, to conclude this thesis, I'd like to gaze beyond the horizon along with the readers, to present a "to-do list", in hope that some of us will be able to implement and verify these ideas, and further unveil the answer to the questions we raised and answered (to some extent) in this thesis.

4.2.1 Lipid polymorphism: a more balanced model and application to reality

Both electrostatic bending of a phospholipid bilayer and the polymorphism of phospholipid – its capability of forming structures other than bilayer – has been studied for decades. Indeed, the very numerically-intensive approach developed by Taheri and Ha [67] has allowed us to perform reliable calculations to determine quantities such as spontaneous curvature. Despite much simpler, our approach has less quantitatively predictive power than theirs. Therefore, the first question is:

Can we make it more powerful while keep the computational cost under control?

To answer this, let's examine some of the approximations we used again.

1. To account for charge correlation, we used the Green's function of D-H equation for a plane ($c = 0$) to approximate that for a slightly cylindrically curved surface ($c \approx 0$). This is hardly convincing. Although the electrical potential for the cylindrical

geometry has long been solved (see Appendix A), the Green's function is yet to be explicitly presented in any literature as far as we know. Therefore, we shall solve for it and use it in the place of planar Green's function.

2. We ignored lipid demixing, assumed that the overall σ_0 distributes evenly on each of the lipids. Were we only interested in the general bending of a monolayer/bilayer, this would be more acceptable, because demixing is not pronounced for a PG/PS mixed monolayer [67]. However, in order to study the distribution of local tension, demixing must be taken into account.

3. We haven't calculated the electrostatic influence on Gaussian curvature k_G in our work, which is certainly of interest. We can accomplish this by solving the D-H equation with spherical boundary condition, which should take a similar form of the solution for a finite sized ion.

By adding more sophistication into our model, the computational cost is expected to raise to some extent. However, we shall keep it in mind that the strength of our model lies in its modest computational cost, and we should figure out which effects and details are most dominant in determining the polymorphic properties, and avoid spending resource on accounting for the subdominant effects.

However much we perfect a model, it's not much more than a toy if we don't apply it to study reality. Therefore, the second question should be:

How can we apply our work to realistic problems?

In the first chapter, we've already listed an abundance of biological, physiological and clinical processes in which the electrostatically tuned polymorphic behaviors of lipids play a central role. The list includes cell fusion and fission, protein-membrane and peptide-membrane interactions, and drug delivery. Contributing to the clarifying of these problems should be the ultimate goal.

In order to accomplish this, at least one thing can be done: to define the "stability" of a mixed phospholipid bilayer. If this can somehow be defined, or depicted by some quantity, we can address problems like drug delivery. Excessive surface tension as used in Chapter 3 is not appropriate here, because an inward surface tension would make the lipids stick closer together while making the bilayer tend to break into inverse-hexagonal structure. LPS doesn't have the same problem, because the polysaccharide chains would deny LPS from forming inverse-hexagonal structure.

4.2.2 Peptide-LPS interaction: a more realistic model and further studies

The works presented in Chapter 3, on the other hand, is relatively new. Despite an abundance of experimental data, computational study of the LPS leaflet, especially the action of AMP against it, has only been carried out recently, most of which are based on Monte-Carlo method. There's much out there to be done. However, before going too far, let's ask ourselves:

How well does our model reflex the realistic scenario?

I find at least the following directions are worthy of trying out:

1. Adopt a lattice structure other than square. Although we've justified the square lattice, we admit that we choose it mainly for convenience. If another structure is proven to be more appropriate, we should happily switch to it. However, B.-Y. Ha (in private communications) stated that the LPS leaflet is more or less fluid-like at body temperature, so approximating the spacial distribution of charged groups by a convenient square lattice is good enough.

2. Allow charged groups to distribute both on and out of the hydrocarbon-water interface. The interface shall locate around the sugar-phosphate part of lipid A, so the carboxyl groups on KDO, as well as other phosphate groups possibly existing in core oligosaccharide, would be out of the interface and completely immersed in water, affecting the strength of electrostatic interaction. At low salt concentration, the difference could be quite pronounced.

3. Account for ionic association more accurately. For example, add the concentration of $MgCl^-$ into the effective n_1.

4. Determine the parameters in a more reliable and convincing way.

5. Depict the sizes and charge distribution of peptides in a more realistic way: the Q charges don't necessarily lie exactly on top of Q binding sites.

After improving the model, we'd naturally ask:

What else can we do with it?

One of the things I can think of is: to calculate the electrostatic influence on a_0 value of LPS. The molecular model used in chapter 2 can readily be migrated here. The γ value and τ value are the intrinsic properties of oil-water interface and hydrocarbon chains, respectively, and won't be too different from the values adopted in chapter 2. Some experimental results are presented in Ref. [93] and [23].

Another more practical problem to tackle is the partition of AMPs between the LPS leaflet and the cytoplasmic membrane (Fig. 4.1). According to this thesis, some AMP molecules have to stay on the LPS leaflet to continuously destabilize it. If there's plenty of AMPs in the aqueous bulk of the system, this isn't too much of an issue. However, when there's only a limited number of AMP molecules in the surrounding (comparing to the number of target gram-negative bacteria), depletion may occur, and the LPS leaflets are expected to accelerate the depletion. This may have a negative impact on the efficiency of AMPs in killing Gram-negative bacteria. Furthermore, similar approach can be extended to study Gram-positive bacteria, because teichoic acid molecules found on the surfaces of their cell walls are also negatively charged. Much work has been done on how AMPs attack the cytoplasmic membrane of bacteria, but the differences brought about by the cell wall are yet to be systematically investigated. Based on the pioneering work presented in this thesis, we can attempt to establish a much more integrated and realistic picture of the mechanism of AMPs killing bacteria.

Despite all the questions we've managed to answer, there are many more questions out there, many of which are exhilarating, that are calling for an answer. We're glad that our works have contributed a few of the many pieces of the puzzle that, once completed, will be among the most brilliant pictures in the human history.

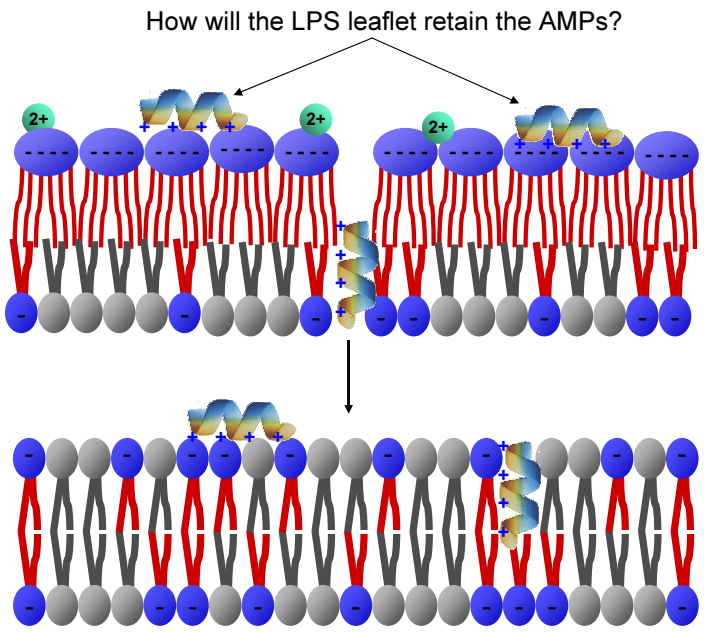

Figure 4.1: Partition of AMPs between the cytoplasmic membrane and the LPS leaflet. The LPS leaflet may deplete AMP molecules surrounding a bacterium, and may enhance its resistance to these peptides.

APPENDICES

Appendix A

Analytical Solution of PB Equation and DH Equation

A.1 Solution of Debye-Hückel equation

A.1.1 Dielectric Discontinuity

The solutions of partial differential equations depend heavily on boundary conditions. In electrostatic problems, one of the most common origin of boundary conditions is dielectric discontinuity, which means at least two bulks of mediums with different dielectric constants are present in the system of interest, in touch with each other and separated by an interface.

In the bio-membrane systems we studied in this thesis, the two mediums are typically water with $\varepsilon = 80$ and the hydrocarbon region of the membrane with $\varepsilon = 2$. In this case, $\varepsilon_l/\varepsilon_w \approx 0$. It's easy to see that the electrostatic field in the water produced by a charge on such an interface is around **twice** as strong as that produced by one completely immersed in water.

A.1.2 Point charge

For a point charge Q immersed in aqueous solution of 1-1 salt with Debye length κ^{-1}, we can solve Eq. 1.12 in spherical coordinate, knowing that the solution should be isotropic i.e. a function of r only, and find:

$$\Psi(r) = \frac{Q}{4\pi\varepsilon}\frac{\exp(-\kappa r)}{r} \tag{A.1}$$

That is, beside the $1/r$ decay of the potential, there is an extra, exponential factor that makes the decadence much faster. This is obviously the screening effect of counterions. A larger κ leads to a steeper decay as we expected. Interestingly, the form in A.1 is identical to "Yukawa potential", $\Psi(r) \propto \exp(-mr)/r$, in nuclear physics, describing a interaction carried by massive boson. Inverse Debye length κ is analog to the mass of the boson.

Eq. A.1 shows that at a distance κ^{-1} from a point charge, the electrical potential is $1/e$ times the value should there be no counterion screening. Besides, a spherical shell of radius κ^{-1} around the charge contains more counterion than shells of any other radii. These can be seen as intuitive way of interpreting κ.

For a finite-size sphere with a uniformly charged surface, Eq. A.1 can be generalized into:

$$\Psi(r) = \frac{Q}{4\pi\varepsilon}\frac{\exp(\kappa a)}{1+\kappa a}\,\frac{\exp(-\kappa r)}{r} \tag{A.2}$$

A.1.3 Plane: electric double layer

Solving Eq. 1.12 for an infinite plane with uniform charge density σ_0 coinciding with the x-y plane gives [52]:

$$\psi(z) = \varphi(0)\, e^{-\kappa z} \tag{A.3}$$
$$\psi(0) = \frac{2\pi\sigma_0}{\varepsilon\kappa} \tag{A.4}$$
$$\Psi(0) = 2\pi\sigma_0 l_b \kappa^{-1} \tag{A.5}$$
$$n(z) = n_0 e^{-\Psi(z)} \tag{A.6}$$

By looking at Eq. A.4, we notice that such linear relationship between potential and surface charge density is quite analogous to a capacitor, namely, a double-plate capacitor with plate separation κ^{-1}.

Such system, with one layer of charge fixed on a surface plus another layer of charge in the close affinity (κ^{-1}) of the surface, is sometimes referred to as *electric double layer* [52].

Here, we assume that both sides of the surface are surrounded by the same type of medium. If, as in bio-membrane, the surface coincides with a dielectric discontinuity and the medium on $z < 0$ side is far smaller than on the $z > 0$ side, the electrical potential (on the $z > 0$ side) will be twice higher.

A.1.4 Flat Membrane: dielectric discontinuity

Consider a flat membrane, abstracted as a slab with finite thickness d, is immersed (from both sides) in water. One of the surfaces carries a uniform charge density σ_0 while the other surface is electrically neutral. Therefore, there are two surfaces on which *varepsilon* is discontinuous. The electrical potential, as produced by the charged surface in the water it faces, is given below:

$$\Psi(0) = 4\pi\sigma_0 l_b \kappa^{-1} \cdot \frac{\varepsilon_l + \varepsilon_w \kappa d}{2\varepsilon_l + \varepsilon_w \kappa d} \tag{A.7}$$

Because, when the electric field penetrates into the membrane, the electric field pointing into the aqueous phase will become weaker (so as to keep the difference of $\vec{D}$ across the charged surface unchanged), making the electric potential in the aqueous phase smaller. Between $\varepsilon_l \ll \varepsilon_w$ and $\varepsilon_w \ll \varepsilon_l$, the difference is a factor of 2.

A.1.5 Cylindrical boundary

Consider a cylindrically bent membrane, whose two monolayers carries charge density σ_a and σ_b, and have curvature radii a and b on their charged surface, and immersed in 1-1 salt solution of inverse Debye length κ_i and κ_o, respectively. Solving Debye-Huckel equation gives [62]:

$$\psi(r < a) = \frac{4\pi\sigma_a}{\kappa_i} \cdot \frac{I_0(\kappa_i r)}{I_1(\kappa_i a)} \cdot \frac{\frac{\varepsilon_l}{\varepsilon_w}\left(\frac{\sigma_b}{\sigma_a \kappa_o a} + \frac{1}{\kappa_o b}\right)\frac{K_0(\kappa_o b)}{K_1(\kappa_o b)} + \ln\left(\frac{b}{a}\right)}{\frac{\varepsilon_l}{\varepsilon_w}\frac{1}{\kappa_o b}\frac{K_0(\kappa_o b)}{K_1(\kappa_o b)} + \frac{\varepsilon_l}{\varepsilon_w}\frac{1}{\kappa_i a}\frac{I_0(\kappa_i a)}{I_1(\kappa_i a)} + \ln\left(\frac{b}{a}\right)} \tag{A.8}$$

$$\psi(r > b) = \frac{4\pi\sigma_b}{\kappa_i} \cdot \frac{K_0(\kappa_o r)}{K_1(\kappa_o a)} \cdot \frac{\frac{\varepsilon_l}{\varepsilon_w}\left(\frac{\sigma_a}{\sigma_b \kappa_i b} + \frac{1}{\kappa_i a}\right)\frac{I_0(\kappa_i a)}{I_1(\kappa_i a)} + \ln\left(\frac{b}{a}\right)}{\frac{\varepsilon_l}{\varepsilon_w}\frac{1}{\kappa_o b}\frac{K_0(\kappa_o b)}{K_1(\kappa_o b)} + \frac{\varepsilon_l}{\varepsilon_w}\frac{1}{\kappa_i a}\frac{I_0(\kappa_i a)}{I_1(\kappa_i a)} + \ln\left(\frac{b}{a}\right)} \tag{A.9}$$

in which functions $I_n(x)$ and $K_n(x)$ are modified Bessel function of the first and the second kind, respectively. Obviously, in the limit of $\frac{\varepsilon_l}{\varepsilon_w \kappa d} \to 0$, the last factor of each

expression drops. And in the limit when $b > a \gg b - a > 0$, which resembles an almost flat membrane, both Eq. A.8 and Eq. A.9 approaches the flat membrane case: Eq. A.7.

By writing this in terms of curvature (for $c < 0$, $a = 1/c$ and $b = 1/c + d$; for $c > 0$, $a = 1/c - d$ and $b = 1/c$), and do an integral over σ to obtain the free energy per area, which is used in chapter 2.

We can expand the potential for small curvature $c = 2/(a + b)$:

$$\psi \approx \psi_0 + c \cdot \psi_1 + c \cdot \psi_2 \tag{A.10}$$

Set $\sigma_a = 0$, $b = a + d$, $\kappa_o = \kappa_i = \kappa$, and expand ψ_0, ψ_1 and ψ_2 for small $x = \varepsilon_l/\varepsilon_w \kappa d$ to the leading order, we have:

$$\psi_0 = \frac{4\pi\sigma_b}{\varepsilon_w \kappa}\left(1 + \frac{x}{\kappa d}\right) + O\left(x^2\right) \tag{A.11}$$

$$\psi_1 = \frac{2\pi\sigma_b}{\varepsilon_w \kappa^2}\left[(\kappa d - 1) + \frac{x}{\kappa d}\right] + O\left(x^2\right) \tag{A.12}$$

$$\psi_2 = \frac{3\pi\sigma_b}{2\varepsilon_w \kappa^3} + O\left(x^2\right) \tag{A.13}$$

A version without dielectric discontinuity can be found in Ref. [60], which is consistent with here.

A.2 Solution of Poisson-Boltzmann equation

We only discuss the solution of the (full) PB equation for a uniformly charged surface immersed in 1-1 electrolyte solution. By solving 1.12, it's found that:

$$\Psi(z) = 2\ln\left(\frac{1 + \gamma e^{-\kappa z}}{1 - \gamma e^{-\kappa z}}\right) \tag{A.14}$$

in which the dimensionless γ is given by

$$\gamma = \sqrt{1 + (\lambda\kappa)^2} - (\lambda\kappa) \tag{A.15}$$

By setting $z = 0$, we find the surface potential to be

$$\Psi_s = -4 \arctan^{-1} \gamma \tag{A.16}$$

At large z, by using $\ln(1 \pm x) = x \mp x^2$, we find:

$$\Psi \approx -4\gamma \exp(-\kappa z) \tag{A.17}$$

Appendix B

Charge Correlation and Fluctuation in Continuous Limit

The following results are mainly taken from Ref. [75]. The scenario is the same as described in section A.1.4. The fluctuation-induced, correlation-associated surface free energy density is given by:

$$\mathcal{F}_{corr} = \frac{1}{2}\int \frac{d^2\vec{q}}{(2\pi)^2}\left\{\ln\left[1+\chi\beta\phi\left(\vec{q}\right)\right]-\chi\beta\phi\left(\vec{q}\right)\right\} \tag{B.1}$$

which takes the form of an inverse Fourier transform. χ is related to the amount of charge presented on the plane:

$$\chi = \sigma_0 + \sigma_1 + 4\sigma_2 = \frac{1}{2\pi l_b \lambda} \tag{B.2}$$

and ϕ describes the electrostatic interaction for charges on the interface:

$$\beta\phi\left(\vec{q}\right) = \frac{4\pi l_b}{\sqrt{\kappa^2+q^2}+\eta q}\left[1+\xi\left(\xi-1\right)\frac{e^{-2qd}}{1-\xi^2 e^{-2qd}}\right] \tag{B.3}$$

in which:

$$\eta = \frac{\varepsilon_l}{\varepsilon_w}, \xi = \frac{\varepsilon_w\sqrt{\kappa^2+q^2}-\varepsilon_l q}{\varepsilon_w\sqrt{\kappa^2+q^2}+\varepsilon_l q} \tag{B.4}$$

Appendix C

Charges in the Vicinity of a Dielectric Discontinuity

Much results can be found in the literatures regarding the electrostatic property of two charges both located on the interface of two mediums with different dielectric constant, or a charged surface coinciding with such an interface [62] [75] [67]. Comparatively, less work has been done on charges locates in the vicinity of such an interface, despite the appearance of such distribution in many biophysical scenarios. For example, in the phospholipid aggregation we studied in chapter 2, the net charge of a phospholipid molecule can locate in its headgroup, completely immersed in water, away from the hydrophilic/ hydrophobic boundary. For an LPS molecule, the anionic groups in the oligosaccharide part obviously can be quite faraway from the hydrophilic/ hydrophobic boundary. In these cases, the approximation that these charges all lie on the interface is too crude. However, we can't simply assume them to be completely immersed in water, because the image charges on the other side of the interface are expected to be not negligible. Therefore, it's necessary to figure out to study charges away from, but in the vicinity of, a dielectric jump.

We start by considering a more general case: water and a medium with a smaller dielectric constant than that of water are separated by an infinite plane, two point charges locates near (or on) this plane in the water with distance z and z' to the plane respectively, and salts are dissolved in water to provide the background Debye screening effect while there's no charges whatsoever in the other medium. For convenience, we assume the projection of their positions on the plane is the origin and $\vec{r}$, respectively. Keep it in mind that $\vec{r}$ is a 2D vector.

The first thing we want to know, naturally, is the electrostatic force $\nu_{DH}(\vec{r})$ between them. According to Netz [102], this can be calculated by an inverse Fourier transform:

$$\nu_{DH}\left(\vec{r}\right)=\int\frac{d\vec{p}}{\left(2\pi\right)^{2}}\cdot\exp\left(i\vec{p}\cdot\vec{r}\right)\nu_{DH}\left(z,z',\vec{p}\right) \tag{C.1}$$

The interaction in the momentum space has been solved, reads:

$$\begin{aligned}\nu_{DH}\left(z,\,z',\,\vec{p}\right) &= \frac{2\pi l_b}{\sqrt{\kappa^2+p^2}}\left[\exp\left(-\left|z-z'\right|\sqrt{\kappa^2+p^2}\right)+\frac{\sqrt{\kappa^2+p^2}-\eta p}{\sqrt{\kappa^2+p^2}+\eta p}\right.\\ &\left.\times\exp\left(-\left|z+z'\right|\sqrt{\kappa^2+p^2}\right)\right]\end{aligned} \tag{C.2}$$

where κ is the inverse Debye length in water, $\eta=\varepsilon_{small}/\varepsilon_{water}$ is the ratio between the dielectric constants.

Analytically performing the inverse Fourier transform Eq. C.1 with the general image function C.2 is not easy. For $\eta=0$ and $z=z'$, the interaction in the position space has been solved:

$$\nu_{DH}\left(\vec{r},\,z\right)=l_b\cdot\left(\frac{e^{-\kappa r}}{r}+\frac{e^{-\kappa\sqrt{r^2+4z^2}}}{\sqrt{r^2+4z^2}}\right) \tag{C.3}$$

For $z\to\infty$, Eq. C.3 becomes $\nu_{DH}\left(\vec{r}\right)=l_b\cdot\frac{e^{-\kappa r}}{r}$, consistent with Eq. A.1. For $z=0$, Eq. C.3 becomes $\nu_{DH}\left(\vec{r}\right)=2l_b\cdot\frac{e^{-\kappa r}}{r}$, consistent with our common sense.

Integrating Eq. C.3 gives the surface potential produced by a uniform charged layer of charge density σ parallel to the interface at a distance z:

$$\psi\left(z\right)=2\pi l_b\sigma\int_0^\infty rdr\cdot\nu_{DH}\left(\vec{r}\right)=2\pi l_b\kappa^{-1}\sigma\cdot\left(1+e^{-2\kappa z}\right) \tag{C.4}$$

As to integrating the general form in Eq. C.2, we haven't arrived at any definite conclusion as of yet. Anyway, we thank J. Rao from Sun Yat-sen University for his attempt to help.

Appendix D

Energy of Charges Alternately Arranged on a Square Lattice

Consider an infinite square lattice of lattice constant a on a plane, on which dwells positive and negative point charges, each of which carries a same amount of charge (only different in sign), that are arranged in the configuration in the left half of Fig. D.1, and the entire system is immersed in electrolyte solution of inverse Debye length κ. Since the lattice is infinite, it's obvious that there are a same amount of positive and negative charges, and the entire plane is electrically neutral. However, for each charge, since the charges on its nearest neighboring lattice sites are of an opposite sign, the overall electrostatic force it feels is non-zero, but slightly attractive (i.e. preventing the charge from moving out of the plane), and the electrostatic energy density of the surface is non-zero either. Here, we aim at calculating the electrostatic energy per site on this lattice.

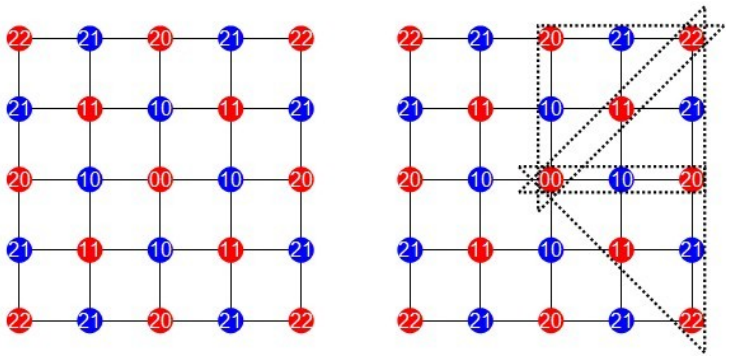

Figure D.1: Scheme for calculating Coulomb energy

The right half of Fig. D.1 depicts the scheme. We put the site of interest at the center, and establish a Cartesian coordinate system. Then, we divide the surface into 8 "semi-quadrants" (Fig. D.1 only shows 3 of them). It's easy to see that each semi-quadrant contains a same amount of sites. Furthermore, for each site in one semi-quadrant, there is another site in any other semi-quadrant that's of the same distance from the origin. For example, all the sites labeled as "21" in the figure are $\sqrt{5}a$ away from the origin. It's also easy to see that sites of the same distance from the origin always carry the same kind of charges. Therefore, we only have to consider one semi-quadrant and multiply that by 8. But before doing that, we noticed that the sites on the boundary between two semi-quadrant are counted twice on each boundary, and 4 times over all. For example, there are only 4 sites labeled "20", and only 4 sites labeled "11", etc.

Based on the arguments above, we can do the calculation as below:

$$E_{site} = k_B T \cdot l_b \cdot \Sigma = k_B T \cdot l_b \cdot \sum_{i=1}^{\infty} \sum_{j=1}^{i} (-1)^{i+j-1} \frac{e^{-\kappa a \sqrt{i^2+j^2}}}{a\sqrt{i^2+j^2}} \cdot k \tag{D.1}$$

in which,

$$k = \begin{cases} 4\,(j=0, j=i) \\ 8\,(otherwise) \end{cases} \tag{D.2}$$

Fig. D.2 shows the (reduced) electrostatic energy per site for several a values.

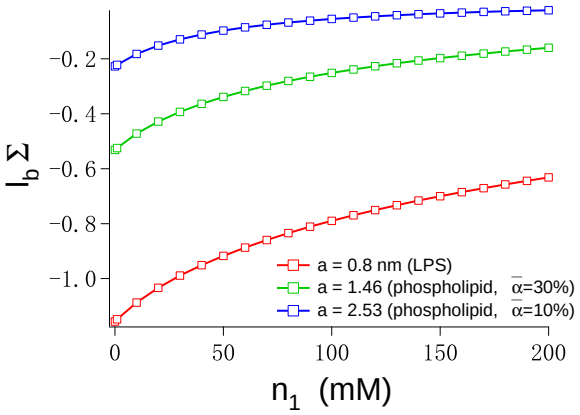

Figure D.2: Magnitude of Σ

Appendix E

Correction Integral in the Mean-field term

As we've discussed in chapter 3 (see Fig. 3.8), a correction term is necessary to depict that no other charged can come too close to an occupied lattice site. Now we express the corresponding energy, $E_{hole} = \Delta \cdot l_b \cdot \mathcal{M}$, and determine $\mathcal{M}$.

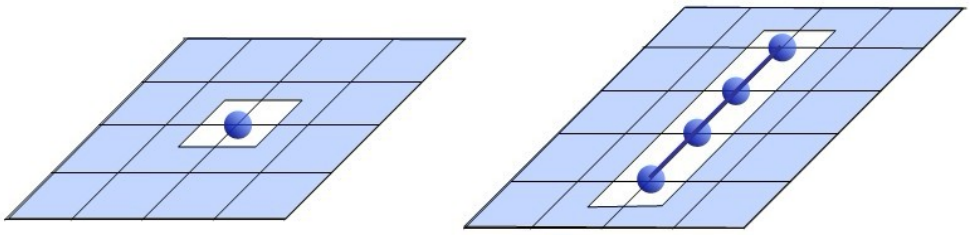

Figure E.1: Calculating the correction term

For an ion (monovalent and divalent alike), it's simple. $\mathcal{M}$, denoted as $\mathcal{M}_1$ in this case, is just the overall Debye-Hückel energy between the ion and all the other point charges in a square region of area a^2 centered around it (left half of Fig. E.1). Notice that here, we ignored the finite distance ($> \delta_i$) between the ion and the plane, because we didn't consider that in the mean-field term, either. In future works when we account for this distance in the mean-field term, we surely need to do the same for the correction term. Therefore,

$$\mathcal{M}_1(\kappa, a) = \int_{-a/2}^{a/2} dx \int_{-a/2}^{a/2} dy \frac{\exp\left(-\kappa\sqrt{x^2+y^2}\right)}{\sqrt{x^2+y^2}} \tag{E.1}$$

For a peptide, it's a bit more tricky. As depicted in the right half of Fig. E.1, for a peptide adopting α-helical structure, it'll occupy Q sites in a row ($Q = 4$ in the figure). The $\mathcal{M}$ here, denoted as $\mathcal{M}_p$, should be the sum of each of the discrete peptide charges (approximated as point charge) with this region.

$$\mathcal{M}_p(\kappa, a) = \sum_{i=1}^{Q} \int_{(-i+1/2)a}^{(Q-i+1/2)a} dx \int_{-a/2}^{a/2} dy \frac{\exp\left(-\kappa\sqrt{x^2+y^2}\right)}{\sqrt{x^2+y^2}} \tag{E.2}$$

Obviously, as $a \to \inf$, $\mathcal{M}_1 \to 2\pi/\kappa$, $\mathcal{M}_p \to 2Q\pi/\kappa$.

Notice that the $\mathcal{M}$ here is not the same as in Ref. [95] (one half for $\mathcal{M}_1$). This is because that Ref. [95] assume the ions are not point charges, but uniformed smeared out in the region. I believe that the author of it plans to depict the limited freedom for bound ions to move around, but we've accounted for that in our calculation as well, in a different way. So our $\mathcal{M}$ is correct within our own theoretical framework.

Appendix F

Entropic Free Energy of Bound Peptides

As stated in section 3.2, when bound onto the lattice depicting the LPS leaflet, each ion occupies one binding site, while each cationic lipid occupies a number of Q (Q = 4 in our calculation) sites. It's expected to introduce some subtlety in the calculation of entropic part of the free energy. In some of the previous works (e.g. [95]), the peptides are treated as if each had occupied only one binding site in the calculation of entropy. This is plausible only when there are few peptides bound on the surface($\sigma_p/\sigma_0 \ll 1$). However, even in Ref. [95], σ_p/σ_0 could be as large as 20%. In this case, the bound ions can only pick among 20% of all the binding sites, while they were assumed to be able to access 80% of all the binding sites. Hence, it's necessary to deal with the issue with more caution.

Assume we have N_0 binding sites, on which N_1 monovalent ions, N_2 divalent ions and N_p peptides are bound. We want to see how many ways there are to arrange them. Let's arrange the peptides first. For convenience, we define one charge on the peptide to be the "head", and assume the orientation of the peptide is fixed. The head of the first peptide can choose from all of the N_0 sites to be bound onto, but once the head is fixed, the remaining $Q-1$ charges are also determined, so there are N_0 ways for this peptide to be bound. The second peptide can choose from the remaining sites for its head to be bound, thus it has $N_0 - Q$ ways to do it. The third peptide has $N_0 - 2Q$ ways to be bound, and the nth peptide has $N_0 - (n-1)Q$ ways. Of course, the peptides themselves are identical, and swapping any two would make no difference. High school maths tells us that the total number ways of arranging the N_p peptides is:

$$\Omega_p = \frac{N_0 \left(N_0 - Q\right) \left(N_0 - 2Q\right) \cdots \left(N_0 - \left(N_p - 1\right)Q\right)}{N_p!} \tag{F.1}$$

If we introduce the concept of "multifactorial"

$$N!^{(k)} = \begin{cases} 1, & 0 \leq N \leq k-1, \quad \text{(F.2)} \\ N \cdot \left(N-k\right)!^{(k)}, & N \geq k. \quad \text{(F.2}') \end{cases}$$

Eq. F.1 can be written as:

$$\Omega_p = \frac{N_0!^{(Q)}}{\left(N_0 - QN_p\right)!^{(Q)} N_p!} \tag{F.3}$$

The arranging of the ions is trivial, and we easily arrive at the total multiplicity:

$$\Omega = \frac{N_0!^{(Q)}}{\left(N_0 - QN_p\right)!^{(Q)} N_p!} \cdot \frac{\left(N_0 - QN_p\right)!}{N_1! N_2! \left(N_0 - QN_p - N_1 - N_2\right)} \tag{F.4}$$

According to several number theory textbooks, the multifactorial can be expressed as:

$$N!^{(k)} = k^{\frac{N-1}{k}} \cdot \frac{\left(\frac{N}{k}\right)!}{\Gamma\left(\frac{1}{k}+1\right)} \tag{F.5}$$

Therefore,

$$\ln\left(N!^{(k)}\right) = \frac{N-1}{k} \ln k + \frac{N}{k} \ln \frac{N}{k} - \ln\left(\Gamma\left(\frac{1}{k}+1\right)\right) = \frac{N}{k} \ln N + C\left(k\right) \tag{F.6}$$

in which $C\left(k\right)$ is a function of k only and will be canceled in the derivation below. Now we can take the logarithm of Eq. F.4:

$$\begin{aligned} \frac{F_{ent}}{k_B T} &= -\ln \Omega = -\frac{N_0}{Q} \ln N_0 + \frac{N_0 - QN_p}{Q} \ln\left(N_0 - QN_p\right) \\ &\quad - \left(N_0 - QN_p\right) \ln\left(N_0 - QN_p\right) + N_p \ln N_p + N_1 \ln N_1 + N_2 \ln N_2 \\ &\quad + \left(N_0 - QN_p - N_1 - N_2\right) \ln\left(N_0 - QN_p - N_1 - N_2\right) \end{aligned} \tag{F.7}$$

The second line is the trivial part, while the second and third terms of the first line are introduce by multifactorial. The first constant term can be dropped.

The chemical potentials $\mu_i^{ent} = \frac{\partial F_{ent}}{\partial N_i}$ for the ions are trivial:

$$\mu_i^{ent} = \frac{N_i}{N_0 - QN_p - N_1 - N_2}; i = 1, 2 \tag{F.8}$$

while the chemical potential for peptide is not as frequently seen, but still easy to work out:

$$\mu_p^{ent} = \frac{N_p \cdot (N_0 - QN_p)^{Q-1}}{(N_0 - QN_p - N_1 - N_2)^Q} \tag{F.9}$$

Obviously, if we set $Q = 1$, everything shall reduce to the forms identical to those in other works.

References

[1] Paul Singleton. *Bacteria in Biology, Biotechnology and Medicine*. 5th edition, 2005.

[2] Dela J. Benos, Sidney A. Simon, and Richard Epand, editors. *Lipid Polymorphism and Membrane Properties*. Current Topics in Membrane. 1997.

[3] Cynthia L Sears. A dynamic partnership: celebrating our gut flora. *Anaerobe*, 11(5):247–51, October 2005.

[4] Dela J. Benos, Sidney A. Simon, and Scott E. Feller, editors. *Computational Modeling of Membrane Bilayers*. Current Topics in Membrane. 2008.

[5] Y Kamio and Hiroshi Nikaido. Outer membrane of Salmonella typhimurium: accessibility of phospholipid head groups to phospholipase c and cyanogen bromide activated dextran in the external medium. *Biochemistry*, 15(12):2561–70, July 1976.

[6] Bruce Alberts, Alexander Johnson, Julian Lewis, Martin Raff, Keith Roberts, and Peter Walter. Chapter 24: Pathogens, Infection, and Innate Immunity. In *Molecular Biology of the Cell*, pages 1485–1538. 2002.

[7] Katsumi Matsuzaki. Why and how are peptide-lipid interactions utilized for self-defense? Magainins and tachyplesins as archetypes. *Biochimica et Biophysica Acta*, 1462:1–10, December 1999.

[8] Michael Zasloff. Antimicrobial peptides of multicellular organisms. *Nature*, 415:389–395, 2002.

[9] D Wade, A Boman, B Wå hlin, C M Drain, D Andreu, H G Boman, and R B Merrifield. All-D amino acid-containing channel-forming antibiotic peptides. *Proceedings of the National Academy of Sciences of the United States of America*, 87(12):4761–4765, June 1990.

[10] Roberto Bessalle, Aviva Kapitkovsky, Alfred Gorea, Itamar Shalit, and Mati Fridkin. All-D-magainin: chirality, antimicrobial activity and proteolytic resistance. *FEBS Letters*, 274(1-2):151–155, November 1990.

[11] Michael Zasloff. Magainins, a class of antimicrobial peptides from Xenopus skin: isolation, characterization of two active forms, and partial cDNA sequence of a precursor. *Proceedings of the National Academy of Sciences of the United States of America*, 84(15):5449–5453, August 1987.

[12] Lin Yang, Thomas M Weiss, Robert I Lehrer, and Huey W Huang. Crystallization of Antimicrobial Pores in Membranes: Magainin and Protegrin. *Biophysical Journal*, 79(4):2002–2009, October 2000.

[13] Hélène Bouvrais, Philippe Méléard, Tanja Pott, Knud J Jensen, Jesper Brask, and John H Ipsen. Softening of POPC membranes by magainin. *Biophysical Chemistry*, 137:7–12, September 2008.

[14] Margitta Dathe, Heike Nikolenko, Jana Meyer, Michael Beyermann, and Michael Bienert. Optimization of the antimicrobial activity of magainin peptides by modification of charge. *FEBS Letters*, 501(2-3):146–150, July 2001.

[15] Sattar Taheri-Araghi and Bae-Yeun Ha. Physical Basis for Membrane-Charge Selectivity of Cationic Antimicrobial Peptides. *Physical Review Letters*, 98(16):168101, April 2007.

[16] Vishnu Dhople, Amy Krukemeyer, and Ayyalusamy Ramamoorthy. The human beta-defensin-3, an antibacterial peptide with multiple biological functions. *Biochimica et biophysica acta*, 1758(9):1499–1512, September 2006.

[17] Lin Yang, Thad A Harroun, Thomas M Weiss, Lai Ding, and Huey W Huang. Barrel-Stave Model or Toroidal Model? A Case Study on Melittin Pores. *Biophysical Journal*, 81(3):1475–1485, September 2001.

[18] Yechiel Shai. Mechanism of the binding, insertion and destabilization of phospholipid bilayer membranes by alpha-helical antimicrobial and cell non-selective membranelytic peptides. *Biochimica et Biophysica Acta*, 1462:55–70, December 1999.

[19] Michael T. Madigan and John M. Martinko. *Brock Biology of Microorganisms*. 11th edition, 2006.

[20] Hiroshi Nikaido and Marti Vaara. Molecular basis of bacterial outer membrane permeability. *Microbiological Reviews*, 49(1):1–32, March 1985.

[21] Martti Vaara. Antibiotic-Supersusceptible Mutants of Escherichia coli and Salmonella typhimurium. *Antimicrobial Agents and Chemotherapy*, 37(11):2255–2260, 1993.

[22] Robert M Shroll and T P Straatsma. Molecular structure of the outer bacterial membrane of Pseudomonas aeruginosa via classical simulation. *Biopolymers*, 65(6):395–407, December 2002.

[23] Christoph Jeworrek, Florian Evers, Jörg Howe, Klaus Brandenburg, Metin Tolan, and Roland Winter. Effects of specific versus nonspecific ionic interactions on the structure and lateral organization of lipopolysaccharides. *Biophysical journal*, 100(9):2169–77, May 2011.

[24] Thomas Abraham, Sarah R Schooling, Mu-Ping Nieh, Norbert Kucerka, Terry J Beveridge, and John Katsaras. Neutron diffraction study of Pseudomonas aeruginosa lipopolysaccharide bilayers. *The Journal of Physical Chemistry B*, 111(10):2477–83, March 2007.

[25] Ilarald Labischinski, Dieter Naumann, Christian Schultz, Shoichi Kusumoto, and Tetsuo Shiba. Comparative X-ray and Fourier-transform-infrared investigations of conformational properties of bacterial and synthetic lipid A of Escherichia coli and Salmonella minnesota as well as partial structures and analogues thereof. *European Journal of Biochemistry*, 665:659–665, 1989.

[26] Stephen G Wilkinson. Bacterial lipopolysaccharides - Themes and variations. *Progress in Lipid Research*, 35(3):283–343, 1996.

[27] Christian R H Raetz and Chris Whitfield. Lipopolysaccharide Endotoxins. *Annual Review of Biochemistry*, 71:635–700, 2002.

[28] Hiroshi Nikaido. Molecular Basis of Bacterial Outer Membrane Permeability Revisited. *Microbiology and Molecular Biology Reviews*, 67(4):593–656, 2003.

[29] Jacob Israelachvili. *Intermolecular and Surface Forces*. 2nd edition, 1991.

[30] P. Nelson. *Biological Physics: Energy, Information, Life*. W. H. Freeman and Company, 2008.

[31] Sek-Wen Hui and Arindam Sen. Effects of lipid packing on polymorphic phase behavior and membrane properties. *Proceedings of the National Academy of Sciences of the United States of America*, 86(15):5825–9, August 1989.

[32] P C Noordam, C J van Echteld, B de Kruijff, A J Verkleij, and J de Gier. Barrier characteristics of membrane model systems containing unsaturated phosphatidylethanolamines. *Chemistry and Physics of Lipids*, 27(3):221–232, October 1980.

[33] Wangchen Wang, Lin Yang, and Huey W Huang. Evidence of cholesterol accumulated in high curvature regions: implication to the curvature elastic energy for lipid mixtures. *Biophysical journal*, 92(8):2819–2830, April 2007.

[34] Pieter R Cullis, Michael J Hope, and Colin P S Tilcock. Lipid polymorphism and the roles of lipids in membranes. *Chemistry and Physics of Lipids*, 40(2-4):127–144, 1986.

[35] Carolyn Newton, Walter Pangborn, Shlom Nir, and Demetrios Papahadjopoulos. Specificity of Ca^{2+} and Mg^{2+} Binding to Phosphatidylserine Vesicles and Resultant Phase Changes of Bilayer Membrane Structure. *Biochimica et Biophysica Acta*, 506:281–287, 1978.

[36] Sattar Taheri-Araghi and Bae-Yeun Ha. Electrostatic bending of lipid membranes: how are lipid and electrostatic properties interrelated? *Langmuir*, 26(18):14737–14746, August 2010.

[37] Demetrios Papahadjopoulos and Shinpei Ohki. Stability of asymmetric phospholipid membranes. *Science*, 164(3883):1075–1077, May 1969.

[38] Hermann Trauble and Hansjorg Eibl. Electrostatic effects on lipid phase transitions: membrane structure and ionic environment. *Proceedings of the National Academy of Sciences of the United States of America*, 71(1):214–219, January 1974.

[39] Demetrios Papahadjopoulos and A Portis. Calcium-induced Lipid Phase Transitions and Membrane Fusion. *Annals of the New York Academy of Science*, 308:50–66, 1978.

[40] P R Cullis and B de Kruijff. Lipid polymorphism and the functional roles of lipids in biological membranes. *Biochimica et Biophysica Acta*, 559(4):399–420, December 1979.

[41] Claus Nielsen, Mark Goulian, and Olaf S Andersen. Energetics of Inclusion-Induced Bilayer Deformations. *Biophysical Journal*, 74(4):1966–1983, April 1998.

[42] Raquel F Epand and Richard M Epand. Modulation of membrane curvature by peptides. *Biopolymers (Peptide Science)*, 55(5):358–63, January 2000.

[43] Andrea Hickel, Sabine Danner-Pongratz, Heinz Amenitsch, Gabor Degovics, Michael Rappolt, Karl Lohner, and Georg Pabst. Influence of antimicrobial peptides on the formation of nonlamellar lipid mesophases. *Biochimica et Biophysica Acta*, 1778(10):2325–2333, October 2008.

[44] Eduardo Perozo, Anna Kloda, D Marien Cortes, and Boris Martinac. Physical principles underlying the transduction of bilayer deformation forces during mechanosensitive channel gating. *Nature Structural Biology*, 9(9):696–703, September 2002.

[45] Christine D Mccallum and Richard M Epand. Insulin Receptor Autophosphorylation and Signaling Is Altered by Modulation of Membrane Physical Properties. *Biochemistry*, 34(6):1815–1824, 1995.

[46] Ming-Tao Lee, Wei-Chin Hung, Fang-Yu Chen, and Huey W Huang. Many-body effect of antimicrobial peptides: on the correlation between lipid's spontaneous curvature and pore formation. *Biophysical journal*, 89(6):4006–16, December 2005.

[47] Ismail M Hafez and Pieter R Cullis. Roles of lipid polymorphism in intracellular delivery. *Advanced Drug Delivery Reviews*, 47(2-3):139–148, April 2001.

[48] Theresa M Allen and Pieter R Cullis. Drug delivery systems: entering the mainstream. *Science*, 303(5665):1818–1822, March 2004.

[49] David Andelman. Electrostatic Properties of Membranes : The Poisson- Boltzmann Theory. In R Lipowsky and E Sackmann, editors, *Handbook of Biological Physics*, volume 1, chapter 12, pages 603–641. Elsevier B.V., 1995.

[50] S A Safran. Curvature elasticity of thin films. *Advances in Physics*, 48(4):395–448, July 1999.

[51] Rob Philips, Jane Kondev, Julie Theriot, and Nigel Orme. Electrostatics for Salty Solutions. In *Physical Biology of the Cell*, chapter 9. 2009.

[52] Meyer B. Jackson. *Molecular and Cellular Biophysics*. Cambridge University Press, 2006.

[53] Stuart McLaughlin. The Electrostatic Properties of Membranes. *Annual Review of Biophysics and Biological Chemistry*, 18:113–136, January 1989.

[54] P A Pincus and S A Safran. Charge fluctuations and membrane attractions. *Europhysics Letters*, 42(1):103–108, April 1998.

[55] Bae-Yeun Ha. Modes of counterion density fluctuations and counterion-mediated attractions between like-charged fluid membranes. *Physical Review E*, 64(3):031507, August 2001.

[56] Itamar Borukhov, David Andelman, and Henri Orland. Steric Effects in Electrolytes: A Modified Poisson-Boltzmann Equation. *Physical Review Letters*, 79(3):435–438, July 1997.

[57] Itamar Borukhov. Adsorption of large ions from an electrolyte solution: a modified PoissonBoltzmann equation. *Electrochimica Acta*, 46(2-3):221–229, November 2000.

[58] Siewert-Jan Marrink, Alex H de Vries, and D Peter Tieleman. Lipids on the move: simulations of membrane pores, domains, stalks and curves. *Biochimica et Biophysica Acta*, 1788(1):149–168, January 2009.

[59] Emanuel Schneck, Thomas Schubert, Oleg V Konovalov, Bonnie E Quinn, Thomas Gutsmann, Klaus Brandenburg, Rafael G Oliveira, David a Pink, and Motomu Tanaka. Quantitative determination of ion distributions in bacterial lipopolysaccharide membranes by grazing-incidence X-ray fluorescence. *Proceedings of the National Academy of Sciences of the United States of America*, 107(20):9147–51, May 2010.

[60] M Winterhalter and Wolfgang Helfrich. Effect of surface charge on the curvature elasticity of membranes. *The Journal of Physical Chemistry*, 92(24):6865–6867, December 1988.

[61] M Winterhalter and Wolfgang Helfrich. Bending elasticity of electrically charged bilayers: coupled monolayers, neutral surfaces, and balancing stresses. *The Journal of Physical Chemistry*, 96(1):327–330, January 1992.

[62] Tom Chou, Marko V Jaric, and Eric D Siggia. Electrostatics of lipid bilayer bending. *Biophysical Journal*, 72(5):2042–2055, May 1997.

[63] Bae-Yeun Ha. Stabilization and destabilization of cell membranes by multivalent ions. *Physical Review E*, 64(5):1–5, October 2001.

[64] Bae-Yeun Ha. Effect of divalent counterions on asymmetrically charged lipid bilayers. *Physical Review E*, 67(3):030901, March 2003.

[65] Yang Li and Bae-Yeun Ha. Molecular theory of asymmetrically charged bilayers: Preferred curvatures. *Europhysics Letters*, 70(3):411–417, May 2005.

[66] A W C Lau and P A Pincus. Charge-Fluctuation-Induced Nonanalytic Bending Rigidity. *Physical Review Letters*, 81(6):1338–1341, August 1998.

[67] Sattar Taheri-Araghi and Bae-Yeun Ha. Electrostatic bending of lipid membranes: how are lipid and electrostatic properties interrelated? *Langmuir*, 26(18):14737–46, September 2010.

[68] Joshua Zimmerberg and Michael M Kozlov. How proteins produce cellular membrane curvature. *Nature Reviews Molecular Cell Biology*, 7(1):9–19, January 2006.

[69] Wolfgang Helfrich. Elastic Properties of Lipid Bilayers: Theory and Possible Experiments. *Zeitschrift für Naturforschung*, 28(c):693–703, 1973.

[70] S Leikin, Michael M Kozlov, Nola L Fuller, and R Peter Rand. Measured effects of diacylglycerol on structural and elastic properties of phospholipid membranes. *Biophysical Journal*, 71(5):2623–2632, November 1996.

[71] Nola L Fuller, Carlos R Benatti, and R Peter Rand. Curvature and Bending Constants for Phosphatidylserine-Containing Membranes. *Biophysical Journal*, 85(3):1667–1674, September 2003.

[72] Sylvio May and Avinoam Ben-Shaul. Molecular theory of lipid-protein interaction and the L_{alpha}-H_{II} transition. *Biophysical Journal*, 76(2):751–67, February 1999.

[73] Stephen H White and Glen I King. Molecular packing and area compressibility of lipid bilayers. *Proceedings of the National Academy of Sciences of the United States of America*, 82(19):6532–6, October 1985.

[74] Lydéric Bocquet, Emmanuel Trizac, and Miguel Aubouy. Effective charge saturation in colloidal suspensions. *The Journal of Chemical Physics*, 117(17):8138–8152, 2002.

[75] Sattar Taheri-Araghi and Bae-Yeun Ha. Charge renormalization and inversion of a highly charged lipid bilayer: Effects of dielectric discontinuities and charge correlations. *Physical Review E*, 72(2):021508, August 2005.

[76] T T Nguyen, A Yu Grosberg, and B I Shklovskii. Screening of a charged particle by multivalent counterions in salty water: Strong charge inversion. *The Journal of Chemical Physics*, 113(3):1110–1125, 2000.

[77] K. Besteman, M. a. G. Zevenbergen, H. A. Heering, and S. G. Lemay. Direct Observation of Charge Inversion by Multivalent Ions as a Universal Electrostatic Phenomenon. *Physical Review Letters*, 93(17):4–7, October 2004.

[78] B I Shklovskii. Screening of a macroion by multivalent ions: correlation-induced inversion of charge. *Physical Review E*, 60(5):5802–5811, November 1999.

[79] David C Morrison and Lorreta Leive. Fractions of lipopolysaccharide from Escherichia coli Olll:B4 prepared by two extraction procedures. *The Journal of Biological Chemistry*, 2750(8):2911–2919, 1976.

[80] Andre Wiese, Jan O Reiners, Klaus Brandenburg, Kazuyoshi Kawahara, Ulrich Zähringer, and Ulrich Seydel. Planar asymmetric lipid bilayers of glycosphingolipid or lipopolysaccharide on one side and phospholipids on the other: membrane potential, porin function, and complement activation. *Biophysical Journal*, 70(1):321–9, January 1996.

[81] Y Takeuchi and Hiroshi Nikaido. Persistence of segregated phospholipid domains in phospholipid–lipopolysaccharide mixed bilayers: studies with spin-labeled phospholipids. *Biochemistry*, 20(3):523–9, February 1981.

[82] Bae-Yeun Ha and D Thirumalai. Bending Rigidity of Stiff Polyelectrolyte Chains: A Single Chain and a Bundle of Multichains. *Macromolecules*, 36(25):9658–9666, December 2003.

[83] C Galanos and O Lüderitz. Electrodialysis of lipopolysaccharides and their conversion to uniform salt forms. *European Journal of Biochemistry*, 54(2):603–10, June 1975.

[84] Hiroshi Nikaido, Yutaka Takeuchi, Shun-Ichi Ohnishi, and Taiji Nakae. Outer membrane of Salmonella typhimurium. Electron spin resonance studies. *Biochimica et Biophysica Acta*, 465(1):152–164, 1976.

[85] F Garcia-del Portillo, John W Foster, Michael E Maguire, and B Brett Fintay. Characterization of the micro-environment of Salmonella typhimunrium-containing vacuoles within MDCK epithelial cells. *Molecular Microbiology*, 6(22):3289–3297, 1992.

[86] S Wee and B J Wilkinson. Increased outer membrane ornithine-containing lipid and lysozyme penetrability of Paracoccus denitrificans grown in a complex medium deficient in divalent cations. *Journal of Bacteriology*, 170(7):3283–6, July 1988.

[87] Richard M Epand and Hans J Vogel. Diversity of antimicrobial peptides and their mechanisms of action. *Biochimica et Biophysica Acta*, 1462(1-2):11–28, December 1999.

[88] Martin W. Bader, William Wiley Navarre, Whitney Shiau, Hiroshi Nikaido, Jonathan G. Frye, Michael McClelland, Ferric C. Fang, and Samuel I. Miller. Regulation of Salmonella typhimurium virulence gene expression by cationic antimicrobial peptides. *Molecular Microbiology*, 50(1):219–230, August 2003.

[89] Joseph B McPhee, Shawn Lewenza, and Robert E W Hancock. Cationic antimicrobial peptides activate a two-component regulatory system, PmrA-PmrB, that regulates resistance to polymyxin B and cationic antimicrobial peptides in Pseudomonas aeruginosa. *Molecular Microbiology*, 50(1):205–217, August 2003.

[90] Eduardo A Groisman. The Pleiotropic Two-Component Regulatory System PhoP-PhoQ. *Journal of Bacteriology*, 183(6):1835–42, 2001.

[91] Steven D Breazeale, Anthony a Ribeiro, and Christian R H Raetz. Origin of lipid A species modified with 4-amino-4-deoxy-L-arabinose in polymyxin-resistant mutants of Escherichia coli. An aminotransferase (ArnB) that generates UDP-4-deoxyl-L-arabinose. *The Journal of Biological Chemistry*, 278(27):24731–9, July 2003.

[92] D A Pink, L Truelstrup Hansen, T A Gill, Bonnie E Quinn, M H Jericho, and T J Beveridge. Divalent Calcium Ions Inhibit the Penetration of Protamine through the Polysaccharide Brush of the Outer Membrane of Gram-Negative Bacteria. *Langmuir*, 19(21):8852–8858, 2003.

[93] S Obst, M Kastowsky, and H Bradaczek. Molecular dynamics simulations of six different fully hydrated monomeric conformers of Escherichia coli re-lipopolysaccharide in the presence and absence of Ca^{2+}. *Biophysical journal*, 72(3):1031–46, March 1997.

[94] M. L Henle, C. D Santangelo, D. M Patel, and P A Pincus. Distribution of counterions near discretely charged planes and rods. *Europhysics Letters*, 66(2):284–290, April 2004.

[95] Roham Rahnamaye Farzami. *Electrostatic Interactions of Peptides with Lipid Membranes : Competitive Binding between Cationic Peptides and Divalent Counterions.* MSc thesis, University of Waterloo, 2010.

[96] Jean-francois Cote, Gerald Perron, and Jacques E Desnoyers. Application of the Bjerrum Association Model to Electrolyte Solutions . III . Temperature and Pressure Dependencies of Association Constants. *Journal of Solution Chemistry*, 27(8):707–718, 1998.

[97] H Krienke and J Barthel. Association concepts in electrolyte solutions. *Journal of Molecular Liquids*, 78:123–138, 1998.

[98] A Travesset and D Vaknin. Bjerrum pairing correlations at charged interfaces. *Europhysics Letters*, 74(1):181–187, April 2006.

[99] E. A. Moelwyn-Hughes. *Physical Chemistry*. 2nd revised edition, 1961.

[100] T. Engel and P. Reid. *Physical Chemistry*. Pearson Education Inc., 2005.

[101] Sattar Taheri-Araghi and Bae-Yeun Ha. Cationic antimicrobial peptides: a physical basis for their selective membrane-disrupting activity. *Soft Matter*, 6(9):1933, 2010.

[102] Roland R Netz. Debye-Hückel theory for interfacial geometries. *Physical Review E*, 60(3):3174–3182, 1999.